NUCLEAR SPIN DYNAMICS AND THERMODYNAMICS OF PULSED NMR IN SOLIDS

Thesis by

Douglas Peter Burum

In Partial Fulfillment of the Requirements

for the Degree of

Doctor of Philosophy

California Institute of Technology

Pasadena, California

1979

(Submitted March 26, 1979)

To Belinda . . .

my wife, and my best friend.

Acknowledgments

I would like to express my sincerest gratitude to Dr. Won-Kyu Rhim. Most of what I know about solid state NMR — indeed, most of what I know about being a scientist — was learned from him. He has been a good friend during the past five years, and our many discussions on all topics of life have been both enlightening and enjoyable.

I would also like to thank my advisor, Dr. Robert Vaughan, for his continuing faith in me and for always providing just the needed mixture of guidance and freedom. It has been good to know that I could always call on him when needed.

Much appreciation goes to my parents for their unfailing love and support through the years and for always allowing me to be the person I was meant to be.

I am grateful to my good friend Ginny Williamson, who saw me through many difficult spots along the way.

Finally, my wife Belinda deserves special thanks for all her love and encouragement, and for adding so much warmth and color to life.

Abstract

The investigations presented in this thesis deal with two basic topics of solid state NMR: coherent averaging of nuclear spin interactions by rf irradiation, and the application of thermodynamics in strongly time dependent interaction frames. In each case new theoretical insights are presented, and these lead to the development of new experiments.

After a general introduction, an extension of coherent averaging theory called the principle of pulse cycle decoupling is presented. This principle greatly facilitates the design and analysis of compound experiments, i.e. techniques which are combinations of several smaller experiments. A number of multiple pulse experiments are analyzed using pulse cycle decoupling and several new techniques are introduced, including 24-pulse and 52-pulse cycles which have a greater ability to resolve anisotropic chemical shifts in solids than any experiment previously developed. The 52-pulse cycle is used to measure proton chemical shift spectra for polycrystalline ice, C_6H_{12}, C_5H_{10} and polyethylene. This new technique is also used to study proton chemical shifts in single crystals of gypsum, $CaSO_4 \cdot 2H_2O$.

The second topic considered in this thesis is the application of thermodynamics to NMR experiments in which the amplitude of the applied rf irradiation is varied in a strongly non-adiabatic fashion. Sources of artificial spin heating are analyzed and methods of eliminating these effects are demonstrated. A calculation is presented of the spin-lattice relaxation time during one basic type of multiple pulse irradiation. Techniques based on this calculation are introduced which measure relaxation times in the laboratory frame, T_1, and the rotating frame, $T_{1\rho}$. A method for determining the first

moment of an NMR spectrum is also developed. These new techniques are demonstrated using a variety of materials, including CaF_2 and C_6F_6.

A simple yet highly flexible pulse sequence generator which is capable of producing all the pulse sequences described in this thesis as well as many more complicated experiments is described in the Appendix.

TABLE OF CONTENTS

Chapter I

GENERAL INTRODUCTION

Section 1

Theoretical Introduction

As indicated in the title, this thesis deals with the dynamics and thermodynamics of nuclear spin systems in solids and their measurment by pulsed NMR techniques. Specifically, it explores the physics of an ensemble of quantum mechanical two level spin systems in contact with one another and also with a classical thermodynamic bath called the lattice. Physically, the term "lattice" refers to the electromagnetic spectrum generated by phonons in the crystal lattice of which the nuclear spins are a part. However, the lattice can be considered simply as a thermodynamic bath with a temperature equal to the physical temperature of the solid. Under many circumstances, the nuclear spin ensemble can also be described by thermodynamics. When this is the case, the spin system can also be considered to have a temperature. At equilibrium this spin temperature is equal to the lattice temperature.

The investigations in this thesis are limited almost exclusively to solids which contain only a single species of nuclear magnetic dipole with gyromagnetic ratio γ and spin $I = \frac{1}{2}$. The spin system is immersed in a strong, constant magnetic field H_o applied along the z-axis.

If it is assumed that the coupling between the spin system and the lattice can be neglected, the Hamiltonian in the laboratory reference frame can be written[1]

$$\mathcal{H}_L = \gamma H_0 I_z + \mathcal{H}_D + \mathcal{H}_C \qquad (1)$$

where $\mathcal{H}_D$ describes the direct dipole-dipole interaction between the nuclei and the chemical shift term, $\mathcal{H}_C$, characterizes the change in the magnetic field at the nuclear site due to the diamagnetism of the surrounding electrons. There are many other smaller Hamiltonian terms which have been neglected in equation 1.

In order to manipulate the spin system, rf irradiation of variable amplitude and phase is applied at some frequency ω near $\omega_0 = \gamma H_0$. By moving to an interaction representation, or "rotating frame", with this characteristic frequency ω the Hamiltonian can be written[1]

$$\mathcal{H}(t) = (\omega_0 - \omega)I_z + \mathcal{H}_{rf}(t) + \mathcal{H}_D^{(z)} + \mathcal{H}_C \ , \qquad (2)$$

where $\mathcal{H}_D^{(z)}$ described the static, or truncated part of the dipole-dipole interaction in this frame. Because the rf irradiation, and thus $\mathcal{H}_{rf}$, are under experimental control, the form of $\mathcal{H}(t)$ can be manipulated in many ways. In particular, it is often desirable to suppress $\mathcal{H}_D^{(z)}$ so that the effects of much weaker interactions such as chemical shift can be observed.

In chapter II, a coherent averaging theory, or "average Hamiltonian theory", based on the Magnus expansion[2] which was first applied to NMR by Evans[3] is extended so that it can be more readily applied to long and complex NMR experiments. This enlarged theory is applied in analyzing and developing a number of experiments designed to eliminate the effects of the homonuclear dipolar interaction in solids and allow the measurement of chemical shift information. Several new experiments of this type are introduced which are more successful than any technique developed previously. One new experiment, a 52-pulse cycle, is analyzed in detail. In order to demonstrate its resolving ability, this technique is used to measure chemical shift spectra for polycrystalline samples of ice, C_6H_{12}, C_5H_{10} and polyethylene. The 52-pulse cycle is also used to determine the chemical shift tensor for protons in gypsum, $CaSO_4 \cdot 2H_2O$.

As was stated earlier, equations (1) and (2) contain no information regarding the interaction of the spin system with the lattice. This interaction is thermodynamic in nature. Therefore one would expect that experiments

designed to measure characteristics of the spin-lattice coupling would involve rf irradiation which was either constant in amplitude or at most varied adiabatically. However, it is demonstrated in chapter III that this need not always be the case.

In chapter III, circumstances are explored under which thermodynamics can be applied to a nuclear spin system in a strongly time dependent interaction frame. As a result, several new experiments are developed which are a valuable contribution to NMR technology. These include methods for measuring thermodynamic spin-lattice coupling parameters and also a new technique for determining the first moment of an NMR spectrum. The theoretical validity and practical applicability of these new experiments are demonstrated using several representative materials, such as C_6F_6, C_6F_{12} and CaF_2.

The Appendix describes a simple pulse sequence generator which is capable of producing all the pulse sequences described in the thesis as well as many more complicated experiments. This instrument represents a practical demonstration that the complexity of the new experiments discussed in this thesis is not an obstacle to their implementation.

References

1. A. Abragam, The Principles of Nuclear Magnetism, Oxford Univ. Press, London (1961).

C. P. Slichter, Principles of Magnetic Resonance, 2nd Edition, Springer-Verlag, Berlin, Heidelberg and New York (1978).

2. W. Magnus, Commun. Pure Appl. Math. 7, 649 (1954).

3. W. A. B. Evans, Ann. Phys. 48, 72 (1968).

Section 2

Instrumentation

The NMR spectrometer[1,2] which was used to perform all the experiments discussed in this thesis is illustrated in Figure 1. RF irradiation at frequencies near 56.4 MHz is applied to the sample in the probe coil either in continuous bursts or as a series of short, nearly square pulses. Four different phases of rf are available with relative shifts of 0^{o}, 90^{o}, 180^{o} and 270^{o}. In the rotating frame these correspond to irradiation along the x, y, -x and -y coordinate axes. Pulse timing and phase channel selection is determined through the use of rf switches, or "gates", which are controlled by the pulse sequence generator described in the Appendix. This instrument is programmed by the PDP 11/10 computer but operates independently. It is capable of producing a wide variety of experiements including sequences of up to 200 pulses.

The receiver is designed to detect the NMR signal between applications of rf irradiation. Both the rf transmitter and the receiver utilize the same coil in the probe. Despite various features designed to protect the receiver from rf irradiation such as the use of crossed diodes and ¼ wave length coaxial cables,[3] there is still a characteristic time interval, or receiver "dead" time, following the end of an rf burst during which the receiver is saturated and accurate data are not available. This gives rise to a minimum sampling time, or sampling "window", between the start of one rf pulse and the beginning of the next equal to the pulse width + the receiver dead time + about ½ μsec during which the signal can be sampled. The receiver dead time for the spectrometer discussed in this thesis varied from 6 μsec to 3 μsec as improvements were made in receiver protection. The typical rf pulse length required to produce a 90^{o} rotation of the nuclear magnetization vectors[4] was 1.5 μsec.

References

1. A detailed description of this spectrometer is given in R. W. Vaughan, D. D. Elleman, L. M. Stacey, W. K. Rhim and J. W. Lee, Rev. Sci. Instrum. 43, 1356 (1972).

2. The spectrometer described in this thesis is representative of current NMR technology. See for example, J. S. Waugh, Advances in Magnetic Resonance, Academic Press, New York and London (1971).

3. I. J. Lowe and C. E. Tarr, J. Phys. E 1, 320 (1968).

I. J. Lowe and C. E. Tarr, J. Phys. E 1, 604 (1968).

4. See chapter II, section 1.

Figure Caption

1. Schematic diagram of the pulse spectrometer.

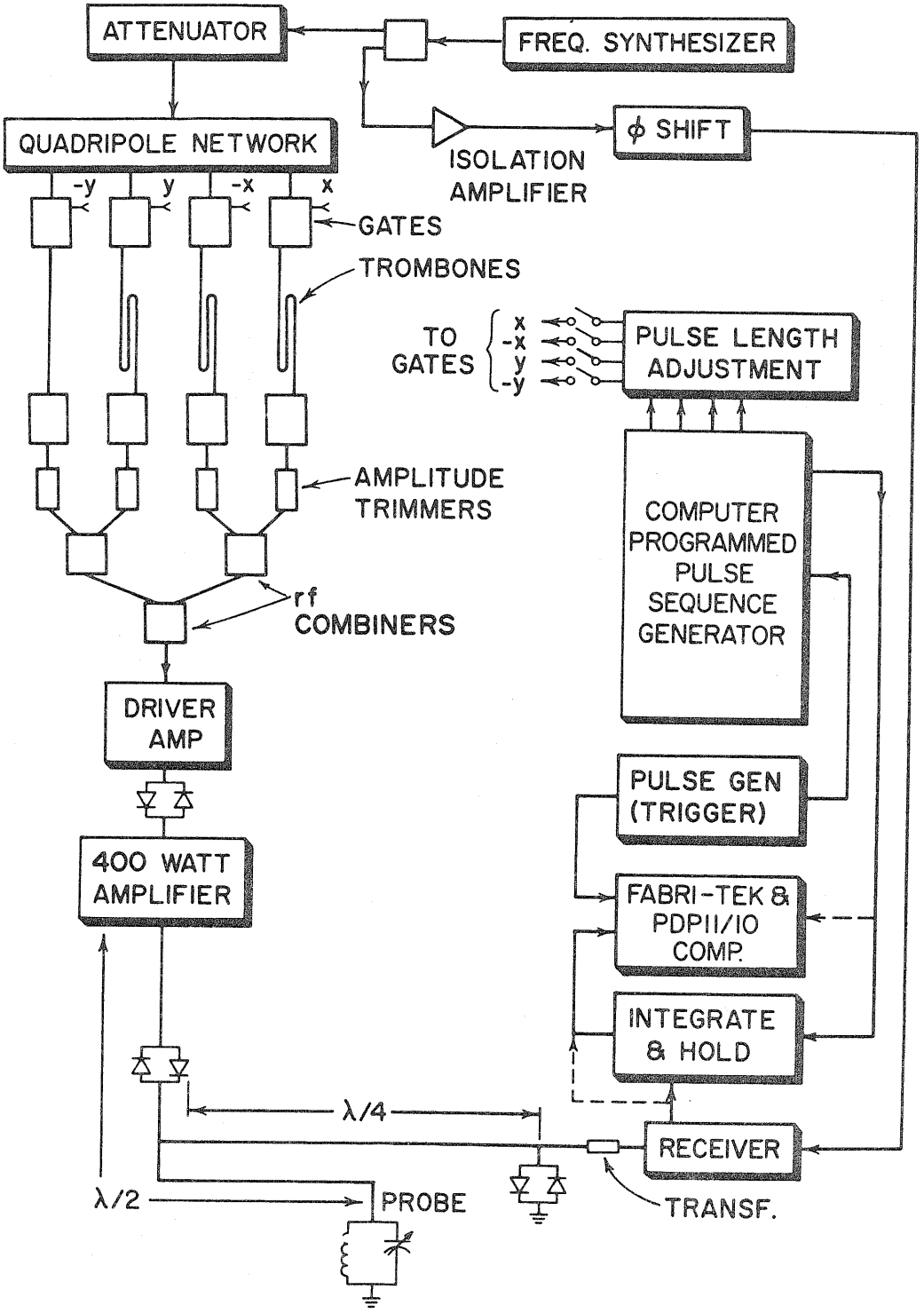
ATTENUATOR
FREQ. SYNTHESIZER
QUADRIPOLE NETWORK
ISOLATION AMPLIFIER
φ SHIFT
-y
y
-x
x
GATES
TROMBONES
TO GATES
x
-x
y
-y
PULSE LENGTH ADJUSTMENT
AMPLITUDE TRIMMERS
COMPUTER PROGRAMMED PULSE SEQUENCE GENERATOR
rf COMBINERS
DRIVER AMP
PULSE GEN (TRIGGER)
400 WATT AMPLIFIER
FABRI-TEK & PDP11/10 COMP.
INTEGRATE & HOLD
λ/4
RECEIVER
λ/2
PROBE
TRANSF.

Fig. 1

Chapter II

NUCLEAR SPIN DYNAMICS IN SOLIDS DURING MULTIPLE PULSE rf IRRADIATION

Section 1

Introduction

This chapter is concerned with understanding and developing experiments designed to eliminate the effects of the homonuclear dipole-dipole interactions in solids described by $\mathcal{H}_D^{(z)}$ to as high an order of magnitude as possible while preserving information regarding weaker interactions such as the chemical shift, $\mathcal{H}_C$. Although determining the strength of $\mathcal{H}_D^{(z)}$ provides valuable information regarding the structure and dynamics of a solid, much more insight is gained if the other interactions such as chemical shift can also be measured. Unfortunately, in most solids the effects of these weaker interactions on conventional NMR experiments are completely obscured by $\mathcal{H}_D^{(z)}$.

Recall from the first section of chapter I that if the interaction between the spin system and the lattice is neglected, the Hamiltonian in the rotating reference frame can be written

$$\mathcal{H}(t) = (\omega_0 - \omega)I_z + \mathcal{H}_{rf} + \mathcal{H}_D^{(z)} + \mathcal{H}_C \qquad (1)$$

where I_x, I_y and I_z are the spin angular momentum operators corresponding to the total spin operator I. The experiments discussed in this chapter are designed in such a way that $\mathcal{H}_{rf}$ has the effect of eliminating $\mathcal{H}_D^{(z)}$. These experiments also invariably reduce, or "scale", the effective magnitude of $\mathcal{H}_C$, but this reduced chemical shift term is observable if the dipolar term $\mathcal{H}_D^{(z)}$ is sufficiently eliminated.

In principle, the amplitude of the rf irradiation in an NMR experiment can be modulated in any way. However, all of the experiments described in this chapter consist of sequences of short rf "pulses" applied along the x, y, -x and -y coordinate axes in the rotating frame.

The Hamiltonian for an ideal, square rf pulse applied along the x-axis can be expressed in the rotating frame as follows:

$$\mathcal{H}_{pulse} = \gamma H_1 I_x \equiv \omega_1 I_x \qquad (2)$$

where the amplitude of the rf magnetic field in the laboratory frame is $2H_1 \cos\omega t$. The time development operator which corresponds to an x-pulse can be expressed as

$$U_{pulse} = \exp(i\omega_1 t\ I_x) \ . \tag{3}$$

The rotation angle of a pulse is determined by its amplitude $\omega_1 = \gamma H_1$ and its width t_w. For example, a pulse for which $\omega_1 t_w = \pi/2$ is referred to as a $(\pi/2)$ pulse or a 90^o pulse. For purposes of analysis, the assumption is often made that the pulses can be considered to have a δ-function shape. The time development operator for a $(\pi/2)_x$ pulse of this type is given by

$$U_{\delta\text{-fn}} = \exp(i\ \pi/2\ I_x) \ . \tag{4}$$

It is convenient to analyze the effects of $\mathcal{H}_{rf}$ on the other Hamiltonian terms in equation 1 by moving to the so called "toggling" frame, i.e. the interaction frame determined by the time development operator U_{rf} corresponding to $\mathcal{H}_{rf}$. In this reference frame the Hamiltonian terms acquire a time dependence due to U_{rf}. For example, the dipolar Hamiltonian in the toggling frame, $\tilde{\mathcal{H}}_D^{(z)}$, is given by

$$\tilde{\mathcal{H}}_D^{(z)} = U_{rf}^{-1} \mathcal{H}_D^{(z)} U_{rf} \ . \tag{5}$$

The effect of an rf pulse in this frame on a Hamiltonian term which is linear in the spin operators I_x, I_y and I_z is to cause a simple rotation. For example, a $(\pi/2)_x$ pulse causes the following transformation of I_z:

$$\exp(-i\ \pi/2\ I_x) I_z \exp(i\ \pi/2\ I_x) = -I_y \tag{6}$$

In section 2, a coherent averaging theory, or "average Hamiltonian" theory, is reviewed. This theory is utilized in the remainder of the chapter in analyzing the effect of $\mathcal{H}_{rf}$ on the other terms in the Hamiltonian.

Perhaps the most successful experiment currently in use which is designed to eliminate the homonuclear dipolar interaction in solids is an 8-pulse sequence called "REV-8". Normally, only single phase information is obtained using this experiment. However, in section 3 it is shown that full quadrature phase information can be obtained using REV-8 by sampling the data more often. This increases the effective data rate and eliminates the need to use special quadrature phase detection apparatus.

Section 4 presents an extension of average Hamiltonian theory which is called the principle of "pulse cycle decoupling." This approach simplifies the design and analysis of compound pulse sequences, i.e. experiments which are combinations of smaller pulse groups. Pulse cycle decoupling is shown to provide a method for the systematic improvement of pulsed NMR experiments. This is demonstrated by the development of several new experiments which resolve chemical shifts in solids more effectively than any techniques previously introduced. One of these experiments, a 52-pulse sequence, is analyzed in detail. This pulse sequence is used to measure proton chemical shifts in ice, C_6H_{12}, C_5H_{10} and polyethylene at liquid N_2 temperature. None of these spectra could be resolved as clearly using previously available techniques such as REV-8.

The applicability of the 52-pulse cycle is further demonstrated in section 5. This section presents the results of a proton chemical shift study performed on single crystals of gypsum, $CaSO_4 \cdot 2H_2O$, at ambient temperature. The results are compared with a similar study which used the REV-8 sequence.

Section 2

Average Hamiltonian Theory

(Most of this section is taken from an article by D. P. Burum and W. K. Rhim, "Analysis of Multiple Pulse NMR in Solids. III" which has been submitted for publication to The Journal of Chemical Physics.)

Average Hamiltonian theory is a formalism based on the Magnus expansion[1] which describes the coherent averaging of terms in the Hamiltonian caused by the applied rf irradiation. This theory was first applied to NMR experiments by Evans[2] and has been discussed in more detail by Haeberlen et al.[3]. It was extended by Rhim et al.[4] in their analysis of the REV-8 experiment to include the effects of rf pulse imperfections.

In the usual rotating frame the Hamiltonian describing the nuclear spin system can be divided into terms describing the rf irradiation, $\mathcal{H}'_{rf}$, and the contributions from internal interactions as follows:

$$\mathcal{H}(t) = \mathcal{H}'_{rf}(t) + \mathcal{H}_0 + \mathcal{H}_D^{(z)} \tag{1}$$

where the off resonance and chemical shift term $\mathcal{H}_0$ and the truncated dipolar Hamiltonian $\mathcal{H}_D^{(z)}$ can be written

$$\mathcal{H}_0 = \sum_i (\Delta\omega + \omega_0\sigma_{zzi})\, I_{zi} \tag{2}$$

and

$$\mathcal{H}_D^{(z)} = \sum_{i<j} \beta_{ij}(\vec{r}_{ij})(\vec{I}_i \cdot \vec{I}_j - 3I_{zi}I_{zj}) \tag{3}$$

$\mathcal{H}'_{rf}$ can be divided into ideal and non-ideal parts as follows:

$$\mathcal{H}'_{rf}(t) = \mathcal{H}_{rf}(t) + \sum_k \mathcal{H}_k(t) \tag{4}$$

where $\mathcal{H}_{rf}(t)$ describes the effect of ideal rf pulses of constant phase and power and exactly the desired length, while the sum over k includes all the error terms which complete the description of the true experimental situation, such as k = P for phase misadjustments, T for phase transients, δ for pulse length misadjustments and ε for rf inhomogeneity. For an x-pulse these can be written as follows:

$$\mathcal{H}_P = -\omega_1 \sin \phi_x \, I_y \tag{5}$$

$$\mathcal{H}_T = \omega_T(t) \, I_y \tag{6}$$

$$\mathcal{H}_\delta = -\frac{\delta_x}{t_w} I_x \tag{7}$$

$$\mathcal{H}_\varepsilon = -\sum_i \frac{\varepsilon_i}{t_w} I_{xi} \tag{8}$$

Here t_w is the pulse width, so that $\omega_1 t_w = \pi/2$, ϕ_x and δ_x are the phase angle and pulse size misadjustments of the x-pulse, ε_i is the error in rotation angle at the i'th nucleus caused by rf inhomogeneity and $\omega_T(t)$ is the rf amplitude orthogonal to the x direction. It is assumed without loss of generality that

$$\sum_i \varepsilon_i = 0 \tag{9}$$

and

$$\int_0^{t_w} \omega_T(t)dt = 0 \tag{10}$$

Similar definitions apply for pulses of different rf phases.

It is convenient to move an interaction representation, or "toggling frame", which

is determined by $\mathcal{H}_{rf}$. In this frame the other terms in the Hamiltonian acquire a time dependence from $\mathcal{H}_{rf}$. For example, the dipolar Hamiltonian in this frame, $\tilde{\mathcal{H}}_D$, is given by

$$\tilde{\mathcal{H}}_D = U_{rf}^{-1} \mathcal{H}_D U_{rf} \tag{11}$$

where U_{rf} is the time development operator determined by $\mathcal{H}_{rf}$.

If $\mathcal{H}_{rf}(t)$ is assumed to be cyclic, with cycle time t_c, i.e.,[5]

$$U_{rf}(Nt_c) = \pm 1 \tag{12}$$

then the usual rotating frame and the toggling frame coincide at times Nt_c. Furthermore, if $\mathcal{H}_{rf}$ is also periodic,

$$\mathcal{H}_{rf}(t + Nt_c) = \mathcal{H}_{rf}(t) \tag{13}$$

then the time development operator in the toggling frame, which we call U_{int}, acquires the useful property

$$U_{int}(Nt_c) = [U_{int}(t_c)]^N \tag{14}$$

This means that the behavior of the system for an arbitrary number of pulse cycles can be deduced from the time development operator for a single cycle.

The Magnus expansion[1,2] can be used to expand $U_{int}(t_c)$ so that it remains unitary no matter where the expansion is truncated:

$$U_{int}(t_c) = \exp\left[-it_c\left(\bar{\mathcal{H}}_{int}^{(0)} + \bar{\mathcal{H}}_{int}^{(1)} + \bar{\mathcal{H}}_{int}^{(2)} + \ldots\right)\right] \tag{15}$$

where

$$\bar{\mathcal{H}}_{int}^{(0)} = t_c^{-1} \int_0^{t_c} \tilde{\mathcal{H}}_{int}(t_1) dt_1 \tag{16}$$

$$\bar{\mathcal{H}}_{int}^{(1)} = (2it_c)^{-1}\int_0^{t_c} dt_2 \int_0^{t_2} dt_1 \left[\tilde{\mathcal{H}}_{int}(t_2), \tilde{\mathcal{H}}_{int}(t_1)\right] \tag{17}$$

$$\bar{\mathcal{H}}_{int}^{(2)} = (6t_c)^{-1}\int_0^{t_c} dt_3 \int_0^{t_3} dt_2 \int_0^{t_2} dt_1 \left\{\left[\tilde{\mathcal{H}}_{int}(t_3), \left(\tilde{\mathcal{H}}_{int}(t_2), \tilde{\mathcal{H}}_{int}(t_1)\right)\right] + \left[\tilde{\mathcal{H}}_{int}(t_1), \left(\tilde{\mathcal{H}}_{int}(t_2), \tilde{\mathcal{H}}_{int}(t_3)\right)\right]\right\} \tag{18}$$

and, of course,

$$\tilde{\mathcal{H}}_{int} = \tilde{\mathcal{H}}_0 + \tilde{\mathcal{H}}_D + \sum_k \tilde{\mathcal{H}}_k \tag{19}$$

By expressing $\tilde{\mathcal{H}}_{int}$ according to equation (19), the various terms in the Magnus expansion can be divided into contributions from each of the Hamiltonian terms in a straightforward way, i.e.,

$$\bar{\mathcal{H}}_{int}^{(0)} = \bar{\mathcal{H}}_0^{(0)} + \bar{\mathcal{H}}_D^{(0)} + \sum_k \bar{\mathcal{H}}_k^{(0)} \tag{20}$$

$$\bar{\mathcal{H}}_{int}^{(1)} = \bar{\mathcal{H}}_0^{(1)} + \bar{\mathcal{H}}_D^{(1)} + \bar{\mathcal{H}}_{DO}^{(1)} + \bar{\mathcal{H}}_{\epsilon D}^{(1)} + \ldots \tag{21}$$

$$\bar{\mathcal{H}}_{int}^{(2)} = \bar{\mathcal{H}}_0^{(2)} + \bar{\mathcal{H}}_D^{(2)} + \bar{\mathcal{H}}_{DO}^{(2)} + \ldots \tag{22}$$

and so forth.

By expressing the time development operator according to the Magnus expansion the problem of observing certain interactions which are normally obscured by other, stronger interactions in solids is reduced to choosing a periodic and cyclic rf pulse sequence which preserves the desired Hamiltonian terms while removing the unwanted terms to as high an order as possible.

REFERENCES

1. W. Magnus, Commun. Pure Appl. Math. 7, 649 (1954).

2. W. A. B. Evans, Ann. Phys. 48, 72 (1968).

3. U. Haeberlen and J. S. Waugh, Phys. Rev. 175, 453 (1968).

4. W. K. Rhim, D. D. Elleman, L. B. Schreiber and R. W. Vaughan, J. Chem. Phys. 59, 3740 (1973).

5. Cases in which $U_{rf}(t_c) = -1$ are of special interest. See, for example: M. E. Stoll, A. J. Vega and R. W. Vaughan, Phys. Rev. A16, 1521 (1977).

Section 3

Extraction of Quadrature Phase Information from Multiple Pulse NMR Signals

(This section is essentially an article by W. K. Rhim and D. P. Burum, Rev. Sci. Instrum. 47, 720 (1976).)

A. INTRODUCTION

Over the last decade, considerable progress has been achieved in the field of high resolution solid state NMR.[1-3] Through the use of multiple pulse techniques, the static dipolar interaction can be averaged out, enabling one to observe relatively smaller interactions such as anisotropic chemical shifts or indirect exchange interactions. Considerable attention has been given to the REV-8 sequence for its simplicity, smaller chemical shift scaling effect, high resolution, and better stability.[3]

In pulsed NMR experiments a quadrature phase detector is often used to observe two components of the free induction decay signal, one in phase and one out of phase with the rf pulse. In this scheme, when applied to multiple pulse NMR experiments in solids, the signal is usually sampled once per cycle and phase detected using the quadrature phase detector.[4,5] However, the multiple pulse sequence contains rf pulses whose phases are mutually orthogonal so that one might expect the signal sampled at two properly chosen windows within a cycle to furnish full quadrature information without the use of a special detector.

In this section, the REV-8 cycle is further analyzed with the goal of retrieving more information from the resultant NMR signal. Several important points which are emphasized are (1) the quadrature phase information which can be obtained from a single phase detector, practically eliminating the need for a conventional quadrature phase detector; (2) the increased signal-to-noise ratio; and (3) the high frequency information which can be made available due to the fact that the 8-pulse sequence allows one to sample the signal at a higher rate.

B. THE 8-PULSE CYCLE

The 8-pulse cycle which will be considered in this section is shown in Fig. 1. All the pulses, expressed by x, y, -x and -y are 90 degree pulses whose phases are directed along the indicated axes in the rotating frame. The spacings between adjacent pulses are τ and 2τ.

The usual receiver blocking time which follows the strong rf pulses and the short values of t_c required for a better averaging effect prevent sampling the NMR signal in the narrow windows. Therefore, only signal detection at the 2τ windows is considered.

C. AVERAGE HAMILTONIANS

The interactions commonly encountered in solid state NMR can be expressed in the rotating frame by the Hamiltonian

$$\mathcal{H}(t) = \mathcal{H}_{rf}(t) + \mathcal{H}_0 + \mathcal{H}_C + \mathcal{H}_D^{(z)} \tag{1}$$

$\mathcal{H}_{rf}(t)$ depends on the nature of the rf excitation, while the resonance offset $\mathcal{H}_0$, the chemical shift $\mathcal{H}_C$, and the truncated dipolar interaction $\mathcal{H}_D^{(z)}$, have the following forms:

$$\mathcal{H}_0 = -\gamma(\omega_o - \omega)\, I_z \tag{2}$$

$$\mathcal{H}_C = -\omega_o \sum_i \sigma_{zzi}\, I_{zi} \tag{3}$$

$$\mathcal{H}_D^{(z)} = \sum_{i<j} B_{ij}(r_{ij})\,(\vec{I}_i \cdot \vec{I}_j - 3I_{zi}I_{zj}) \tag{4}$$

If the first few pulses are considered pre-pulses and the 8-pulse cycle is redefined, average Hamiltonian theory can be applied to analyze the signal appearing at each of the 2τ windows shown in figure 1. This analysis shows that the average dipolar interaction vanishes at all 2τ windows. However, the sum $\mathcal{H}_0 + \mathcal{H}_C$ results in a different, non zero average Hamiltonian at each 2τ window in the 8-pulse cycle when averaged over t_c. These average Hamiltonians, $\bar{\mathcal{H}}_{0\alpha}^{(0)}$, ($\alpha$ = 1,2,3 or 4) at the α-th 2τ window in each cycle are given by:

$$\bar{\mathcal{H}}_{01}^{(0)} = \tfrac{1}{3}\sum_i (\Delta\omega + \omega_o\sigma_{zz})\,(I_{xi} + I_{zi}) = \bar{\mathcal{H}}_{03}^{(0)} \tag{5a}$$

$$\bar{\mathcal{H}}_{02}^{(0)} = \tfrac{1}{3}\sum_i (\Delta\omega + \omega_o\sigma_{zz})\,(I_{yi} + I_{zi}) \tag{5b}$$

$$\bar{\mathcal{H}}_{04}^{(0)} = \tfrac{1}{3}\sum_i (\Delta\omega + \omega_o \sigma_{zz})\,(I_{zi} - I_{yi}) \tag{5c}$$

Since the chemical shift and resonance offset Hamiltonians have essentially the same form, it is assumed for simplicity that $\alpha_{zzi} = 0$ in order to describe the development of the system in a pictorial way. Then eq. (5a)-(5c) can be rewritten in the following form:

$$\bar{\mathcal{H}}_{\alpha}^{(0)} = \gamma \vec{H}_{\alpha} \cdot \vec{I} \quad (\text{for } \alpha = 1, 2, 3, \text{ and } 4) \tag{6}$$

where $$\vec{H}_1 = \tfrac{1}{3}\frac{\Delta\omega}{\gamma}(\hat{x} + \hat{y}) = \vec{H}_3 \tag{7a}$$

$$\vec{H}_2 = \tfrac{1}{3}\frac{\Delta\omega}{\gamma}(\hat{y} + \hat{z}) \tag{7b}$$

$$\vec{H}_4 = \tfrac{1}{3}\frac{\Delta\omega}{\gamma}(-\hat{y} + \hat{z}) \tag{7c}$$

and $\hat{x}$, $\hat{y}$, and $\hat{z}$ are unit vectors in the rotating frame. Of course, the vectors $\vec{H}_{\alpha}$ will serve as the effective fields in the rotating frame. Therefore, given the initial magnetization vectors in the various windows of the first 8-pulse cycle, each magnetization vector will appear to precess around its own effective field with angular frequency $\gamma|\vec{H}_{\alpha}| = \frac{\sqrt{2}}{3}\omega$ (Fig. 2).

If δ-function rf pulses are assumed, the magnetization vector at each window in the first 8-pulse cycle can be obtained by alternately applying 90° rotations due to the rf pulses and appropriate precessions due to the resonance offset during the windows. Beginning with the magnetization in thermal equilibrium along z-axis, the initial vectors so obtained can be drawn as in Figure 2 when $\omega \approx 0$. Therefore, if the signal is sampled once per cycle, the result is a stroboscopic view in which the magnetization seems to precess around $\vec{H}_{\alpha}$ starting from $\vec{M}_{\alpha}$ as shown in figure 2, $\alpha = 1, 2, 3$, and 4.

Since the $\vec{H}_{\alpha}$ vectors are all tilted by 45° from the z-axis, the projections of the precessing magnetization vectors on the x-y plane will trace out ellipses whose short axes measure $1/\sqrt{2}$ times the long axes. When the NMR signal is phase detected along the y-axis, the M_y components which are expected at each window are shown in Figure 3. The first four traces in Figure 3 are just those which one would expect to obtain if the magnetization of a given isochromat was measured at only one of the windows in each cycle. The last trace in this figure is the composite of the first four traces which is observed when the signal is sampled at all 2τ windows.

D. THE NARROW SPECTRUM CASE

It is a well known property of the discrete, fast Fourier transform that the bandwidth of the transformed spectrum depends directly upon the sampling rate of the input data. Thus, if the time between sampling of the input points is T, the total width of the transformed spectrum will be $\frac{2\pi}{T}$, and signals of frequency greater than $\pm \pi/T$ will be reflected back into the range $\frac{2\pi}{T}$. When the NMR signal is sampled at all 4 of the 2τ windows, the time between successive complex points is $t_c/2$, so that the transformed spectral band width is $\frac{4\pi}{t_c}$.

In this section, it is assumed that the NMR spectral width is much smaller than $\frac{2\pi}{t_c}$, so that the entire spectrum can be located near exact resonance. As was described in the previous section, the magnetization M_α, stroboscopically observed at the α-th window (α = 1, 2, 3, 4) will appear to precess around $\vec{H}_\alpha$ with angular frequency $\gamma|\vec{H}_\alpha| = \omega_r$ ($\omega_r = \sqrt{2}\omega/3$). In this case, it is assumed that the y-component of the magnetization at each window, $(M_y)_\alpha$, satisfies the following relations:

$$(M_y)_1 = M_o \cos(\omega_r t) = (M_y)_3 \tag{8a}$$

$$-(M_y)_2 = \frac{M_o}{\sqrt{2}} \sin(\omega_r t) = (M_y)_4 \tag{8b}$$

The degree to which this assumption is valid will become clear when the more general "Wide Spectrum Case" is analyzed in the next sub-section. The following are important consequences of this situation: (i) relations (8a)-(8b) provide quadrature phase information. If the amplitudes are matched by multiplying $(M_y)_2$ by $-\sqrt{2}$ and $(M_y)_4$ by $\sqrt{2}$, the signals from the four windows combine to produce two traces which can be treated as the real and imaginary parts of a complex video signal proportional to $M_o \exp(i\omega_r t)$. Therefore, the complex Fourier transformed spectrum will unambiguously exploit the direction in which each isochromat is precessing. One should realize, however, that (8a) and (8b) are only orthogonal when the detector phase is set either along the x- or y-axis in the rotating frame. (At this point it may be worthwhile to mention that for the 4-pulse WAHUHA cycle[1] the signals at the two wide windows differ in phase by 120° when the detector phase is set along the x- or y-axis. Also, the observation of a baseline shift is inevitable for that cycle unless a special prepulse is applied.) (ii) Since signal is coherent and noise is random, one can expect enhancement of the signal

to noise ratio by a factor of $\sqrt{3}$ when utilizing the signals obtained at all 4 windows.

In order to demonstrate some of these effects experimentally, perfluorocyclohexane was chosen as a sample and the REV-8 sequence was applied at -60^{o} C.[6] In this case the signal was sampled only at the first two windows. Trace (A) in Fig. 4 is the digitized signal so obtained, and traces (B) and (C) are the computer separated signals from (A). Notice the predicted orthogonality in phase as well as the amplitude difference. Inasmuch as the usual algorithms are designed to work with complex quantities, the trace (A) becomes an ideal input for a fast Fourier transform computation when the amplitude difference between (B) and (C) is corrected.

The top trace of Fig. 5 is the real part of the Fourier transform of trace (B) alone. As one would expect, this spectrum is symmetric about the resonance point, since only single phase information was Fourier transformed. The real part of the Fourier transform of trace (C) in Fig. 4 is an antisymmetric spectrum, as shown by the second trace in Fig. 5. Note that the amplitude of this spectrum is reduced compared to the top spectrum. Of course, the logical way to handle the data of Fig. 4 trace (A) is to multiply trace (C) by $\sqrt{2}$, recombine (B) and (C), and take the full complex Fourier transform of the resultant trace. The lower two curves in Fig. 5 are the absorption and the dispersion spectra so obtained. Now the images have disappeared and the direction in which each isochromat is precessing is apparent.

The same procedure was repeated, but this time for frozen C_6F_6[7] and a different resonance offset frequency (5 KHz above the liquid C_6F_6 resonance point). Fig. 6 shows the real and imaginary parts of the familiar chemical shift powder pattern so obtained. No additional correction was made, although the spectrum was nearly 9 KHz wide.

E. THE WIDE SPECTRUM CASE

In this sub-section the more general situation is considered in which the spectral width may be comparable to $2\pi/t_c$ and may be located over any region within the bandwidth $\pm 2\pi/t_c$. The types of errors which are introduced and schemes for correcting these errors are discussed. For simplicity, the signal due to an isochromat is analyzed.

1. Sampling at 2 Windows Only

Consider first the case in which only the first and second windows are sampled to form a complex input to the Fourier transformation. The analysis of this case is relatively simple, and the symmetry properties of the errors provide a very simple method for error correction. The signal sampled at the first window (i.e. right after the first pulse) can be expressed as A cos ($\omega_r t$) if the isochromat is off resonance by frequency $\omega_r/2\pi$ during the rf burst. A is a constant which is proportional to the intensity of the undistorted absorption spectrum at this same frequency. In general the precession of the magnetization during the time between the start of the sequence and the start of the second window in the first cycle must be taken into account in determining the initial magnetization at the second window. It is the deviation of this magnetization from its ideal value which gives rise to the spectral distortions described below. The resulting signal can be expressed as:

$$I_{\omega_r}(t) = A(A_2 \cos\phi_2 \sin\omega_r t + A_2 \sin\phi_2 \cos\omega_r t) + C_2$$

The amplitude A_2, phase change ϕ_2 and the constant shift C_2 are all functions of $\omega\tau$. They can be expressed in the following way:

$$A_2 = [(1 - 8C_2^2)/2]^{1/2}$$

$$\phi_2 = \sin^{-1}[(\sin\omega\tau \sin 2\omega\tau - C_2)/A_2]$$

$$C_2 = \tfrac{1}{4}[\cos\omega\tau \sin 2\omega\tau - \sin\omega\tau \sin 2\omega\tau]$$

where $\omega_r = \frac{\sqrt{2}}{3}\omega$.

Now, the complex input signal for the fast Fourier transform at frequency $\omega_r/2\pi$ can be expressed by

$$f_{\omega_r}(t) = R_{\omega_r}(t) + iI_{\omega_r}(t)$$

$$= A \cos\omega_r t + iA[A_2 \cos\phi_2 \sin\omega_r t + A_2 \sin\phi_2 \cos\omega_r t] + iC_2$$

$$= Ae^{i\omega_r t} + i[2K \sin(\omega_r t + \phi) + C_2] \tag{9a}$$

where

$$K \equiv \frac{A}{2}\left[(A_2 \cos\phi_2 - 1)^2 + A_2^2 \sin^2\phi_2\right]^{\frac{1}{2}}$$

and

$$\phi \equiv \tan^{-1}[(A_2 \sin\phi_2)/(A_2 \cos\phi_2 - 1)] + \pi$$

The first term in eq. (9a) is the ideal signal, while the second and third terms represent the errors produced by the resonance offset effect in the first cycle. The effect of these error terms on the spectrum is more easily seen in eq. (9b).

$$f(t) = Ae^{i\omega_r t} Be^{i\psi} - Ke^{-i(\omega_r t + \phi)} + iC_2 \tag{9b}$$

where

$$B \equiv [(1 + K\cos\phi)^2 + (K\sin\phi)^2]^{\frac{1}{2}}$$

$$\psi \equiv \tan^{-1}\frac{K\sin\phi}{1 + K\cos\phi} \quad (+\pi \text{ if } 1 + K\cos\phi < 0)$$

B and ψ in this equation indicate the amplitude and phase distortion of the main spectrum caused by the errors. The second term produces an image at $-\omega_r$, and the third term results in a sharp spike at $\omega_r = 0$. Thus, if the spectrum extends over $\omega_r = 0$, it will be distorted by the central spike, and the image will be superimposed on the spectrum. It is very difficult to correct for this effect. Fortunately, the error terms tend to be small near $\omega_r = 0$. In fact, after the dispersion curve is multiplied by $\sqrt{2}$, the error terms in eq. (9a) will contribute only $\sim .06\%$ at $\frac{\omega}{2\pi} = \pm 5$ KH$_z$ and $\sim 1.3\%$ at ± 5 KH$_z$, which is negligible in most practical situations.

If the spectrum does not overlap $\omega_r = 0$, however, correction of those errors becomes rather simple. It is easy to see in this case that one can merely discard the second term in eq. (9b), and correct the signal by rotating it by $-\psi$ and multiplying it by 1/B. Fig. 7 shows 1/B and ψ as functions of resonance offset frequency when $\tau = 5\mu$sec. While these are useful in estimating the amount of expected error, there is yet an easier way to correct these errors.

It can be shown that the Fourier transform of the error terms in (9a) is antisymmetric in the absorption part and symmetric in the dispersion part about $\omega_r = 0$. As long as the entire spectrum is located on one side of $\omega_r = 0$, therefore, the error can be removed by adding $U(-\omega_r)$ to $U(\omega_r)$ in the absorption part, and subtracting $V(-\omega_r)$ from $V(\omega_r)$ in the dispersion part, where the spectrum can be expressed as $U(\omega_r) + iV(\omega_r)$.

The two-window sampling case, then, provides full complex information about the precessing magnetization, increases the signal to noise ratio by a factor of $\sqrt{3}/2$, and provides a very simple way of correcting off resonance errors even for wide spectra as long as the entire spectrum can be located on one side of $\omega_r = 0$.

2. Sampling at All Four Windows

The basic procedure which is followed in analyzing the spectrum obtained when all four windows are used for sampling is essentially identical to that which was followed in the 2-window case. The actual expressions are much more complicated, however, and will not be repeated here. Again, for simplicity, the signal resulting from an isochromat is analyzed, and it is assumed that the amplitude normalizations described above have been performed.

If the magnetization is taken to be initially along the z-axis and the 8-pulse sequence is applied as a series of classical rotations, the signals which result at each of the four windows can be expressed in the following form:

$$\begin{aligned} &A_\alpha \cos(\omega_r t + \phi_\alpha) + C_\alpha \qquad \alpha = 1, 3 \\ &A_\alpha \sin(\omega_r t + \phi_\alpha) + C_\alpha \qquad \alpha = 2, 4 \end{aligned} \tag{10}$$

where the factors A_α, ϕ_α and C_α are functions of $\omega\tau$ and are determined by the excess precession in the first cycle.

When the detector phase is set along the y-axis, consideration of the direction of the effective field for each window reveals that

$$C_1 = C_3 = 0 \quad \text{and} \quad \phi_1 = 0$$

and A_1 can be set to unity for convenience.

Of course, in this case the data points sampled at windows 1 and 3, when taken together, provide the real part of the complex Fourier transform input, while those from windows 2 and 4 make up the imaginary part. This can be expressed in the following way:

$$
\begin{aligned}
R(nt_c) &= \cos(\omega_r n t_c) \\
R[(n+\tfrac{1}{2})t_c] &= A_3 \cos[\omega_r(n+\tfrac{1}{2})t_c + \phi_3)] + C_3 \\
I(nt_c) &= A_2 \sin(\omega_r n t_c + \phi_2) + C_2 \\
I[(n+\tfrac{1}{2})t_c] &= A_4 \sin[\omega_r(n+\tfrac{1}{2})t_c + \phi_4)] + C_4
\end{aligned}
\tag{11}
$$

These discrete points can be replaced for analytical purposes by the following pair of continuous curves:

$$
\begin{aligned}
R(t) &= \tfrac{1}{2}[\cos(\omega_r t) + A_3 \cos(\omega_r t + \phi_3)] \\
&\quad + \tfrac{1}{2}[\cos(\omega_r t) - A_3 \cos(\omega_r t + \phi_3)] \cos(2\pi t/t_c) \qquad (12) \\
I(t) &= \tfrac{1}{2}[A_2 \sin(\omega_r t + \phi_2) + A_4 \sin(\omega_r t + \phi_4) + C_2 + C_4] \\
&\quad + \tfrac{1}{2}[A_2 \sin(\omega_r t + \phi_2) - A_4 \sin(\omega_r t + \phi_4) + C_2 - C_4] \cos(2\pi \frac{t}{t_c})
\end{aligned}
$$

Through the use of trigonometric identities, the complex function represented by equation (12) can be expressed in the following form:

$$
\begin{aligned}
f(t) &= R(t) + iI(t) \\
&= e^{i\omega_r t} B e^{i\psi} + \epsilon_1 \exp(-i\omega_r t) + \epsilon_2 \exp[i(\omega_r + \frac{2\pi}{t_c})t] \qquad (13) \\
&\quad + \epsilon_3 \exp[i(\omega_r - \frac{2\pi}{t_c})t] + \epsilon_4 \exp[-i(\omega_r + \frac{2\pi}{t_c})t] \\
&\quad + \epsilon_5 \exp[-i(\omega_r - \frac{2\pi}{t_c})t] + \epsilon_6 \exp[i\frac{2\pi}{t_c}] + \epsilon_7 (-i\frac{2\pi}{t_c}) + \epsilon_8
\end{aligned}
$$

B and ψ in the first term of equation (13) above indicate the amplitude and phase distortion of the isochromat signal at frequency ω_r. The ϵ_i's are all error factors. Namely, ϵ_1 gives rise to a small mirror image of the spectrum, while ϵ_2-ϵ_5 give rise to sidebands at $\pm\omega_r \pm \frac{2\pi}{t_c}$. Finally, ϵ_6 and ϵ_7 produce sharp spikes at the extreme edges of the transformed spectrum, while ϵ_8 produces a similar spike at $\omega_r = 0$.

As was true in the 2 window case, these errors are difficult to correct if they are superimposed on the "true" spectrum. Table 1 shows the size of some of these errors at a few representative frequencies. However, if the spectrum can be positioned such that it does not overlap the points $\omega_r = 0$ and $\pm \frac{\pi}{t_c}$, none of these errors overlap the spectrum, and the phase and amplitude distortion (see the first term in eq. (13)) can be corrected by a simple rotation and amplitude normalization. B and ψ can be rigorously calculated and can be used to correct the main spectrum. Figure 8 shows 1/B and ψ over the full frequency range $\pm \frac{2\pi}{t_c}$, assuming $\tau = 5\mu$sec. It is interesting to note that $\pm \frac{\pi}{t_c}$ is just the full spectral bandwidth for the single window sampling case.

References

1. U. Haeberlen and J. S. Waugh, Phys. Rev. 175, 453 (1968).

2. P. Mansfield, J. Phys. C4, 1444 (1971).

3. W.-K. Rhim, D. D. Elleman and R. W. Vaughan, J. Chem. Phys. 9, 3740 (1973).

4. J. D. Ellett, Jr., M. G. Gibby, U. Haeberlen, L. M. Huber, M. Mehring, A. Pines, and J. S. Waugh, Adv. Magn. Reson. 5, 117 (1971).

5. R. W. Vaughan, D. D. Elleman, L. M. Stacey, W-K. Rhim and J. W. Lee, Rev. Sci. Instr. 43, 1356 (1972).

6. J. D. Ellett, Jr., U. Haeberlen and J. S. Waugh, J. Amer. Chem. Soc. 92, 411 (1970).

7. M. Mehring, R. G. Griffin, and J. S. Waugh, J. Chem. Phys. 55, 746, (1971).

Table I. Relative error magnitudes in eq. (13), with respect to the undistorted signal amplitude, for representative offset frequencies (t_c = 60 μsec).

$\omega/2\pi$ (in KH_z)	ϵ_1 (in%)	$\epsilon_2 + \epsilon_3$ or $\epsilon_4 + \epsilon_5$ (in %)
25	35	38
15	13	23
5	5	4
0	0	0
- 5	5	2
-15	26	7
-25	87	37

Figure Captions

Fig. 1 The 8-pulse cycle discussed in this paper. x, y, and z indicate the rf phase in the rotating frame. τ is used to indicate the time interval between pulses, and the 8-pulse cycle time $t_c = 12\ \tau$.

Fig. 2 The magnetization vectors $\vec{M}_\alpha$ (α = 1, 2, 3, 4) as observed during the 1st 8-pulse cycle, and the effective field vectors $\vec{H}_\alpha$ around which they will stroboscopically precess.

Fig. 3 Stroboscopic views of the magnetization $\vec{M}_\alpha$ precessing around their effective fields $\vec{H}_\alpha$. Each magnetization traces an ellipse on the x-y plane. When the detector phase is set along the y-axis, the top four curves are obtained if only one window is sampled in each cycle. The last curve is the composite which is obtained if all four windows are sampled.

Fig. 4 NMR signal obtained for frozen C_6F_{12} at -60°C when the first two windows in each cycle were sampled. (A) is the signal as it was initially obtained. (B) and (C) are the two traces obtained from (A) by computer separation.

Fig. 5 Fourier transformations of various traces from Fig. 4. The top two spectra are the real parts of the transformations of traces (B) and (C) respectively. The other two spectra are the absorption and dispersion parts of the transformation of a curve obtained by multiplying (C) by $\sqrt{2}$ to normalize its amplitude, and recombining it with (B). The frequency scale is in terms of actual changes of the oscillator frequency away from resonance.

Fig. 6 F^{19} powder pattern obtained from frozen C_6F_6. The first and second $2\ \tau$ windows were sampled to form a complex input for Fourier transformation. The scale is in terms of actual changes of the oscillator frequency away from resonance (1 KH_z/division). No error corrections were applied to this spectrum.

Fig. 7 The quantities 1/B and ψ vs. resonance offset frequency for the two window sampling case, as used in eq. (9b). Note that these quantities are functions of $\omega\tau$, and that this figure uses the particular value $\tau = 5\mu$sec.

Fig. 8 The quantities 1/B and ψ vs. resonance offset frequency for the four window sampling case, as expressed in eq. (13). Note that these quantities are functions of $\omega\tau$, and that this figure uses the particular value $\tau = 5\mu$sec.

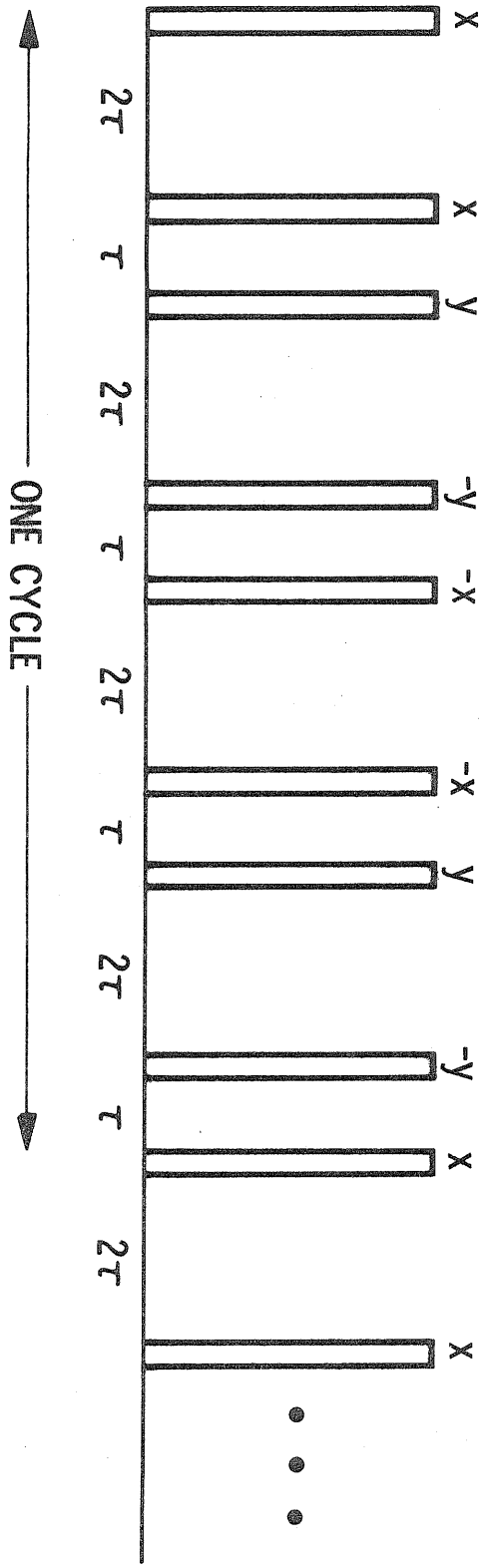

Fig. 1

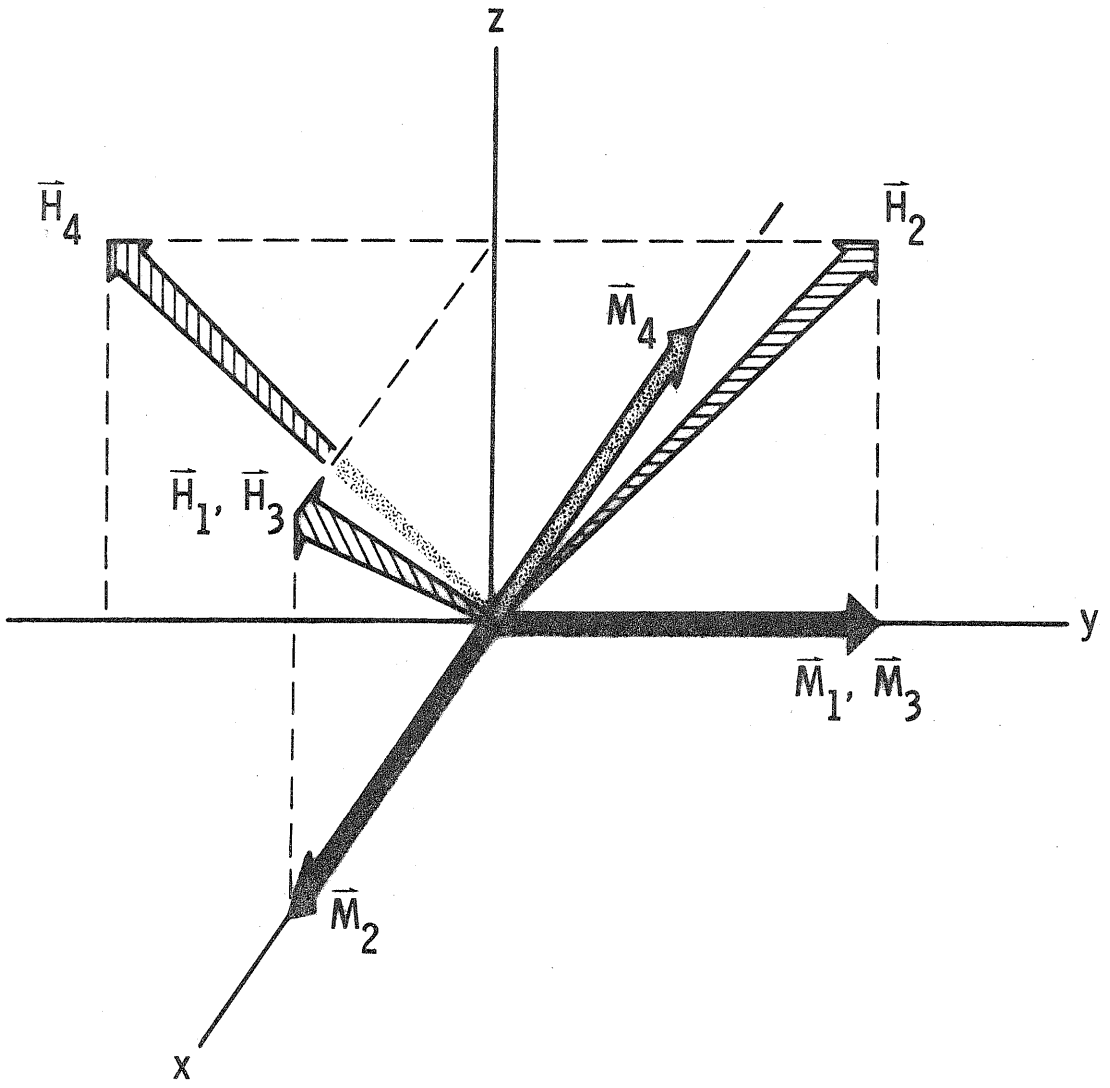

Fig. 2

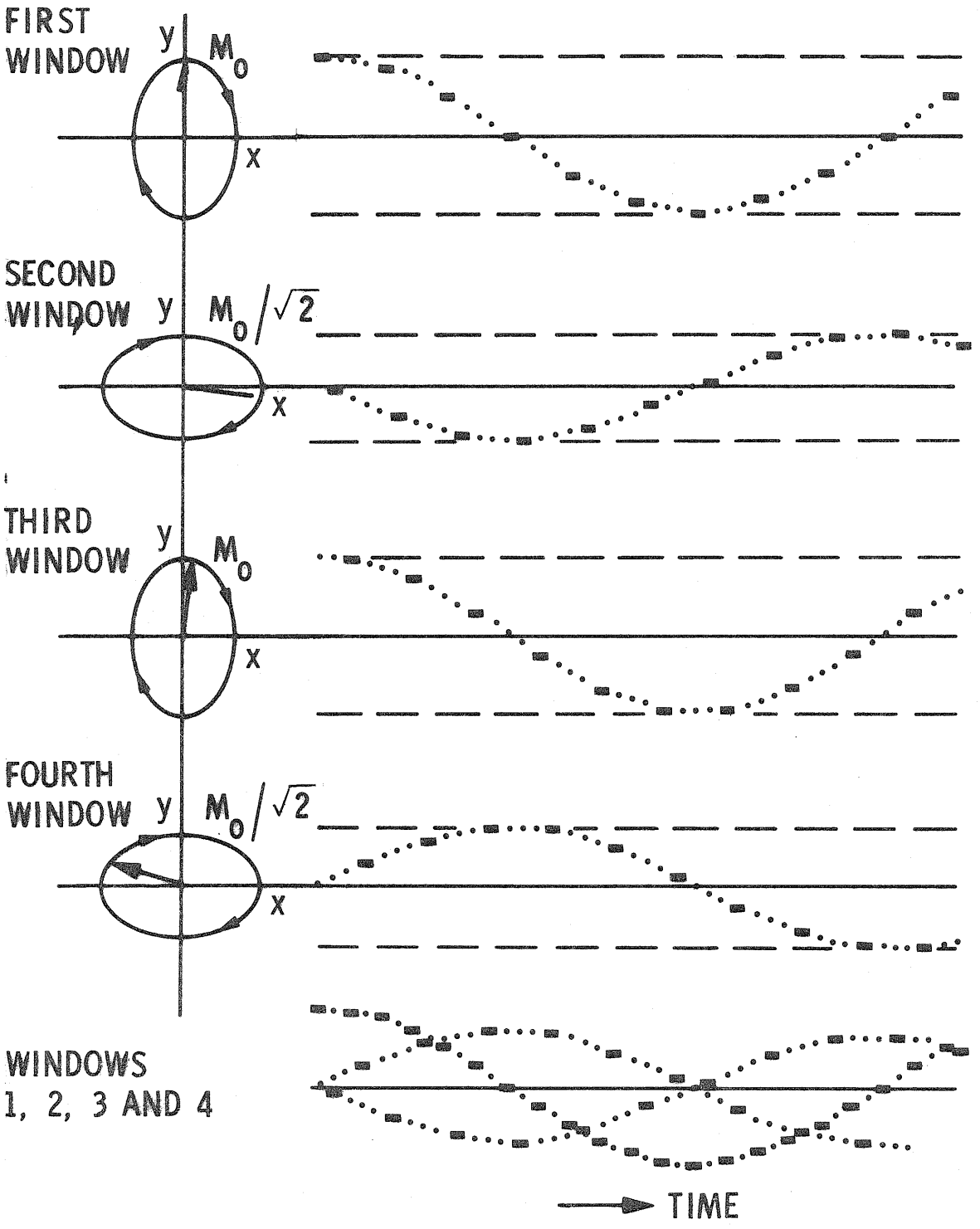
FIRST WINDOW
y
M_0
x
SECOND WINDOW
y
$M_0/\sqrt{2}$
x
THIRD WINDOW
y
M_0
x
FOURTH WINDOW
y
$M_0/\sqrt{2}$
x
WINDOWS 1, 2, 3 AND 4
TIME

Fig. 3

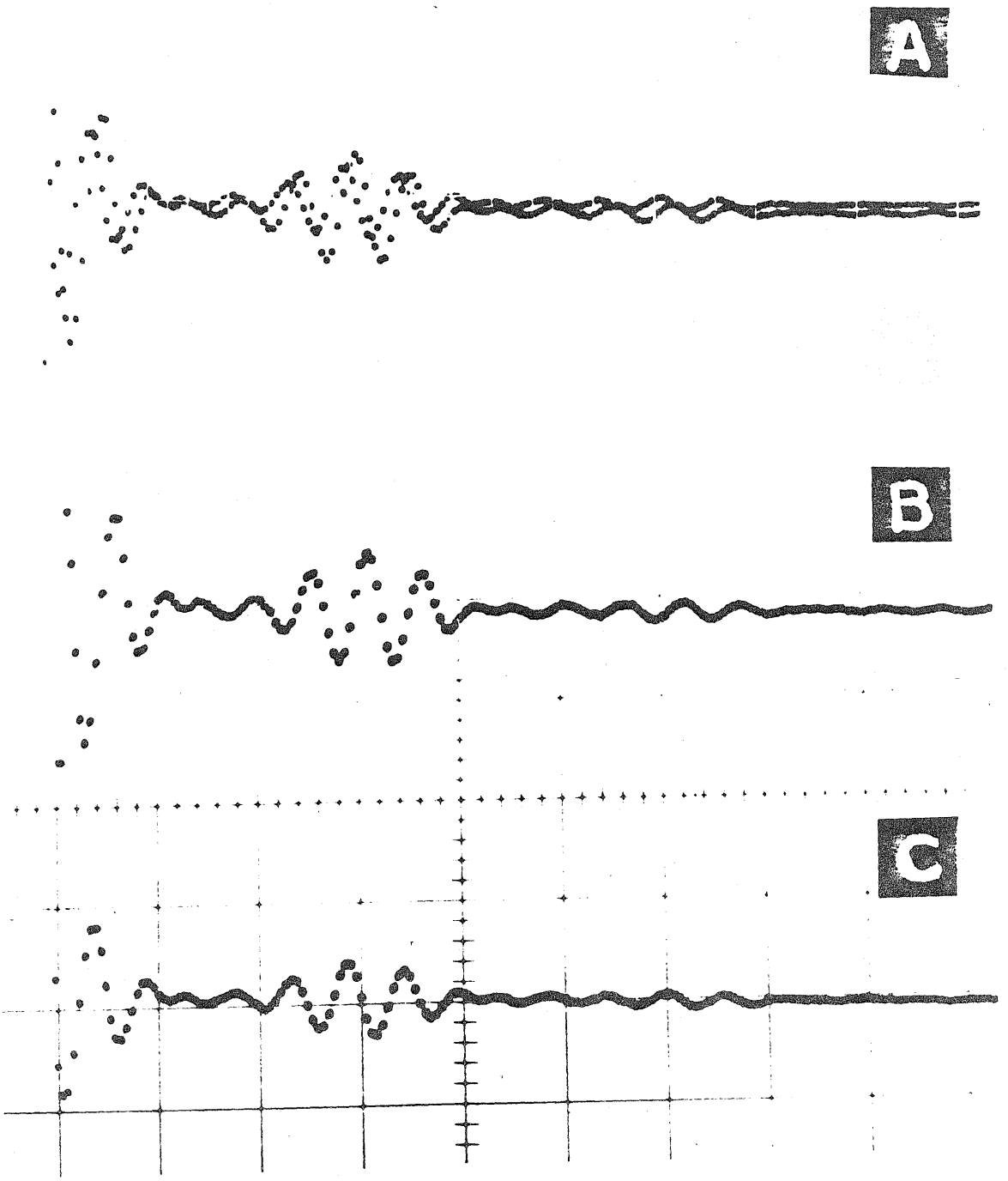

Fig. 4

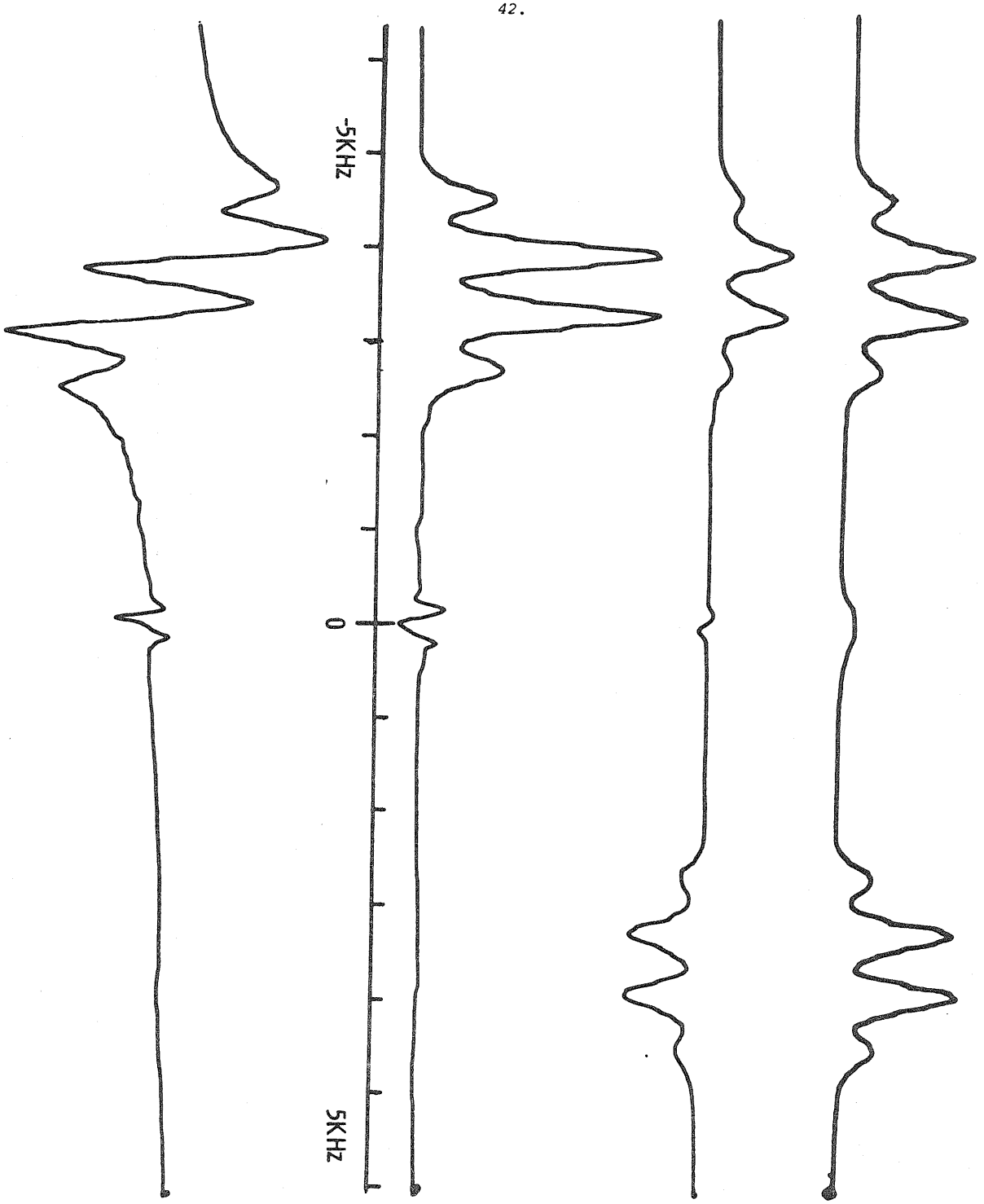

Fig. 5

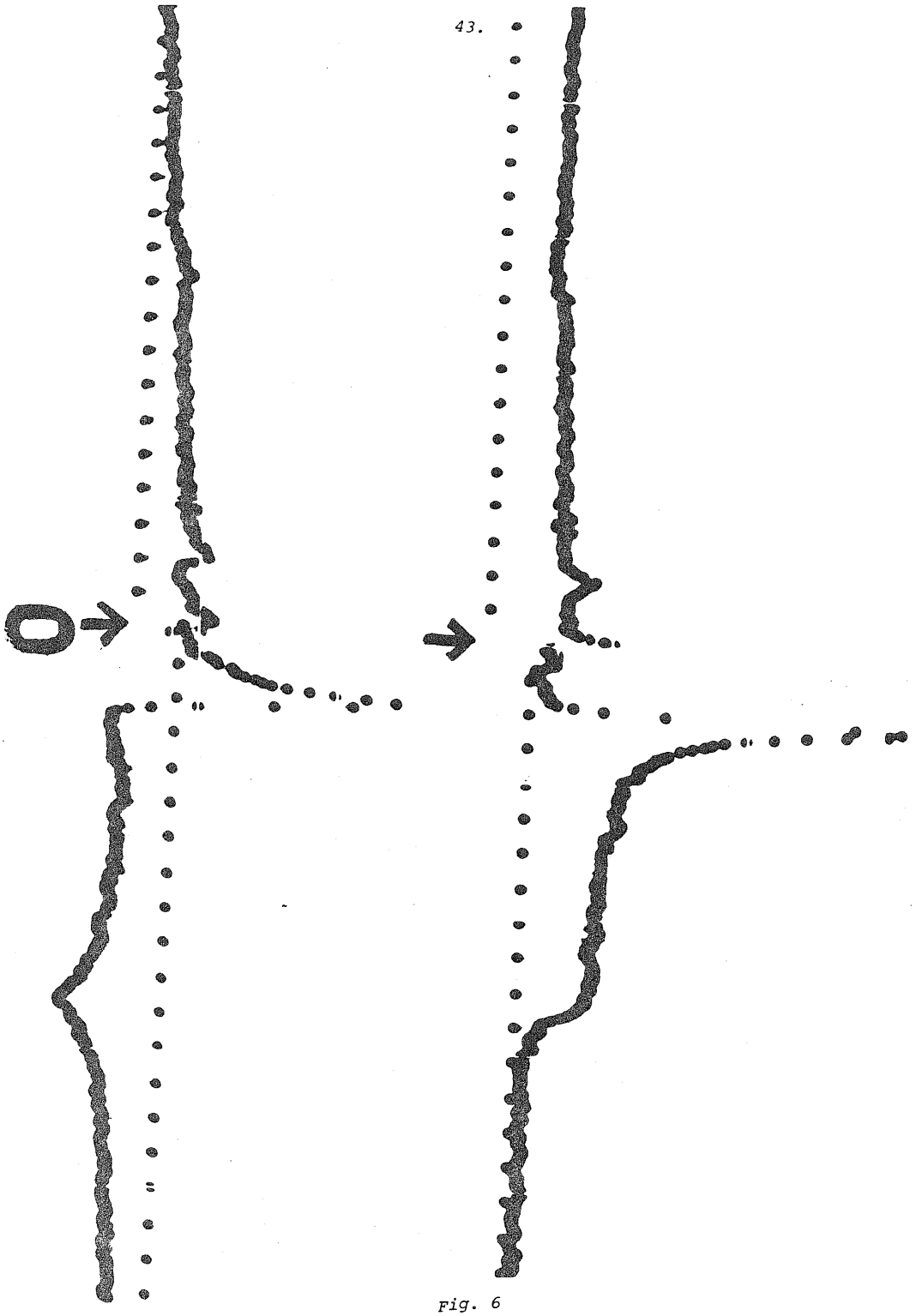

Fig. 6

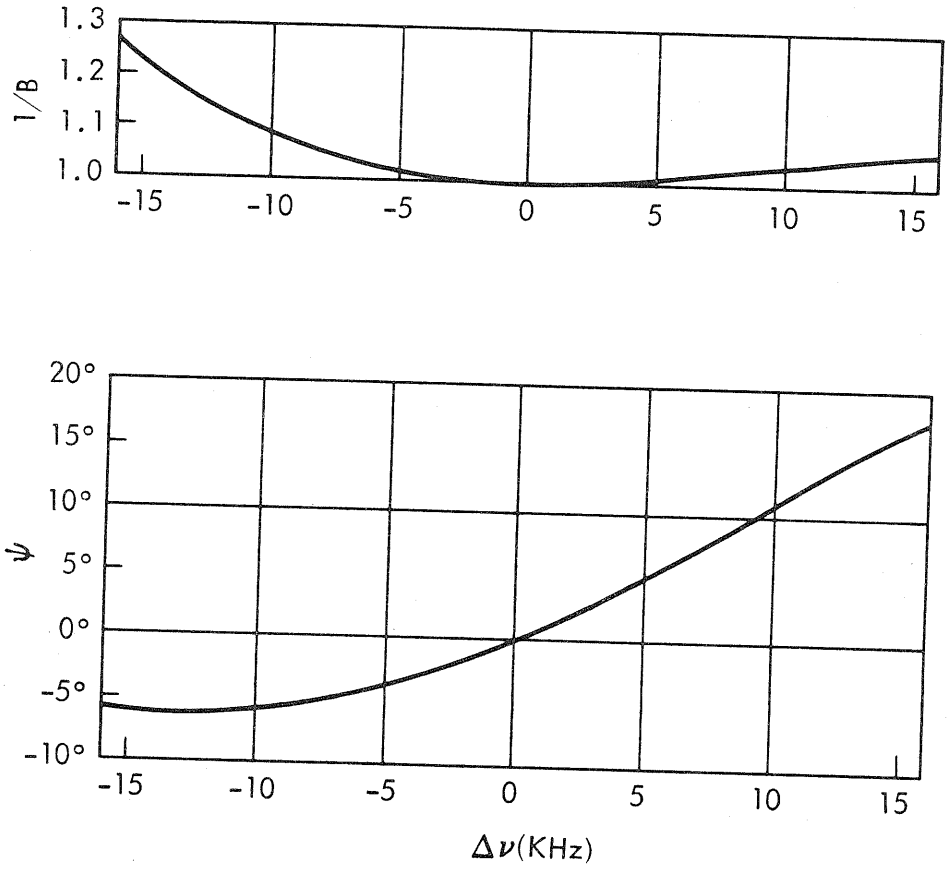

Fig. 7

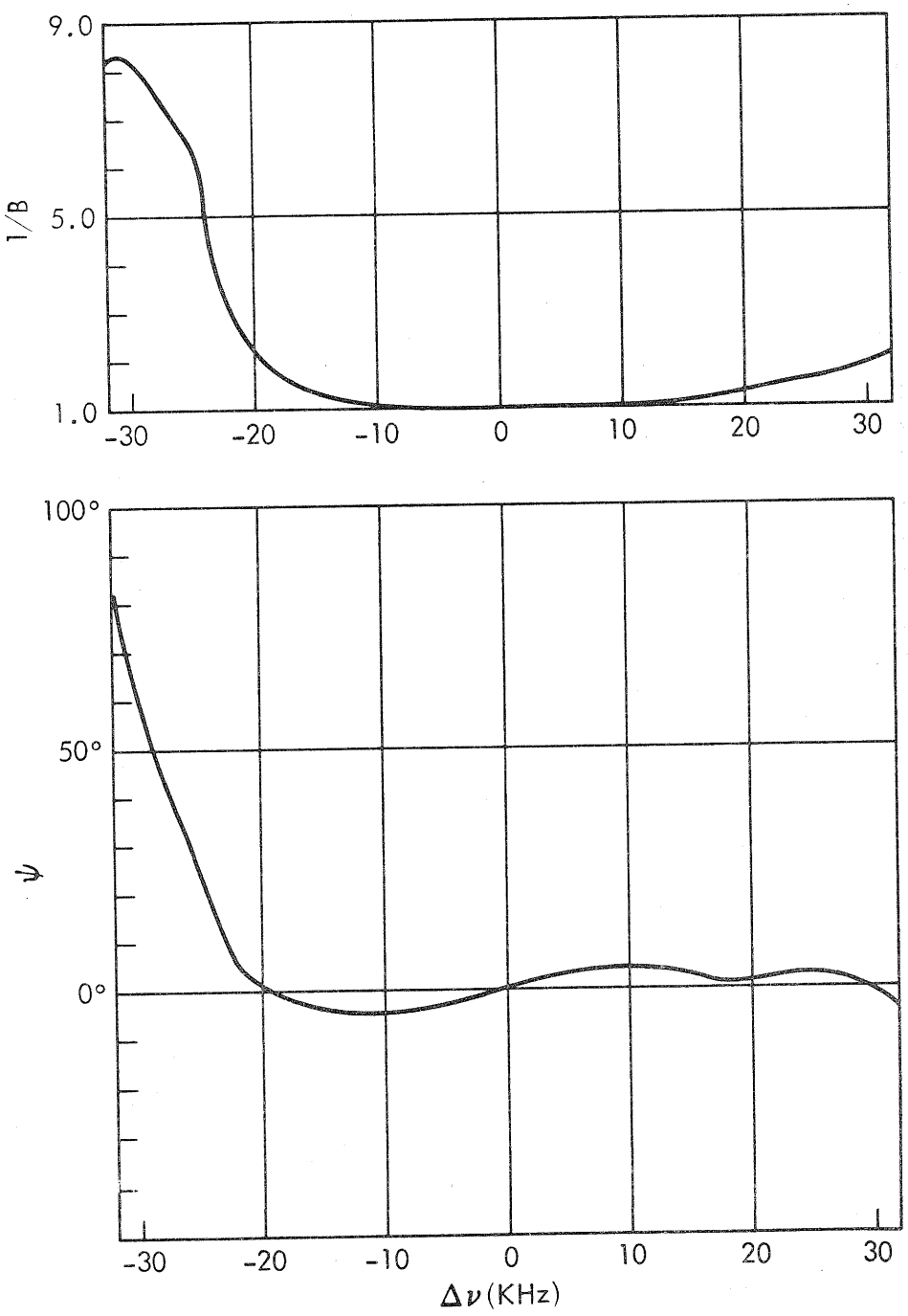

Fig. 8

Section 4

Pulse Cycle Decoupling Theory and the Design of Compound Cycles

(This section is taken from two articles by D. P. Burum and W. K. Rhim, "Analysis of Multiple Pulse NMR in Solids. III", and "An Improved NMR Technique for Homonuclear Dipolar Decoupling in Solids: Application to Polycrystalline Ice", to be published April 1, 1979 in The Journal of Chemical Physics.)

A. INTRODUCTION

In this section, principles are introduced which greatly simplify the process of designing and analyzing compound pulse cycles. These principles are demonstrated through application in the design and analysis of several cycles, including a new 52-pulse cycle which combines six different REV-8 cycles and has substantially more resolving power than previously available techniques. Also, a new 24-pulse cycle is introduced which combines three different REV-8 cycles and has a resolving ability equivalent to that of the 52-pulse cycle.

It was suggested by Haeberlen[1] that REV-8 multiple pulse cycles[2,3,4] might be combined to form compound cycles which eliminate the effects of the homonuclear dipolar interaction in solids to higher orders of magnitude. Nevertheless, there has been no real attempt to do this in practice, presumably because of uncertainty regarding how to combine different pulse cycles without reintroducing undesired Hamiltonian terms, especially those cross terms between the dipolar interaction and various pulse imperfections. Also, the need to analyze long and seemingly complicated pulse cycles appeared to pose problems. There has been an attempt by Haeberlen[1,5] to implement the suggestion of Mansfield[6] that three WAHUHA cycles be combined to form a compound cycle. However, the resulting 14-pulse cycle has shown little improvement compared to REV-8 because it does not eliminate those first order dipolar cross terms involving pulse imperfections which are removed by REV-8.

Average Hamiltonian theory is extended in this section through exploring the conditions under which a given term in the Hamiltonian expansion for a compound cycle is given by a sum of separate contributions from each of the pulse groups making up the entire cycle. Under such conditions

the cycle is said to "decouple" with regard to that Hamiltonian term, and this principle of decoupling provides a method for systematically combining pulse groups into compound cycles in order to achieve enhanced performance. This method is illustrated by a logical development from the 2-pulse solid echo sequence[7] to the WAHUHA,[8] the REV-8 and finally the new 24-pulse and 52-pulse cycles. During this development the 14-pulse cycle of Haeberlen[1,5] is discussed, and it is shown that three WAHUHA cycles can be combined in a different way to form an equivalent 12-pulse cycle. A large number of average Hamiltonian terms are calculated for the 52-pulse cycle, and an experimental analysis follows with tentative explanations of which terms are governing the performance of the cycle under various experimental conditions. The resolution of the 52-pulse cycle is compared with results obtained using REV-8. Finally, axially symmetric proton chemical shift tensor components are reported without detailed discussion for polycrystalline samples of ice, C_6H_{12}, C_5H_{10} and polyethylene, all measured near liquid N_2 temperature. Several alternate versions of the 52-pulse cycle are presented in the appendix.

B. Pulse Cycle Decoupling

One approach to the design of improved pulse cycles is to create compound cycles which combine various pulse groups with known characteristics in order to systematically eliminate undesired Hamiltonian terms to as high an order as possible. However, this is difficult in general since there is no simple way of predicting what the terms for a compound cycle formed from these sub-groups will be. Nevertheless, the process of designing a compound cycle can be greatly simplified through the principle of pulse cycle decoupling. Whenever a given Hamiltonian term in the Magnus expansion for a compound cycle is simply

an algebraic sum of separate contributions from each of the pulse groups which make up the entire compound cycle, the cycle is said to decouple with regard to that Hamiltonian term. This is clearly the case for all pulse cycles with regard to zero-order Hamiltonian terms, as can be seen from equation (16) of section 2. **In fact, zero order terms are a trivial case of pulse cycle decoupling.**

In this sub-section, conditions are presented under which a compound cycle will also decouple for higher order Hamiltonian terms. The principle of pulse cycle decoupling will be shown to provide a method for combining pulse groups in such a way that additional unwanted Hamiltonian terms are eliminated without reintroducing any of the undesired terms which vanish for each of the pulse groups considered separately. This same principle also greatly simplifies the analysis of compound cycles.

Consider a compound cycle composed of m sub-intervals, $0 \equiv \ell_0 < \ell_1 \ldots < \ell_m \equiv t_c$. It is straightforward to show by changing the limits of integration in equation (17) of section 2 that for any Hamiltonian in the toggling frame, $\tilde{\mathcal{H}}_A$, the first order term in the Magnus expansion is given by

$$\bar{\mathcal{H}}_A^{(1)} = t_c^{-1} \sum_{j=1}^{m} t_{cj} \bar{\mathcal{H}}_{Aj}^{(1)} + (2it_c)^{-1} \sum_{j=2}^{m} \sum_{k=1}^{j} t_{cj} t_{ck} \bar{\mathcal{H}}_{Aj}^{(0)} \bar{\mathcal{H}}_{Ak}^{(0)} \tag{1}$$

where $\bar{\mathcal{H}}_{Aj}^{(0)}$ and $\bar{\mathcal{H}}_{Aj}^{(1)}$ are simply $\bar{\mathcal{H}}_A^{(0)}$ and $\bar{\mathcal{H}}_A^{(1)}$ calculated for the j'th sub-interval using equations (16) and (17), of section 2,

$$\bar{\mathcal{H}}_{Aj}^{(0)} \equiv t_{cj}^{-1} \int_{\ell_{j-1}}^{\ell_j} \tilde{\mathcal{H}}_A(t_1) dt_1 \tag{2}$$

$$\bar{\mathcal{H}}_{Aj}^{(1)} \equiv (2it_c)^{-1}\int_{\ell_{j-1}}^{\ell_j} dt_2 \int_{\ell_{j-1}}^{t_2} dt_1 \,[\tilde{\mathcal{H}}_A(t_2), \tilde{\mathcal{H}}_A(t_1)] \tag{3}$$

with

$$t_{cj} \equiv \ell_j - \ell_{j-1} \tag{4}$$

From this it is clear that if $\bar{\mathcal{H}}_{Aj}^{(0)}$ vanishes for each of the sub-intervals $0 < j \leq m$ the cycle decouples for $\bar{\mathcal{H}}_A^{(1)}$, i.e.,

$$\bar{\mathcal{H}}_A^{(1)} = t_c^{-1}\sum_{j=1}^{m} t_{cj}\bar{\mathcal{H}}_{Aj}^{(1)} \tag{5}$$

In fact, even if $\bar{\mathcal{H}}_{Aj}^{(0)}$ only vanishes for each sub-interval when δ-function pulses are assumed, i.e., $\bar{\mathcal{H}}_{Aj}^{(0)}$ depends on pulse width t_w to first order, $\bar{\mathcal{H}}_{Aj}^{(0)}\bar{\mathcal{H}}_{Ak}^{(0)}$ in equation (23) will be second order in t_w. Thus $\bar{\mathcal{H}}_A^{(1)}$ will decouple to first order in t_w, i.e.,

$$\bar{\mathcal{H}}_A^{(1)} = t_c^{-1}\sum_{j=1}^{m} t_{cj}\,\bar{\mathcal{H}}_{Aj}^{(1)} + \mathcal{O}(t_w^2) \tag{6}$$

From equation (18) of section 2, it can be shown in a similar way that if $\bar{\mathcal{H}}_{Aj}^{(0)}$ vanishes for each of the sub-intervals, the cycle also decouples for $\bar{\mathcal{H}}_A^{(2)}$, i.e.,

$$\bar{\mathcal{H}}_A^{(2)} = t_c^{-1}\sum_{j=1}^{m} t_{cj}\,\bar{\mathcal{H}}_{Aj}^{(2)} \tag{7}$$

where $\bar{\mathcal{H}}^{(2)}_{Aj}$ is defined as $\bar{\mathcal{H}}^{(2)}_{A}$ calculated for a single sub-interval. **Finite pulse width effects will be neglected for Hamiltonian** terms of second or higher order. Therefore, even if $\bar{\mathcal{H}}^{(0)}_{Aj}$ only vanishes for each sub-interval under the δ-function pulse assumption equation **(7)** will still be considered valid.

Finally, if $\bar{\mathcal{H}}^{(0)}_{Aj}$ vanishes over each sub-interval then for any other Hamiltonian $\tilde{\mathcal{H}}_B$ the cycle will also decouple with regard to $\bar{\mathcal{H}}^{(1)}_{AB}$:

$$\bar{\mathcal{H}}^{(1)}_{AB} = t_c^{-1} \sum_{j=1}^{m} t_{cj} \, \bar{\mathcal{H}}^{(1)}_{ABj} \tag{8}$$

where $\bar{\mathcal{H}}^{(1)}_{ABj}$ is defined simply as $\bar{\mathcal{H}}^{(1)}_{AB}$ calculated for the j'th sub-interval. Of course if $\bar{\mathcal{H}}^{(0)}_{Aj}$ vanishes over each sub-interval only when δ-function pulses are assumed, the cycle may not decouple to first order in t_w with regard to $\bar{\mathcal{H}}^{(1)}_{AB}$, depending upon $\tilde{\mathcal{H}}_B$.

These rules can be summarized as follows: if, for some Hamiltonian $\tilde{\mathcal{H}}_A$, $\bar{\mathcal{H}}^{(0)}_{Aj}$ vanishes over each sub-interval of a compound cycle, the cycle will decouple with regard to $\bar{\mathcal{H}}^{(1)}_{A}$, $\bar{\mathcal{H}}^{(2)}_{A}$ and $\bar{\mathcal{H}}^{(1)}_{AB}$ regardless of the behavior of $\tilde{\mathcal{H}}_B$. Furthermore, if $\bar{\mathcal{H}}^{(0)}_{Aj}$ vanishes over each sub-interval only when δ-function pulses are assumed the cycle still decouples to first order in t_w with regard to $\bar{\mathcal{H}}^{(1)}_{A}$, and the cycle also decouples with regard to $\bar{\mathcal{H}}^{(2)}_{A}$ and $\bar{\mathcal{H}}^{(1)}_{AB}$ under the δ-function pulse assumption.

It is difficult to extend these results to Hamiltonian terms of arbitrary order because no general expression is available for $\bar{\mathcal{H}}^{(n)}_{A}$. However, there is a simple expression for $\bar{\mathcal{H}}^{(n)}_{A}$ for at least one special case. We make the following mathematical definition:

$$\bar{\bar{\mathcal{H}}}_A^{(n)} \equiv (-i)^n t_c^{-1} \int_0^{t_c} dt_{n+1} \int_0^{t_{n+1}} dt_n \cdots \int_0^{t_2} dt_1$$

$$\tilde{\mathcal{H}}_A(t_{n+1}) \tilde{\mathcal{H}}_A(t_n) \cdots \tilde{\mathcal{H}}_A(t_1) \tag{9}$$

Haeberlen et al. have shown[9] that if for a given cycle $\bar{\mathcal{H}}_A^{(j)} = 0$ for all $j < n$, then $\bar{\mathcal{H}}_A^{(n)} = \bar{\bar{\mathcal{H}}}_A^{(n)}$. If one assumes that this cycle is composed of two sub-groups, $0 \equiv \ell_0 < \ell_1 < \ell_2 \equiv t_c$, then by changing the limits of integration in equation (31) it is straightforward to obtain the following equation:

$$\bar{\mathcal{H}}_A^{(n)} = t_c^{-1} \left\{ t_{c1} \bar{\bar{\mathcal{H}}}_{A1}^{(n)} + t_{c2} \bar{\bar{\mathcal{H}}}_{A2}^{(n)} - i t_{c1} t_{c2} \left(\bar{\bar{\mathcal{H}}}_{A2}^{(0)} \bar{\bar{\mathcal{H}}}_{A1}^{(n-1)} + \bar{\bar{\mathcal{H}}}_{A2}^{(1)} \bar{\bar{\mathcal{H}}}_{A1}^{(n-2)} + \cdots + \bar{\bar{\mathcal{H}}}_{A2}^{(n-1)} \bar{\bar{\mathcal{H}}}_{A1}^{(0)} \right) \right\} \tag{10}$$

where

$$\bar{\bar{\mathcal{H}}}_{A1}^{(j)} \equiv (-i)^n t_c^{-1} \int_0^{\ell_1} dt_{n+1} \int_0^{t_{n+1}} dt_n \cdots \int_0^{t_2} dt_1$$

$$\tilde{\mathcal{H}}_A(t_{n+1}) \tilde{\mathcal{H}}_A(t_n) \cdots \tilde{\mathcal{H}}_A(t_1) \tag{11}$$

and a similar definition applies to $\bar{\bar{\mathcal{H}}}_{A2}^{(j)}$.

From equation (11) it is clear that there are a number of circumstances under which the cycle will decouple. Perhaps the most important case can be summarized as follows. If

$$\bar{\mathcal{H}}_A^{(j)} = 0 \quad , \qquad \forall j < n \tag{12}$$

and

$$\bar{\bar{\mathcal{H}}}_{A1}^{(j)} = \bar{\bar{\mathcal{H}}}_{A2}^{(j)} = 0 \quad , \qquad \forall j < \begin{matrix} (n/2-1) \text{ for even } n \\ (n-1)/2 \text{ for odd } n \end{matrix} \tag{13}$$

then

$$\bar{\mathcal{H}}_A^{(n)} = \bar{\bar{\mathcal{H}}}_A^{(n)} = t_c^{-1} \left\{ t_{c1} \bar{\bar{\mathcal{H}}}_{A1}^{(n)} + t_{c2} \bar{\bar{\mathcal{H}}}_{A2}^{(n)} \right\} \tag{14}$$

but it is not necessarily true that $\bar{\bar{\mathcal{H}}}_{A1}^{(n)} = \bar{\mathcal{H}}_{A1}^{(n)}$ or $\bar{\bar{\mathcal{H}}}_{A2}^{(n)} = \bar{\mathcal{H}}_{A2}^{(n)}$. It is simple to extend equation **(14)** to m sub-intervals. Equation **(13)** is replaced by

$$\bar{\mathcal{H}}_{A1}^{(j)} = \bar{\mathcal{H}}_{A2}^{(j)} = \ldots = \bar{\mathcal{H}}_{Am}^{(j)} = 0 \quad , \quad \forall j < \begin{matrix} (n/2-1) \text{ for even } n \\ (n-1)/2 \text{ for odd } n \end{matrix} \tag{15}$$

and the result is then

$$\bar{\mathcal{H}}_A^{(n)} = t_c^{-1} \sum_{j=1}^{m} t_{cj} \bar{\bar{\mathcal{H}}}_{Aj}^{(n)} \tag{16}$$

Of course, in order for the compound cycle to decouple with regard to a higher order cross term such as $\bar{\mathcal{H}}_{AB}^{(n)}$, equations **(12)**, **(15)** and **(16)** must be satisfied for $\tilde{\mathcal{H}}_A + \tilde{\mathcal{H}}_B$.

C. Reflection Symmetry

In the design of pulse cycles much use has previously been made[1,6] of the principle of reflection symmetry.[10,11] If a Hamiltonian in the toggling frame $\tilde{\mathcal{H}}_A$ has reflection symmetry, that is if

$$\tilde{\mathcal{H}}_A(t) = \tilde{\mathcal{H}}_A(t_c - t) \qquad \text{for } 0 < t < t_c \tag{17}$$

then $\bar{\mathcal{H}}_A^{(j)}$ vanishes for all odd j. Moreover, if $\tilde{\mathcal{H}}_B$ also has reflection symmetry, then $\bar{\mathcal{H}}_B^{(j)}$ and $\bar{\mathcal{H}}_{AB}^{(j)}$ also vanish for all odd j.

This principle can be useful when analyzing the properties of sub-cycles within compound cycles. However, it is more or less accidental that sub-cycles within the 52-pulse cycle discussed below

have reflection symmetry, and the improved resolution of the cycle does not arise from this symmetry. In fact, the sub-intervals within the 24-pulse cycle introduced below do not all have reflection symmetry, yet the principle of pulse cycle decoupling shows that this cycle is essentially equivalent to the 52-pulse cycle, and indeed the two cycles have been shown in practice to have comparable resolving abilities.

C. DESIGN OF COMPOUND CYCLES

Pulse cycle decoupling has obvious applications in simplifying the calculation of average Hamiltonian terms for compound cycles. Perhaps an even more important use of this concept is as an aid in the design of pulse cycles. After the introduction of some useful notation, the application of the decoupling principle to pulse cycle design will be illustrated by several examples in which **a series of compound cycles designed to remove the effects of the homonuclear dipolar interaction while preserving off resonance and chemical shift information will be developed.**

Notation

It is very helpful in designing pulse cycles to use a notation similar to that of Mansfield[6] which focuses attention on the state of the Hamiltonian in the toggling frame. Specifically, a pulse cycle is expressed according to the state of $\tilde{I}_z = U_{rf}^{-1} I_z U_{rf}$. For instance, one version of the solid echo sequence,

$$\tau - \left(\frac{\pi}{2}\right)_x - \tau - \left(\frac{\pi}{2}\right)_y - \tau \qquad (18)$$

can be written simply as

$$(I_z, -I_y, I_x) \qquad (19)$$

Only $\pi/2$ pulses of four different rf phases, $(\pi/2)_x$, $(\pi/2)_{-x}$, $(\pi/2)_y$ and $(\pi/2)_{-y}$, will be considered. Therefore, a unique pulse sequence will be determined by each series of $\tilde{I}_z$ states such as expression (19)

In order to illustrate the various features of this notation, the WAHUHA 4-pulse cycle will be considered as an example, one version of which can be written

$$\tau - \left(\frac{\pi}{2}\right)_{-x} - \tau - \left(\frac{\pi}{2}\right)_{y} - 2\tau - \left(\frac{\pi}{2}\right)_{-y} - \tau - \left(\frac{\pi}{2}\right)_{x} - \tau \qquad (20)$$

Pulse timing information is easily included in this notation. For instance the pulse cycle in expression (20) can be written either as a single pulse group,

$$(I_z, I_y, 2I_x, I_y, I_z) \qquad (21)$$

or as a combination of two solid echo pulse groups, i.e.,

$$(I_z, I_y, I_x)(I_x, I_y, I_z) \qquad (22)$$

There are usually many possible versions of a given pulse cycle. For instance, the cycle

$$\tau - \left(\frac{\pi}{2}\right)_{x} - \tau - \left(\frac{\pi}{2}\right)_{y} - 2\tau - \left(\frac{\pi}{2}\right)_{-y} - \tau - \left(\frac{\pi}{2}\right)_{-x} - \tau \qquad (23)$$

is also a version of WAHUHA, and is written in this notation as

$$(I_z, -I_y, I_x)(I_x, -I_y, I_z) \qquad (24)$$

In order to study the characteristics of a pulse cycle which do not depend on which specific version of the cycle is used, the six possible

states for $\tilde{I}_z$, which are $\pm I_x$, $\pm I_y$ and $\pm I_z$, will be written simply as A, $\bar{A}$, B, $\bar{B}$, C and $\bar{C}$, where of course $\bar{A} = -A$ etc. and A, B and C are mutually orthogonal. In this notation the WAHUHA cycle is written simply as

$$(ABC)(CBA) \tag{25}$$

where the substitution $A = I_z$, $B = I_y$, $C = I_x$ gives the version shown in expression **(20)** and $A = I_z$, $B = -I_y$, $C = I_x$ gives expression **(23)**.

Four important points should be remembered about this notation when combining pulse groups to form compound cycles:

(i) An extra pulse will be required between two pulse groups when the first state of the second pulse group is not the same as the last state of the first pulse group. For example, the two WAHUHA cycles which make up the following pulse group,

$$(ABC)(CBA)(CAB)(BAC) \tag{26}$$

cannot be joined without inserting an extra $(\pi/2)$ pulse between (CBA) and (CAB). This extra pulse does not belong to either WAHUHA cycle. Therefore the entire compound cycle is not a simple combination of two WAHUHA sub-cycles, and it may not decouple as one might otherwise expect.

(ii) A (π)-pulse will be required if two pulse groups are joined which cause a pair of adjacent states such as $A\bar{A}$. Therefore pulse cycles like the following will be avoided in this **section.**

$$(ABC)(CBA)(\bar{A}\bar{B}\bar{C})(\bar{C}\bar{B}\bar{A}) \tag{27}$$

(iii) The fact that a pulse sequence begins and ends with the same $\tilde{I}_z$ state does not guarantee that it is a cycle. For a cycle the following must be true,

$$U_{rf}(t_c) = \pm 1 \tag{28}$$

while the fact that a sequence starts and ends with the same $\tilde{I}_z$ state only shows that

$$\tilde{I}_z(t_c) = U_{rf}^{-1}(t_c) I_z U_{rf}(t_c) = I_z \tag{29}$$

This is a necessary, but not a sufficient condition for the sequence to be a cycle. For example, while

$$(ABC)(CBA) \tag{30}$$

is a cycle,

$$(ABC)(\bar{C}\bar{B}A) \tag{31}$$

is not a cycle.

One can be sure, however, that if two cycles are joined side by side or one complete cycle is inserted somewhere inside another one, the resulting sequence is a cycle. Also, any pulse sequence such as (ABC) (CBA) which has reflection symmetry is a cycle.

(iv) The arrangement of the pulse groups within a compound cycle can be important even when the cycle decouples if the Hamiltonian term being considered depends on $\tilde{I}_x$, $\tilde{I}_y$ or on the specific rf pulses used to generate the cycle. For example, assume that the following compound cycle decouples with regard to both $\bar{\mathscr{H}}_D^{(1)}$ and $\bar{\mathscr{H}}_{\varepsilon D}^{(1)}$:

$$(ABC)(CAB)(BAC)(CBA) \tag{32}$$

$\tilde{\mathscr{H}}_D$ depends only on $\tilde{I}_z$ but $\tilde{\mathscr{H}}_\varepsilon$ also depends on the state of $\tilde{I}_x$ and $\tilde{I}_y$ and on the specific pulses used to generate the cycle. Therefore, if the sub-groups in expression **(32)** are rearranged to form a different cycle, such as

$$(CAB)(BAC)(CBA)(ABC) \tag{33}$$

$\bar{\mathscr{H}}_D^{(1)}$ will be unaffected, but $\bar{\mathscr{H}}_{\varepsilon D}^{(1)}$ may be different for the two cases.

One important advantage of the notation introduced **here** is that it makes the chemical shift scaling factor for any cycle immediately available, assuming δ-function pulses. Consider for example the WAHUHA cycle given in expression **(20)**. Since $\tilde{\mathscr{H}}_0 = \sum_i (\Delta\omega + \omega_0\sigma_{zzi})\tilde{I}_{zi}$ it is apparent from the $\tilde{I}_z$ states shown in expression (22) that the integral of $\tilde{\mathscr{H}}_0$ over a cycle is $2\tau(I_x + I_y + I_z)$, and that the cycle time is 6τ. **Thus it can be seen from equation (16) of section 2 that**

$$\bar{\mathscr{H}}_0^{(0)} = \frac{1}{3}\sum_i (\Delta\omega + \omega_0\sigma_{zzi})(I_{xi} + I_{yi} + I_{zi}) \tag{34}$$

Since the chemical shift scaling factor is given by $||\mathscr{H}_0||/||\bar{\mathscr{H}}_0^{(0)}||$, one **finds by computing the length of the vector in equation (34) that the** scaling factor in this case is $\sqrt{3}$. The same result could have been obtained just as easily from expression **(25)**. The feature of making the scaling factor readily available is an important advantage of this notation when designing a pulse cycle for measuring chemical shifts.

The Solid Echo Pulse Group

The solid echo pulse sequence is a basic building block. For this sequence, assuming δ-function pulses, $\bar{\mathcal{H}}_D^{(0)} = \mathcal{H}_D^{(x)} + \mathcal{H}_D^{(y)} + \mathcal{H}_D^{(z)} = 0$, where $\mathcal{H}_D^{(x)}$ and $\mathcal{H}_D^{(y)}$ are obtained by substituting I_x or I_y for I_z in equation (37) of section 2. Therefore it is clear from the principle of pulse cycle decoupling that any compound cycle composed of solid echo sequences will decouple assuming δ-function pulses with regard to $\bar{\mathcal{H}}_D^{(1)}$, $\bar{\mathcal{H}}_D^{(2)}$ and all first order dipolar cross terms such as $\bar{\mathcal{H}}_{DO}^{(1)}$, $\bar{\mathcal{H}}_{\delta D}^{(1)}$ etc. In fact, the cycle will decouple with regard to $\bar{\mathcal{H}}_D^{(0)}$ when finite pulse widths are considered, and with regard to $\bar{\mathcal{H}}_D^{(1)}$ when calculated to first order in t_w. Since these terms will be simple algebraic sums of the contributions from the individual solid echo pulse groups, the objective is to form a compound cycle by combining different versions of the solid echo pulse sequence in such a way that the algebraic sums vanish.

It is convenient at this point to define two types of "compensated" sets of pulse groups. Assume that a compound cycle is being designed which will decouple with regard to some Hamiltonian term $\bar{\mathcal{H}}_A^{(n)}$. Then a set of pulse groups is a compensated set of the first kind with regard to $\bar{\mathcal{H}}_A^{(n)}$ if it will make no net contribution to $\bar{\mathcal{H}}_A^{(n)}$ as long as each member of the set is included somewhere in the compound cycle. Compensated sets of the first kind are usually associated with Hamiltonian terms such as $\bar{\mathcal{H}}_D^{(1)}$, $\bar{\mathcal{H}}_{DO}^{(1)}$ etc. which depend only on the states of $\tilde{I}_z$. Terms such as $\bar{\mathcal{H}}_{\varepsilon D}^{(1)}$, $\bar{\mathcal{H}}_{\delta D}^{(1)}$, etc. which also depend on $\tilde{I}_x$, $\tilde{I}_y$ or on the specific rf pulses are often associated with compensated sets of the second kind. These are sets of pulse groups which must be included in the compound cycle in a specific order, and the members of the set must be either adjacent to each other or separated by complete subcycles.

There are only two ways in which the members of a compensated set of the second kind may be rearranged:

(i) The members of the set may be cyclically permuted, e.g. if {(ABC)(CAB)(BCA)} is a compensated set of the second kind then so are {(CAB)(BCA)(ABC)} and {(BCA)(ABC)(CAB)},

(ii) Adjacent cycles within the set may be interchanged. For example, {(ABC)(CBA)($A\bar{B}C$)($C\bar{B}A$)(ACB)} can be rearranged to form {($A\bar{B}C$)($C\bar{B}A$)(ABC)(CBA)(ACB)}.

Table 1 summarizes the sets of solid echo pulse groups which are compensated sets of the first kind with regard to $\bar{\mathscr{H}}_D^{(0)}$, $\bar{\mathscr{H}}_D^{(1)}$, $\bar{\mathscr{H}}_{DO}^{(1)}$, and $\bar{\mathscr{H}}_D^{(2)}$. The generalized notation used in the table is a straightforward extension of the notation introduced earlier for representing pulse sequences. Recall that A, B and C represent states of $\tilde{I}_z$, that $\bar{A} = -A$ etc. and that A, B and C are mutually orthogonal. Since $\tilde{\mathscr{H}}_D^{(z)}$ is readily determined from $\tilde{I}_z$ by substitution in equation (3) of section 2, i.e.,

$$\tilde{\mathscr{H}}_D^{(z)} = \sum_{i<j} \beta_{ij}(\vec{I}_i \cdot \vec{I}_j - 3I_{zi}I_{zj}) \tag{35}$$

it can be written in a generalized form according to $\tilde{I}_z$. For example, if $\tilde{I}_z = A$, $\tilde{\mathscr{H}}_D^{(z)} = \mathscr{H}_D^{(a)}$ where $\mathscr{H}_D^{(a)}$ is given by

$$\mathscr{H}_D^{(a)} = \sum_{i<j} \beta_{ij}(\vec{I}_i \cdot \vec{I}_j - 3A_iA_j) \tag{36}$$

Of course, $\tilde{\mathscr{H}}_D^{(z)}$ is not affected by the sign of $\tilde{I}_z$, i.e., if $\tilde{I}_z = \bar{A}$, $\tilde{\mathscr{H}}_D^{(z)} = \mathscr{H}_D^{(a)}$. Thus, for the pulse group ($A\bar{B}C$) $\tilde{\mathscr{H}}_D^{(z)}$ is given by the following series of states:

$$\tilde{\mathcal{H}}_D^{(z)} = \mathcal{H}_D^{(a)} \qquad 0 < t < \tau$$

$$\tilde{\mathcal{H}}_D^{(z)} = \mathcal{H}_D^{(b)} \qquad \tau < t < 2\tau$$

$$\tilde{\mathcal{H}}_D^{(z)} = \mathcal{H}_D^{(c)} \qquad 2\tau < t < 3\tau \tag{37}$$

The compensated sets in Table 1 were determined in a very straightforward manner. First, a general result for each Hamiltonian term was calculated using the above notation. This insured that the result for any specific solid echo group could be obtained simply by substituting the proper $\tilde{I}_z$ and $\tilde{\mathcal{H}}_D^{(z)}$ states into the general result. Then, from these general results it was determined which combinations of solid echo groups would form compensated sets. Usually this could be done by inspection, but if necessary the results for all possible solid echo groups could be readily tabulated by substitution into the general results and then compared to determine the compensated sets. For $\bar{\mathcal{H}}_D^{(1)}$, $\bar{\mathcal{H}}_{DO}^{(1)}$ and $\mathcal{H}_D^{(2)}$ the compensated sets were determined assuming δ-function pulses. Notice however that {(ABC), (CBA)} is a compensated set for $\bar{\mathcal{H}}_D^{(1)}$ if it is calculated to first order in t_w.

In order to illustrate the procedure followed in generating Table 1, the term $\bar{\mathcal{H}}_D^{(1)}$ will be considered as an example. If the formula for a first order term given in equation (17) of section 2 is applied to the solid echo group (ABC), the following result is obtained assuming δ-function pulses:

$$\bar{\mathcal{H}}_D^{(1)} = -\left(\frac{i\tau}{6}\right)\left\{\left[\mathcal{H}_D^{(b)}, \mathcal{H}_D^{(a)}\right] + \left[\mathcal{H}_D^{(c)}, \mathcal{H}_D^{(a)} + \mathcal{H}_D^{(b)}\right]\right\} \tag{38}$$

Recalling that

$$\mathcal{H}_D^{(a)} + \mathcal{H}_D^{(b)} + \mathcal{H}_D^{(c)} = 0 \tag{39}$$

it is clear that the last term in equation (38) vanishes, giving the general result shown in the table:

$$\bar{\mathcal{H}}_D^{(1)} = -\left(\frac{i\tau}{6}\right)\left[\mathcal{H}_D^{(b)}, \mathcal{H}_D^{(a)}\right] \tag{40}$$

It is clear from this formula that the sign of $\tilde{I}_z$ will not affect $\bar{\mathcal{H}}_D^{(1)}$. Thus equation (40) also applies to $(A\bar{B}C)$, $(\bar{A}B\bar{C})$, etc. **The goal now is to find solid echo groups for which the sign of $\bar{\mathcal{H}}_D^{(1)}$ will be reversed.** One possibility is to switch the order of A and B, i.e., (BAC). Also, because of equation (39) the desired result can be obtained by switching either A and C or B and C, i.e., (CBA) and (ACB). Thus three simple compensated sets for $\bar{\mathcal{H}}_D^{(1)}$ are {(ABC), (BAC)}, {(ABC), (CBA)} and {(ABC), (ACB)}. The other results in Table 1 were obtained in a similar manner.

WAHUHA AND REV-8

It is clear from Table 1 that {(ABC), (CBA)} is a compensated set of the first kind with regard to both $\bar{\mathcal{H}}_D^{(1)}$ calculated to first order in t_w and also $\bar{\mathcal{H}}_{DO}^{(1)}$ calculated assuming δ-function pulses. In fact, **the expression (ABC)(CBA) by itself represents the 4-pulse WAHUHA cycle.**[8]

In order to eliminate $\bar{\mathcal{H}}_D^{(0)}$ for finite pulse widths a compound cycle can be constructed by combining the four solid echo groups (ABC), (CBA), $(A\bar{B}C)$ and $(C\bar{B}A)$. **Notice from Table 1 that both {(ABC), (CBA)} and {$(A\bar{B}C)$, $(C\bar{B}A)$}** are compensated sets of the first kind with regard to $\bar{\mathcal{H}}_D^{(1)}$ and $\bar{\mathcal{H}}_{DO}^{(1)}$, while {(ABC), $(C\bar{B}A)$} and {$(A\bar{B}C)(CBA)$} are compensated sets for $\bar{\mathcal{H}}_D^{(0)}$ calculated for finite pulse widths. Thus $\bar{\mathcal{H}}_D^{(0)}$ for finite pulse widths, $\bar{\mathcal{H}}_D^{(1)}$ calculated to first order in t_w

and $\bar{\mathcal{H}}_{DO}^{(1)}$ for δ-function pulses will all vanish for any compound cycle composed of these four pulse groups. There are two ways to combine these pulse groups so that extra pulses between the solid echo groups are not required, namely

$$(ABC)(CBA)(\bar{A}\bar{B}\bar{C})(\bar{C}\bar{B}\bar{A}) \tag{41}$$

and

$$(ABC)(\bar{C}\bar{B}\bar{A})(\bar{A}\bar{B}\bar{C})(CBA) \tag{42}$$

These expressions represent the two basic forms of the REV-8 cycle[2-4]. An important property which is not obvious from Table 1 but which has been demonstrated previously is that both expressions **(41)** and **(42)** are compensated sets of the second kind with regard to all first order cross terms between $\tilde{\mathcal{H}}_D$ and the various pulse imperfection Hamiltonians calculated assuming δ-function pulses. This means that all cross terms such as $\bar{\mathcal{H}}_{\delta D}^{(1)}$, $\bar{\mathcal{H}}_{\varepsilon D}^{(1)}$, etc., vanish for REV-8. Expressions **(41)** and **(42)** are actually the same compensated set. This can be seen by making a cyclic permutation on **(41)** to obtain

$$(CBA)(\bar{A}\bar{B}\bar{C})(\bar{C}\bar{B}\bar{A})(ABC) \tag{43}$$

and then making the substitution A' = C, B' = B, C' = A to obtain expression **(42)**.

An interesting comparison can be made at this point between the usefulness of pulse cycle decoupling and of reflection symmetry in the design of pulse cycles. Since the REV-8 cycles described by expressions **(41)** and **(42)** both decouple with regard to $\bar{\mathcal{H}}_{DO}^{(1)}$ assuming δ-function pulses, it is apparent from Table 1 that this term vanishes for both forms of REV-8. However $\tilde{I}_z$, and therefore $\tilde{\mathcal{H}}_0$, does not have

reflection symmetry in expression (41). Thus the principle of reflection symmetry cannot predict that $\bar{\mathcal{H}}_{DO}^{(1)}$ vanishes for expression (41), and on this basis one might be misled regarding the effect of $\bar{\mathcal{H}}_{DO}^{(1)}$ on the performance of the two cycles.

The 14-Pulse and 12-Pulse Cycles

Clearly, the next step is to design a compound cycle which removes $\bar{\mathcal{H}}_{D}^{(2)}$. Pulse cycles have been suggested previously by Evans[12], Haeberlen and Waugh[9], and Mansfield[6] which eliminate $\bar{\mathcal{H}}_{D}^{(2)}$ as well as $\bar{\mathcal{H}}_{D}^{(0)}$, $\bar{\mathcal{H}}_{D}^{(1)}$ and $\bar{\mathcal{H}}_{DO}^{(1)}$. However, none of these cycles show substantial improvement over the WAHUHA sequence because none of them remove the first order dipolar cross terms which are eliminated by REV-8. For example, the "72 τ complementary doubly symmetrized" cycle proposed by Mansfield[6] bears some resemblance to the new 52-pulse cycle discussed below. However, it requires eighty $\pi/2$ pulses and makes no attempt to remove the dipolar cross terms involving such pulse imperfections as pulse length and phase misadjustments and phase transients. More recently Haeberlen[1,5] has used a 14-pulse cycle which generates a series of $\tilde{I}_z$ states originally suggested by Mansfield[6]:

$$(ABC)(CBA)(BAC)(CAB)(ACB)(BCA) \qquad (44)$$

Since this cycle combines three WAHUHA cycles it is clear from the principle of decoupling that $\bar{\mathcal{H}}_{D}^{(0)} = \bar{\mathcal{H}}_{DO}^{(1)} = 0$ assuming δ-function pulses, and $\bar{\mathcal{H}}_{D}^{(1)}$ vanishes when computed to first order in t_w. Furthermore, expression (44) satisfies the requirement given in Table 1 for $\bar{\mathcal{H}}_{D}^{(2)}$ to vanish, namely that it be composed of equal numbers of solid echo groups with A, B and C as the middle state. In order to generate

expression (44) two extra pulses surrounding the center two solid echo groups are required, making a total of 14 pulses.

Because the cycle described by expression (44) decouples, the solid echo groups in the cycle can be rearranged so that extra pulses are not needed:

$$(ABC)(CBA)(ACB)(BAC)(CAB)(BCA) \tag{45}$$

Since $\bar{\mathcal{H}}_D^{(0)}$, $\bar{\mathcal{H}}_D^{(1)}$, $\bar{\mathcal{H}}_{DO}^{(1)}$ and $\bar{\mathcal{H}}_D^{(2)}$ also vanish for this 12-pulse cycle, it can be expected to have a resolving power equivalent to the 14-pulse cycle.

Experimentally, the 14-pulse and 12-pulses cycles have been found to be equivalent to each other, but in most cases their resolving ability is less than for REV-8. Clearly this is because the 12-pulse and 14-pulse cycles do not remove those dipolar cross terms such as $\bar{\mathcal{H}}_{\delta D}^{(1)}$ and $\bar{\mathcal{H}}_{\varepsilon D}^{(1)}$ which are eliminated by REV-8.

The 24-Pulse and 52-Pulse Cycles

The principle of pulse cycle decoupling assures us that we may combine different versions of REV-8 in order to eliminate $\bar{\mathcal{H}}_D^{(2)}$ without reintroducing any of the dipolar terms which vanish for REV-8, including dipolar cross terms such as $\bar{\mathcal{H}}_{TD}^{(1)}$, $\bar{\mathcal{H}}_{PD}^{(1)}$ etc. Following the example of the 14-pulse cycle , **consider the following series of $\tilde{I}_z$ states:**

$$[ABC][A\bar{B}C][BAC][B\bar{A}C][ACB][A\bar{C}B] \tag{46}$$

where the square brackets indicate reflection symmetry, e.g., [ABC] = (ABC)(CBA).

Expression (46) represents three different versions of REV-8 combined in such a way that $\bar{\mathcal{H}}_D^{(2)}$ vanishes for the cycle as a whole, and this is what is desired. However, in order to generate the pulse groups in the order shown in expression (46) it is necessary to insert two extra $\pi/2$ pulses surrounding the center REV-8 cycle. Since these extra pulses are not part of the REV-8 cycles the possibility arises that dipolar terms which vanish for REV-8 may not vanish for this cycle.

One way to solve this problem is to rearrange the solid echo groups in expression (46) so that extra pulses are no longer needed. One must be more careful than in the case of the 14-pulse cycle because the REV-8 cycles are compensated sets of the second kind. Nevertheless, by inserting one entire REV-8 cycle inside another one the compensated properties of the REV-8 cycles are preserved and the following 24-pulse cycle is produced:

$$[ABC][A\bar{B}C][ACB](A\bar{C}B)[BAC][B\bar{A}C](B\bar{C}A) \qquad (47)$$

This cycle was discovered only recently and will be analyzed in detail in a later paper. However, our initial measurements indicate that the resolving ability of this 24-pulse cycle is equivalent to that of the 52-pulse cycle which is analyzed in this section. Of course, many other versions of this 24-pulse cycle are possible, the main criteria being:

(i) Three REV-8 cycles are combined in accordance with the rules for compensated sets of the second kind, and

(ii) The resulting compound cycle contains equal numbers of solid echo groups with A, B and C as the middle state.

There is another way in which one can use the principle of pulse cycle decoupling in order to correct for the effects of the two extra pulses required by expression (46), namely we can combine different versions of this cycle in order to eliminate the undesired Hamiltonian terms created by the extra pulses. Fortunately, all of the first order dipolar terms which vanish for REV-8 also vanish for the pulse cycle described by expression (46). However, $\bar{\mathcal{H}}_D^{(0)}$ no longer vanishes if finite pulse widths are considered. For example if $A = I_z$, $B = -I_y$ and $C = I_x$, one obtains

$$\bar{\mathcal{H}}_D^{(0)} = t_w(18\pi i\tau)^{-1}\,[I_x, \mathcal{H}_D^{(z)}] \tag{48}$$

Since $\bar{\mathcal{H}}_D^{(0)}$ would vanish if the extra pulses were not needed to generate expression (46), it is natural to explore the behavior of $\bar{\mathcal{H}}_D^{(0)}$ as a function of the rf phases of the extra pulses. If the rf phases of these two pulses are reversed, with all other pulses remaining unchanged, expression (46) becomes

$$[ABC][A\bar{B}C][\bar{B}\bar{A}C][\bar{B}AC][ACB][A\bar{C}B] \tag{49}$$

and $\bar{\mathcal{H}}_D^{(0)}$ for this expression is just the negative of $\bar{\mathcal{H}}_D^{(0)}$ in equation (48). Thus expressions (46) and (49) can be combined to form a compound cycle for which $\bar{\mathcal{H}}_D^{(0)} = 0$:

$$[ABC][A\bar{B}C][BAC][B\bar{A}C][ACB][A\bar{C}B][ABC][A\bar{B}C][\bar{B}\bar{A}C][\bar{B}AC][ACB][A\bar{C}B] \tag{50}$$

This is one version of the 52-pulse cycle.

There are many other combinations of twelve 4-pulse groups which are just as readily produced and can be expected to show similar capabilities for homonuclear dipolar decoupling. The main criteria for constructing these cycles can be summarized as follows:

(i) The compound cycle is formed by rearranging the 4-pulse groups within six REV-8 cycles according to the rules discussed above for compensated sets of the second kind.

(ii) Equal numbers of solid echo groups with A, B and C as the middle state, disregarding bars over the states, are contained in the compound cycle.

(iii) Four extra pulses are inserted between pulse groups in such a way that the third and fourth extra pulses are reversed in phase relative to the first and second pulses.

In practice, 52-pulse cycles which satisfy these three criteria can differ somewhat in performance due to their properties with regard to "second averaging"[13] of non-vanishing Hamiltonian terms. This effect is discussed in the next section. The version of the 52-pulse cycle which has the most favorable characteristics of those tried so far can be expressed as follows:

$$[ABC][ACB][B\bar{A}C][BAC][A\bar{C}B][A\bar{B}C][ABC][ACB][\bar{B}AC][\bar{B}\bar{A}C][A\bar{C}B][A\bar{B}C] \qquad (51)$$

Notice that $\bar{\mathscr{H}}_D^{(0)}$, $\bar{\mathscr{H}}_D^{(1)}$, $\bar{\mathscr{H}}_{DO}^{(1)}$ and $\bar{\mathscr{H}}_D^{(2)}$ all vanish (for δ-function pulses) over each quarter of this cycle. Also, expression (51) has reflection symmetry for $\tilde{\mathscr{H}}_D^{(z)}$. Therefore, the principle of reflection symmetry tells one that $\bar{\mathscr{H}}_D^{(3)} = 0$ for the cycle as a whole.

D. SPECIFIC rf PULSE CYCLES

The pulse cycles discussed in the previous sub-section were expressed in a general notation which emphasizes the states of $\tilde{I}_z$. This sub-section presents specific versions of these cycles expressed in terms of rf pulses. All of the cycles are constructed using solid echo pulse groups such as

$$\tau - \left(\frac{\pi}{2}\right)_x - \tau - \left(\frac{\pi}{2}\right)_{-y} - \tau \qquad (52)$$

For simplicity, solid echo groups will be expressed according to the rf phases of the two pulses. For instance, the solid echo sequence in expression (52) will be written simply $(X\bar{Y})$. Four versions of WAHUHA, which will be called 1a, 1b, 2a and 2b, can be expressed as follows:

$$\begin{aligned} 1a &= (XY)(\bar{Y}\bar{X}) \\ 1b &= (\bar{X}Y)(\bar{Y}X) \\ 2a &= (YX)(\bar{X}\bar{Y}) \\ 2b &= (\bar{Y}X)(\bar{X}Y) \end{aligned} \qquad (53)$$

Of course, 1a1b = 1 and 2a2b = 2 form two versions of REV-8.

Using this notation, one version of the 14-pulse cycle discussed in the previous section can be written

$$1a\left(\frac{\pi}{2}\right)_x 1a\left(\frac{\pi}{2}\right)_{-x} 2a \qquad (54)$$

and the corresponding 12-pulse cycle is written

$$1a(YX)\ 2a(\bar{X}\bar{Y}) \qquad (55)$$

These cycles produce the series of $\tilde{I}_z$ states given in expressions (44) and (45) if the substitution is made $A = I_z$, $B = -I_y$ and $C = I_x$. For this same substitution, the following pulse cycle produces the series of $\tilde{I}_z$ states given in expression (47):

$$*1a*1b*2a*(\bar{Y}X)\ 2a2b(\bar{X}Y) \tag{56}$$

This is a 24-pulse cycle with a cycle time of 36 τ. The signal may be sampled in each of the windows indicated by a * without distorting the results unless the spectrum contains frequency components comparable to or greater than $(12\ \tau)^{-1}$.

The 52-pulse cycle which is analyzed in the next section can be written

$$*1a*2a\left(\frac{\pi}{2}\right)_x 1a1b\left(\frac{\pi}{2}\right)_{-x} 2b*1b*1a*2a\left(\frac{\pi}{2}\right)_{-x} 1a1b\left(\frac{\pi}{2}\right)_x 1b*2b \tag{57}$$

This cycle contains 12 of the 4-pulse groups defined in equation (53) along with 4 extra $\pi/2$ pulses, and it produces the series of $\tilde{I}_z$ states given in expression (51) if the substitution $A = I_z$, $B = -I_y$ and $C = I_x$ is made. The cycle may be sampled in each of the windows indicated by a * in expression (55).

It should be possible to obtain quadrature phase information from the 24-pulse and 52-pulse cycles by sampling in other windows, as was demonstrated in section 3 for the REV-8 cycle.

E. ANALYSIS OF THE 52-PULSE CYCLE

Hamiltonian Terms

Table 2 lists terms in the Magnus expansion for the 52-pulse cycle given in expression (55). First order terms which vanished when δ-function pulses were assumed were recalculated by including the effects of finite pulse widths to first order in t_w except for $\bar{\mathscr{H}}^{(1)}_{PD}$ and $\bar{\mathscr{H}}^{(1)}_{TD}$. Cross terms between pulse errors were assumed to have no effect and were not included, and terms of second or higher order were calculated assuming δ-function pulses. The only important term which did not decouple and was too complex to calculate for the cycle as a whole is $\bar{\mathscr{H}}^{(2)}_{DO}$.

Because of the symmetry of the 52-pulse cycle and its decoupling properties the calculation of the first non-vanishing pure dipolar term, $\bar{\mathscr{H}}^{(4)}_{D}$, was reduced to a summing of the contributions of only three versions of the 2-pulse solid echo group. This allowed the term to be obtained with relative ease, whereas the calculation would otherwise have been extremely laborious.

The practical value of Table 2 will become more apparent in the next section as the behavior of the 52-pulse cycle is experimentally analyzed.

Experimental Analysis

Figure 1 shows the results from a measurement of the apparent off resonance frequency $\Delta\omega^+$ as a function of the actual resonance offset $\Delta\omega$ for the 52-pulse cycle applied to a water sample. The least squares fit shown in the figure gives a scaling factor of 2.78, which is in good agreement with the theoretical value of 2.81 calculated using $\bar{\mathscr{H}}^{(0)}_{0}$ from Table 2 with τ = 3.0 μsec and t_w = 1.5 μsec. It is not as simple a task to predict the resolution of the 52-pulse cycle under various

experimental conditions from the terms in Table 2. However, a significant improvement compared to the REV-8 cycle is expected under all conditions since $\bar{\mathscr{H}}_D^{(2)}$ and $\bar{\mathscr{H}}_D^{(3)}$ vanish for the 52-pulse cycle along with all of those line broadening terms which vanish for REV-8.

A number of measurements have been made on a single crystal of CaF_2 which give an overall picture of the cycle's performance and allow some tentative conclusions to be drawn as to which of the Hamiltonian terms in the Magnus expansion determine the resolution. An undoped, spherical crystal of CaF_2 was chosen as the sample for the measurements so that the resolution could not be limited by dopants, bulk susceptibility, or effects due to molecular motion. Limitation of the resolution due to paramagnetic impurities has been observed in 52-pulse experiments even for U-doped CaF_2 with $T_1 \simeq 3$ sec. Substantial spectral broadening due to bulk susceptibility has also been observed in CaF_2 powder samples. One example is shown in Figure 2, which compares spectra from a polycrystalline sample of undoped CaF_2 and a spherical crystal of the same material oriented with the (100) axis parallel to H_0. These spectra were obtained using the 52-pulse cycle with $\tau = 2.8$ μsec and $\Delta\omega/2\pi = 2.3$ kHz. Part (a) of the figure agrees well with a value for the spectral width of roughly 12 ppm which was predicted by comparing two hypothetical CaF_2 crystallites assumed to be ellipsoidal with axial ratios $b/a = c/a = 0.1$ for one and $b/a = 1.0$, $c/a = 0.1$ for the other. The value -28.0×10^{-6} cgs units[14] for the bulk susceptibility of CaF_2 and the tables of Osborn[15] were used in this calculation.

Figure 3 illustrates typical behavior of the exponential decay time of the signal during the pulse train, T_2^+, as a function of $\Delta\omega$. For this measurement τ = 2.8 μsec, and the CaF_2 sphere was oriented with the (100) crystal axis parallel to H_0.

Comparison with the dashed theoretical curve shows that below $\Delta\omega/2\pi$ = -3 kHz the resolution is determined by a term that is linear in $\Delta\omega$, the most likely candidate being $\bar{\mathcal{H}}_{DO}^{(1)}$ (see Table 2). However, this term apparently has little effect for 1 kHz $\leq \Delta\omega/2\pi \leq$ 4 kHz. In this region of constant T_2^+, which is called the high resolution "plateau", T_2^+ is obviously determined by terms in the Hamiltonian expansion which do not depend on $\Delta\omega$. Further measurements at this crystal orientation have shown that as τ is increased the heighth and width of this plateau tend to decrease, although the plateau is always found in the same region of $\Delta\omega/2\pi$, and the resolution becomes dependent on $\Delta\omega$.

Greater insight into which Hamiltonian terms are limiting T_2^+ in the high resolution plateau can be gained from Figure 4, which presents experimental data for T_2^+ as a function of crystal orientation for two values of τ, 2.0 μsec and 7.0 μsec, at two different values of $\Delta\omega/2\pi$, 1 kHz and 2.5 kHz. From this figure the following observations can be made:

(i) When the (100) crystal axis is parallel to H_0, which is the orientation of strongest dipolar coupling, T_2^+ depends on τ^{-2} for a given $\Delta\omega$.

(ii) For τ = 7.0 μsec T_2^+ depends on $\Delta\omega^{-1}$ at all orientations.

(iii) The more rounded shape of the two curves for τ = 2.8 μsec as compared to the "propellor" shape of the curves for τ = 7.0 μsec indicates a weaker dependence on the strength of the dipolar coupling for τ = 2.8 μsec than for τ = 7.0 μsec.

(iv) The curves for τ = 2.8 μsec show only a slight dependence on $\Delta\omega$.

From the first 3 observations it may be concluded that the two curves for τ = 7.0 μsec are governed by that part of $\bar{\mathcal{H}}_{DO}^{(2)}$ which is proportional to $\Delta\omega\tau^2||\mathcal{H}_D^{(z)}||^2$. Observations (iii) and (iv) indicate that, except when H_0 is nearly parallel to the (100) crystal axis, T_2^+ is limited by one or more terms which do not depend on $\Delta\omega$ and at most vary linearly with the strength of the dipolar interaction. The most likely candidates are the first order cross terms between the dipolar Hamiltonian and the various pulse errors. All of these terms vanish assuming δ-function pulses and depend on $t_w \tau^{-1} ||\mathcal{H}_D^{(z)}||$ when calculated to first order in t_w, and all of them are independent of $\Delta\omega$. Thus, one would expect the resolution to improve as τ is increased whenever T_2^+ is governed by these cross terms. This prediction is confirmed by the results of additional measurements made in the plateau region of $\Delta\omega/2\pi$ for values of τ between 2.8 and 5 μsec and with the (111) crystal axis parallel to H_0. Experience has shown that misadjustment of the pulse lengths and faulty positioning of the sample in the rf coil have the strongest effect on resolution. Thus it is most likely that T_2^+ is limited by $\bar{\mathcal{H}}_{\delta D}^{(1)}$ and $\bar{\mathcal{H}}_{\varepsilon D}^{(1)}$ when it is not governed by $\bar{\mathcal{H}}_{DO}^{(1)}$ or $\bar{\mathcal{H}}_{DO}^{(2)}$.

The question of what causes the asymmetry with regard to $\Delta\omega$ in Figure 2 is not completely solved. It is most likely that those terms in the average Hamiltonian expansion which do not depend on $\Delta\omega$ and are linear in the spin operators alter the direction, but not the magnitude, of $\bar{\mathscr{H}}_0^{(0)}$, causing it to have a more pronounced second averaging effect on $\bar{\mathscr{H}}_{D0}^{(1)}$ above resonance than below resonance.

Experimental comparisons confirm that the 52-pulse cycle has consistently better resolution than REV-8, as can be predicted from Table 2. One example is shown in Figure 5, which compares proton spectra from the two cycles for one orientation of a single crystal of gypsum[16], $CaSO_4 \cdot 2H_2O$. These spectra were measured at ambient temperature with $\tau = 2.8$ μsec and $\Delta\omega/2\pi = 2$ kHz. This example is typical of the improved resolution available using the 52-pulse and 24-pulse cycles, including those alternate versions discussed below.

F. EXPERIMENTAL RESULTS

As a further demonstration of the resolving power of the 52-pulse cycle, axially symmetric proton chemical shift tensor components are presented in this sub-section for polycrystalline samples of several organic compounds and for polycrystalline ice.

Figure 6 compares the resolution of the 52-pulse cycle with that of REV-8 for a polycrystalline sample of cyclohexane, C_6H_{12}, at liquid N_2 temperature. Despite broadening due to bulk susceptibility effects, an axially symmetric chemical shift tensor is clearly resolved which

was not obtained using REV-8. For both spectra in the figure τ was 3.0 μsec. Similar results have been obtained for cyclopentane, C_5H_{10}, and polyethylene at liquid N_2 temperature. These results are summarized in Table 3 along with the tensor components for ice which are discussed below.

All of the measurements in Table 3 were made in the high resolution plateau region of frequency, 1 kHz $\leq \Delta\omega/2\pi \leq$ 4 kHz, and with τ = 3.0 μsec.

An important example of a substance for which chemical shifts were very difficult to resolve until now is polycrystalline ice.[17] Figure 7 contrasts the results from the 52-pulse sequence with those from the REV-8 cycle when applied to naturally abundant protons in ice near liquid N_2 temperature. For both cycles τ = 3.0 μsec. The powder spectrum appears to be axially symmetric with $\sigma_{\parallel}$ = 11.2 ± 1 ppm and $\sigma_{\perp}$ = -17.5 ± 1 ppm relative to TMS, and there also appears to be an isotropic shift relative to liquid water of -5.3 ± 1 ppm. Preliminary spectra have also been obtained near -90°C which yield the same tensor components but also show spectral broadening and shape distortions which are apparently due to molecular motion. These results may be compared with a measurement made by Pines et al.[18] on 99% deuterated ice at -90°C. They obtained $\sigma_{\parallel}$ = 15 ± 2 ppm and $\sigma_{\perp}$ = -19 ± 2 ppm relative to TMS, with an isotropic shift relative to liquid water of 2 ± 1 ppm, and their spectrum shows no sign of effects due to molecular motion. Thus it appears that definite differences exist between the chemical shifts and the dynamic behaviors of natural and deuterated ice.

G. ALTERNATE VERSIONS OF THE 52-PULSE CYCLE

There are many other combinations of REV-8 cycles which satisfy the requirements discussed in this section for eliminating $\bar{\mathscr{H}}_D^{(2)}$ without reintroducing any of the dipolar Hamiltonian terms eliminated by REV-8. Most of those tried so far have shown a resolving power near resonance similar to that of the 24-pulse and 52-pulse cycles discussed in this section, but several have not shown a high resolution plateau which extended over as wide a range of frequency as that shown in Figure 3.

One alternate version of the 52-pulse cycle eliminates $\bar{\mathscr{H}}_{DO}^{(1)}$ calculated to first order in t_w as well as all the other dipolar terms that vanish for the 52-pulse cycle analyzed in this section. This alternate 52-pulse cycle combines two versions of REV-8 which can be written as follows:

$$\begin{aligned} 3 &= 3a3b \\ 4 &= 4a4b \end{aligned} \tag{58}$$

where

$$\begin{aligned} 3a &= (XY)(Y\bar{X}) \\ 3b &= (X\bar{Y})(\bar{Y}\bar{X}) \\ 4a &= (YX)(X\bar{Y}) \\ 4b &= (Y\bar{X})(\bar{X}\bar{Y}) \end{aligned} \tag{59}$$

The full cycle can be written

$$3a3b\left(\frac{\pi}{2}\right)_x 3a3b\left(\frac{\pi}{2}\right)_{-x} 4a4b4b4a\left(\frac{\pi}{2}\right)_{-x} 3a3b\left(\frac{\pi}{2}\right)_x 3a3b \tag{60}$$

Another 52-pulse cycle is designed to eliminate $\bar{\mathscr{H}}_{\varepsilon D}^{(1)}$ and $\bar{\mathscr{H}}_{\delta D}^{(1)}$ (assuming $\delta_x = \delta_{-x} = \delta_y = \delta_{-y}$) calculated to first order in t_w. It uses the pulse groups given in equation (59) and can be written

$$3a\left(\frac{\pi}{2}\right)_x 3a3b\left(\frac{\pi}{2}\right)_{-x} 3a3b3b4a\left(\frac{\pi}{2}\right)_{-x} 3a3b\left(\frac{\pi}{2}\right)_x 4a4b4b \tag{61}$$

Another 52-pulse cycle which is composed of unseparated REV-8 cycles from equation (53) can be written as follows:

$$1\left(\frac{\pi}{2}\right)_x 1\left(\frac{\pi}{2}\right)_{-x} 22\left(\frac{\pi}{2}\right)_{-x} 1\left(\frac{\pi}{2}\right)_x 1 \tag{62}$$

Experimental measurements indicate that this cycle has a narrower plateau in the same region of $\Delta\omega/2\pi$ as in Figure 3.

Many other combinations of REV-8 cycles are possible, for instance

$$1a\left(\frac{\pi}{2}\right)_x 1a2a2b1b\left(\frac{\pi}{2}\right)_{-x} 1b1a\left(\frac{\pi}{2}\right)_{-x} 1a2a2b1b\left(\frac{\pi}{2}\right)_x 1b \tag{63}$$

and even a 26-pulse cycle,

$$1a\left(\frac{\pi}{2}\right)_x 1a1b\left(\frac{\pi}{2}\right)_{-x} 1b\left(\frac{\pi}{2}\right)_{-x} 2a2b\left(\frac{\pi}{2}\right)_x \tag{64}$$

which might be difficult to use in practice due to difficulties such as a scarcity of sampling windows. Clearly the approach to pulse cycle design discussed in this section provides a great deal of flexibility which should lead to the development of pulse cycles with even greater resolving power than the 24-pulse and 52-pulse cycles.

REFERENCES

1. U. Haeberlen, High Resolution NMR in Solids, Selective Averaging, (Academic Press, New York, 1976).
2. W. K. Rhim, D. D. Elleman and R. W. Vaughan, J. Chem. Phys. 59, 3740 (1973).
3. W. K. Rhim, D. D. Elleman, L. B. Schreiber and R. W. Vaughan, J. Chem. Phys. 60, 4595 (1974).
4. Section 3.
5. U. Haeberlen, private communication.
6. P. Mansfield, J. Phys. C: Solid State 4, 1444 (1971).
7. J. G. Powles and P. Mansfield, Phys. Lett. 2, 58 (1962).
   J. G. Powles and J. H. Strange, Proc. Phys. Soc. 82, 6 (1963).
   P. Mansfield, Phys. Rev. A137, 961 (1965).
8. J. S. Waugh, L. Huber and U. Haeberlen, Phys. Rev. Lett. 20, 180 (1968).
9. U. Haeberlen and J. S. Waugh, Phys. Rev. 175, 453 (1968).
10. P. Mansfield, Phys. Lett. A32, 485 (1970).
11. C. H. Wang and J. D. Ramshaw, Phys. Rev. B6, 3253 (1972).
12. W. A. B. Evans, Ann. Phys. 48, 72 (1968).
13. U. Haeberlen, J. D. Ellet, Jr. and J. S. Waugh, J. Chem. Phys. 55, 53 (1971).
    A. Pines and J. S. Waugh, J. Magn. Res. 8, 354 (1972).
14. Handbook of Chemistry and Physics, edited by R. C. Weast (Chemical Rubber, Cleaveland, OH, 1974) 55th ed., p. E122.
15. J. A. Osborn, Phys. Rev. 67, 351 (1945).
16. Section 5.

17. A chemical shift powder spectrum for ice measured using the REV-8 experiment was reported by L. M. Ryan, R. C. Wilson and B. C. Gerstein, Chem. Phys. Lett. 52, 341 (1977).

17. A. Pines, D. J. Ruben, S. Vega and M. Mehring, Phys. Rev. Lett. 36, 110 (1976).

Table 1
COMPENSATED SETS OF SOLID ECHO PULSE GROUPS[a]

Hamiltonian Term	Result for (ABC)	Compensated Sets	Comments	
$\bar{\mathcal{H}}_D^{(1)}$	$-\left(\frac{i\tau}{6}\right)\left[\mathcal{H}_D^{(b)}, \mathcal{H}_D^{(a)}\right]$	$\{(ABC), (CBA)\}$	First order in t_w	Bar over any state has no effect
		$\{(ABC), (BAC)\}$	δ-function pulses only	
		$\{(ABC), (ACB)\}$	δ-function pulses only	
$\bar{\mathcal{H}}_{DO}^{(1)}$	$\left(\frac{i\tau}{3}\right)\left[\mathcal{H}_D^{(c)}, B\right]$	$\{(ABC), (CBA)\}$	δ-function pulses only	Bar over A and C has no effect
		$\{(ABC), (\bar{A}B\bar{C})\}$	δ-function pulses only	
$\bar{\mathcal{H}}_D^{(0)}$	$\left(\frac{t_w}{6\tau}\right)\left\{\mathcal{H}_D^{(a)} - \mathcal{H}_D^{(c)}\right.$	$\{(ABC), (C\bar{B}A)\}$	Finite pulse width	Assumes no pulse - immediately precedes the solid echo group
	$- \left(\frac{6}{\pi}\right)\sum_{i<j}\beta_{ij}\left((A_i + C_i)B_j\right.$	$\{(ABC), (\bar{C}\bar{B}\bar{A})\}$	Finite pulse width	
	$\left.\left. + B_i(A_j + C_j)\right)\right\}$			

Table 1
COMPENSATED SETS OF SOLID ECHO PULSE GROUPS[a] (Continued)

Hamiltonian Term	Result for (ABC)	Compensated Sets	Comments	
$\overline{\mathcal{H}}_D^{(2)}$	$-\left(\frac{\tau^2}{18}\right)\left[\mathcal{H}_D^{(a)}-\mathcal{H}_D^{(c)},\left(\mathcal{H}_D^{(a)},\mathcal{H}_D^{(b)}\right)\right]$	{(xAx),(xBx),(xCx)}[b]	δ-function pulses only	Bar over any state has no effect

[a] The generalized notation used in this table is explained in the text.

[b] Any substitution of states may be made for x that results in each solid echo pulse group containing A, B and C.

Table 2
AVERAGE HAMILTONIAN TERMS FOR THE 52-PULSE CYCLE

Hamiltonian Term	52-Pulse Cycle Result	Comments
$\bar{\mathscr{H}}_0^{(0)}$[a]	$\frac{1}{9}\sum_i(\Delta\omega + \omega_0\sigma_{zzi})(1+a)(2I_{xi} - I_{yi} + 2I_{zi})$	Finite pulse width included
$\bar{\mathscr{H}}_0^{(1)}$	$\frac{\tau}{9}\sum_i(\Delta\omega + \omega_0\sigma_{zzi})^2(8I_x + I_y - 6I_z)$	δ-finite pulses assumed
$\bar{\mathscr{H}}_D^{(0)}$	0	Finite pulse width included
$\bar{\mathscr{H}}_D^{(1)}$	0	Finite pulse width included
$\bar{\mathscr{H}}_{DO}^{(1)}$[b]	$\frac{t_w}{36}\sum_k(\Delta\omega + \omega_0\sigma_{zzk})\Big\{i[I_{yk}, Z] + 4i[I_{xk}, Y] - \frac{4}{\pi}\Big(2[I_{xk} + I_{zk}, (I_y, Z)] + [3I_{xk} - I_{yk} + 4I_{zk}, (I_z, Y)] + [-6I_{xk} + 4I_{yk} - 7I_{zk}, (I_x, Y)]\Big)\Big\}$	Finite pulse width included only to first order in t_w
$\bar{\mathscr{H}}_D^{(2)}$	0	δ-function pulses assumed
$\bar{\mathscr{H}}_D^{(3)}$	0	δ-function pulses assumed

Table 2
AVERAGE HAMILTONIAN TERMS FOR THE 52-PULSE CYCLE (Continued)

Hamiltonian Term	52-Pulse Cycle Result	Comments
$\bar{\mathscr{H}}_{D}^{(4)}$ [b]	$\left(\frac{\tau^4}{432}\right)\Big\{4\Big[(X, Z), \big(Y - Z, [X, Y]\big)\Big] + 2\Big(X[Z, (X,Y)]X + Y[X, (X, Y)]Y\Big)$ $- Z[X, (X, Y)]Z - X^2YX^2 - Y^2ZY^2 + Z^2YZ^2 - XYXYX + YZYZY$ $- ZYZYZ + X^5 + Y^5 + Z^5$	δ-function pulses assumed
$\bar{\mathscr{H}}_{P}^{(0)}$	$\left(\frac{1}{36\tau}\right)\Big\{6(\sin\phi_y - \sin\phi_{-y})I_x - 5(\sin\phi_x - \sin\phi_{-x})I_y\Big\}$	
$\bar{\mathscr{H}}_{PO}^{(1)}$	$\left(\frac{1}{18}\right)\sum_i(\Delta\omega + \omega_0\sigma_{zzi})\Big\{3(\sin\phi_x - \sin\phi_{-x})(I_{xi} + 3I_{yi} + I_{zi})$ $+ (\sin\phi_y - \sin\phi_{-y})(-2I_{xi} + I_{yi} - 7I_{zi}) + 2I_{yi}\sin\phi_x$ $- I_{xi}\sin\phi_{-x})\Big\}$	δ-function pulses assumed
$\bar{\mathscr{H}}_{PD}^{(1)}$	0	δ-function pulses assumed
$\bar{\mathscr{H}}_{PT}^{(0)}$ [c]	$\left(\frac{J_1}{36\tau}\right)(4I_x - 2I_y + 5I_z)$	
$\bar{\mathscr{H}}_{TO}^{(1)}$ [c]	$\left(\frac{1}{18}\right)\sum_i(\Delta\omega + \omega_0\sigma_{zzi})(2J_1(11I_{xi} + 2I_{yi} - 7I_{zi}) - J_2(I_{xi} + 2I_{yi})$	δ-function pulses assumed
$\bar{\mathscr{H}}_{TD}^{(1)}$	0	δ-function pulses assumed

Table 2
AVERAGE HAMILTONIAN TERMS FOR THE 52-PULSE CYCLE (Continued)

Hamiltonian Term	52-Pulse Cycle Result	Comments
$\bar{\mathcal{H}}_{\delta}^{(0)}$	$\left(\frac{1}{36}\right)\left\{5(-\delta_x + \delta_{-x})I_x + 2(-\delta_y + \delta_{-y})I_y\right\}$	
$\bar{\mathcal{H}}_{\delta O}^{(1)}$	$\left(\frac{1}{36}\right)\sum_i(\Delta\omega + \omega_0\sigma_{zzi})\left\{(\delta_x - \delta_{-x})(22I_{zi} - 3I_{yi} - 3I_{xi})\right.$ $\left. + 2(\delta_y - \delta_{-y})(I_{zi} + I_{xi} + 3I_{yi}) - 2\left(2(\delta_x + \delta_{-x}) + (\delta_y + \delta_{-y})\right)I_{zi}\right\}$	δ-function pulses assumed
$\bar{\mathcal{H}}_{\delta D}^{(1)}{}^{b,d}$	$\left(\frac{t_w}{9\pi i\tau}\right)\delta\left\{[I_y, X] + [I_x, Y] + 2i(X - Z)\right\}$	First order in t_w only
$\bar{\mathcal{H}}_{\varepsilon}^{(0)}$	0	
$\bar{\mathcal{H}}_{\varepsilon O}^{(1)}$	$-\left(\frac{1}{3}\right)\sum_i \varepsilon_i(\Delta\omega + \omega_0\sigma_{zzi})I_{zi}$	δ-function pulses assumed
$\bar{\mathcal{H}}_{\varepsilon D}^{(1)}{}^{e}$	$-\left(\frac{t_w}{3\pi}\right)\sum_{i<j}\beta_{ij}\varepsilon_i\left\{2(I_{xi}I_{xj} - I_{zi}I_{zj}) - (I_{xi}I_{zj} + I_{zi}I_{xj}\right.$ $\left. - I_{zi}I_{yj} - I_{yi}I_{zj})\right\}$	First order in t_w only

Table 2
AVERAGE HAMILTONIAN TERMS FOR THE 52-PULSE CYCLE (Continued)

NOTES:

[a] $a_a = \left(\frac{t_w}{2\tau}\right)\left(\frac{4}{\pi} - 1\right)$

[b] $X \equiv \mathcal{H}_D^{(x)}$, $Y \equiv \mathcal{H}_D^{(y)}$, $Z \equiv \mathcal{H}_D^{(z)}$

[c] $J_1 = \int_0^{t_w} \omega_T(t)\ (\sin \omega_1 t - \cos \omega_1 t)dt$

$J_2 = \int_0^{t_w} \omega_T(t)\ (\sin \omega_1 t + \cos \omega_1 t)dt$

[d] It is assumed for this calculation that $\delta_x = \delta_y = \delta_{-x} = \delta_{-y} \equiv \delta$

[e] It is assumed that ω_1 is constant over a scale of molecular dimensions

Table 3
PROTON CHEMICAL SHIFT COMPONENTS[a] FOR SEVERAL SOLIDS[b]

	$\sigma_\perp$	$\sigma_\parallel$	σ_0	$\sigma_\parallel - \sigma_\perp$
Ice	-17.5	11.2	-10.6	28.7
C_6H_{12}	-5.0	3.9	-2.7	8.9
C_5H_{10}	-4.3	4.1	-1.1	8.4
Polyethylene	-3.5	2.4	-0.5	5.9

[a] Chemical shift values are in ppm relative to TMS.

[b] All measurements were made using the 52-pulse cycle at liquid N_2 temperature with τ = 3.0 μsec and 1 kHz $\leq \Delta\omega/2\pi \leq$ 4 kHz.

Figure Captions

1. Apparent off resonance, $\Delta\omega^{+}/2\pi$, as a function of actual resonance offset, $\Delta\omega/2\pi$, for the 52-pulse cycle applied to a water sample. The solid line is a least squares fit to the data.

2. Demonstration of spectral broadening due to bulk susceptibility: (a) spectrum from a polycrystalline sample of undoped CaF_2; (b) spectrum from a spherical single crystal of the same material oriented with $H_0 \,||\, (100)$. Both spectra were obtained using the 52-pulse cycle with τ = 2.8 μsec and $\Delta\omega/2\pi$ = 2.3 kHz.

3. Exponential decay time, T_2^{+}, as a function of off resonance for the 52-pulse cycle applied to a spherical CaF_2 crystal oriented with $H_0 \,||\, (100)$. The dashed curve is a theoretical fit for $\Delta\omega/2\pi \leq -2.0$ kHz which varies as $2\pi/\Delta\omega$.

4. Decay time, T_2^{+}, as a function of CaF_2 crystal orientation for two values of τ, 2.0 μsec and 7.0 μsec, at two different values of $\Delta\omega/2\pi$, 1 kHz and 2.5 kHz.

5. Comparison of the resolving power of REV-8 (part a) and the 52-pulse cycle (part b) for a single crystal of gypsum at one orientation. For both spectra τ = 2.8 μsec. The scale is in ppm relative to TMS.

6. Comparison of the resolving power of REV-8 and the 52-pulse cycle for a polycrystalline sample of cyclohexane at liquid N_2 temperature. For both spectra τ = 3.0 μsec. The scale is in ppm relative to TMS and the chemical shift tensor components shown in the figure are given in Table 3.

7. Comparison of the resolving power of REV-8 (part A) and the 52-pulse cycle (part B) for naturally abundant protons in polycrystalline ice at liquid N_2 temperature. For both spectra τ = 3.0 μsec. The scale is in ppm relative to TMS and the dashed line shows the liquid resonance position. The chemical shift tensor components for part B are given in Table 3.

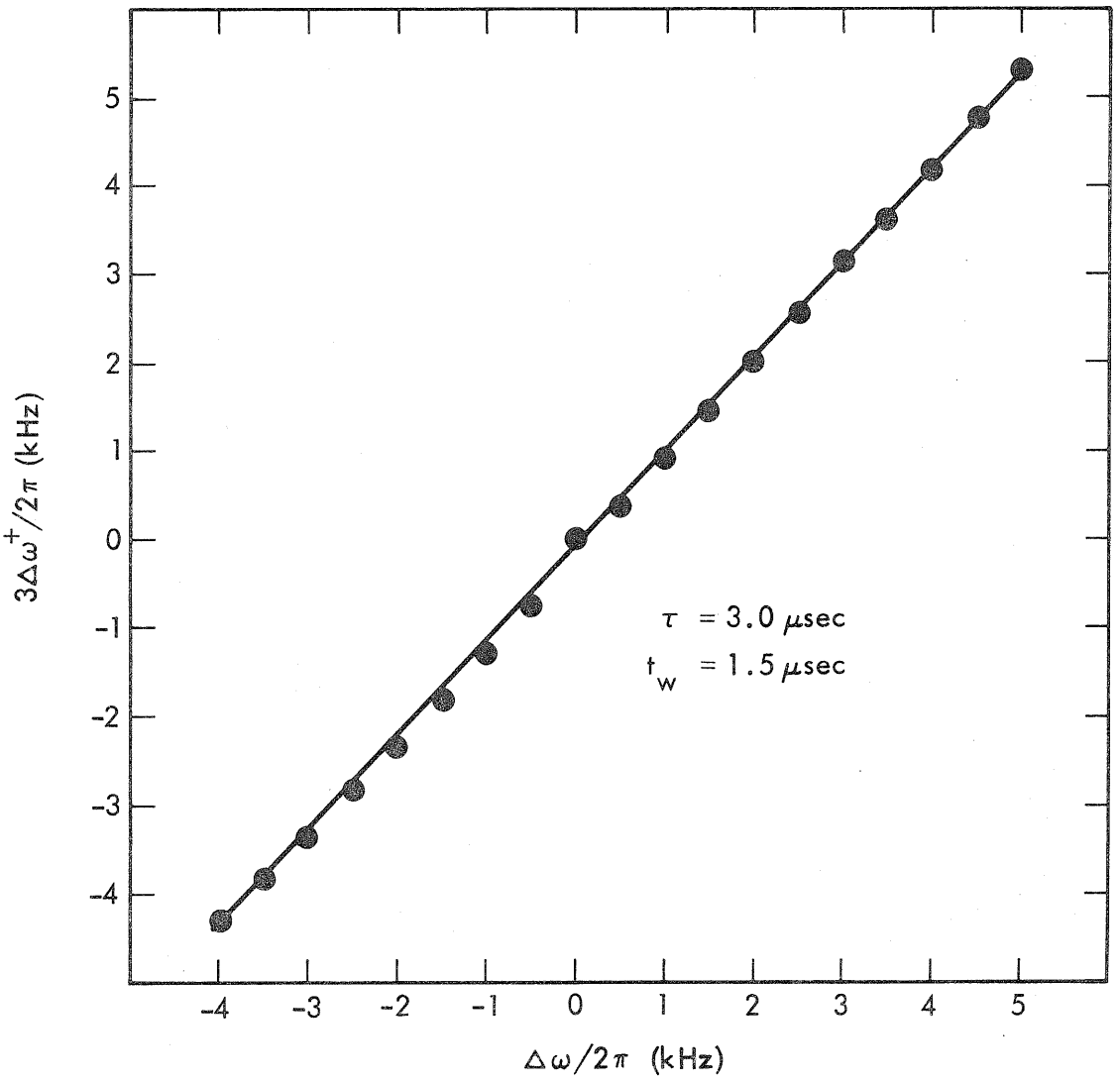
$3\Delta\omega^{+}/2\pi$ (kHz)
5
4
3
2
1
0
-1
-2
-3
-4
τ = 3.0 μsec
t_w = 1.5 μsec
-4
-3
-2
-1
0
1
2
3
4
5
$\Delta\omega/2\pi$ (kHz)

Fig. 1

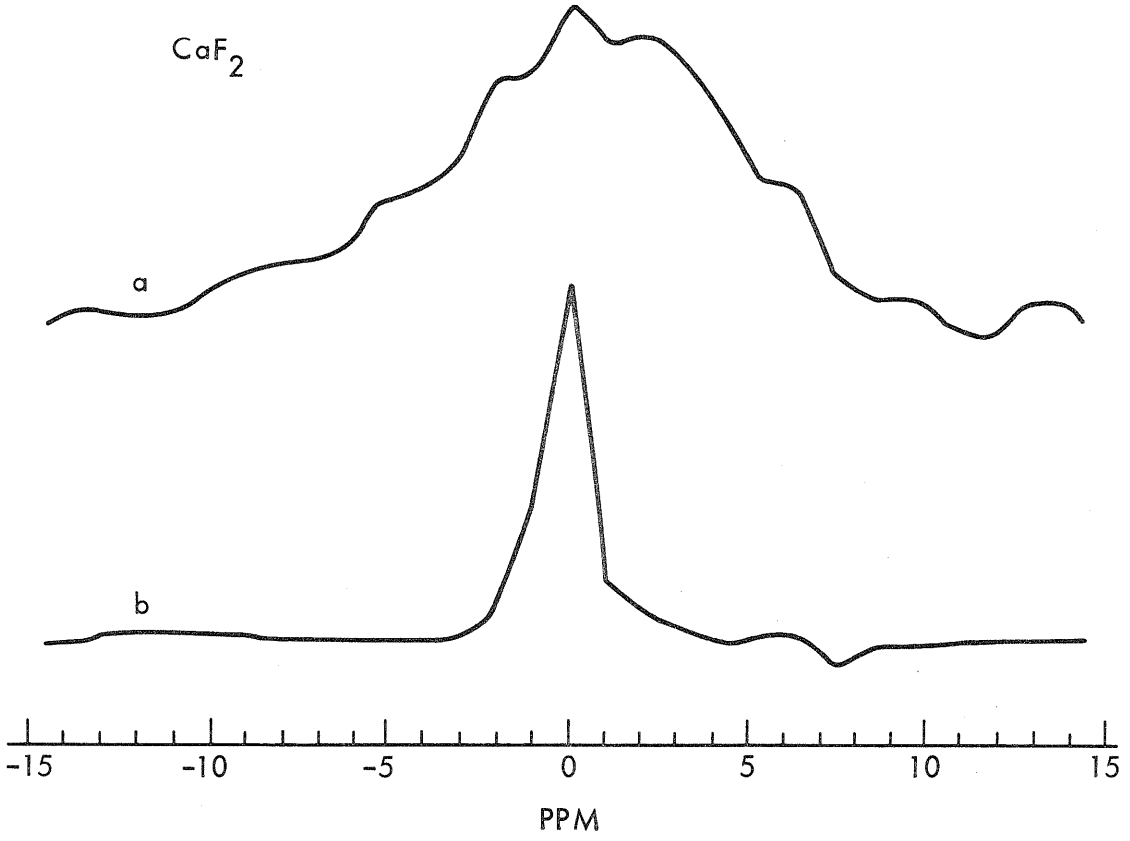

Fig. 2

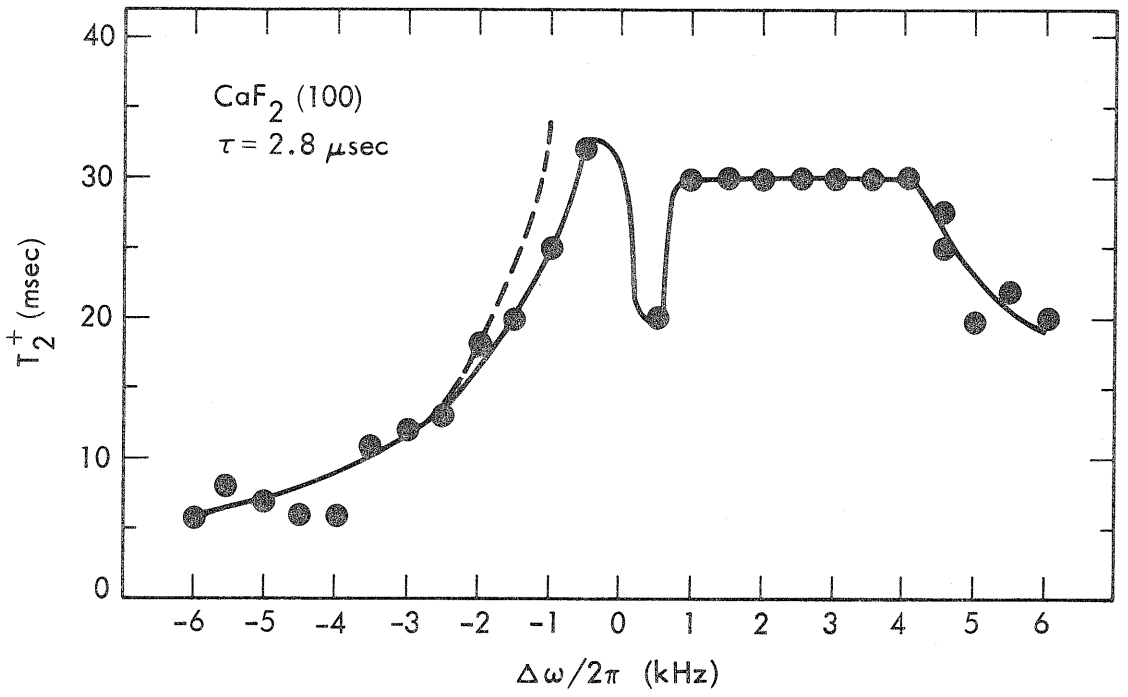
40
30
20
10
0
CaF_2 (100)
$\tau = 2.8\ \mu sec$
T_2^+ (msec)
-6 -5 -4 -3 -2 -1 0 1 2 3 4 5 6
$\Delta\omega/2\pi$ (kHz)

Fig. 3

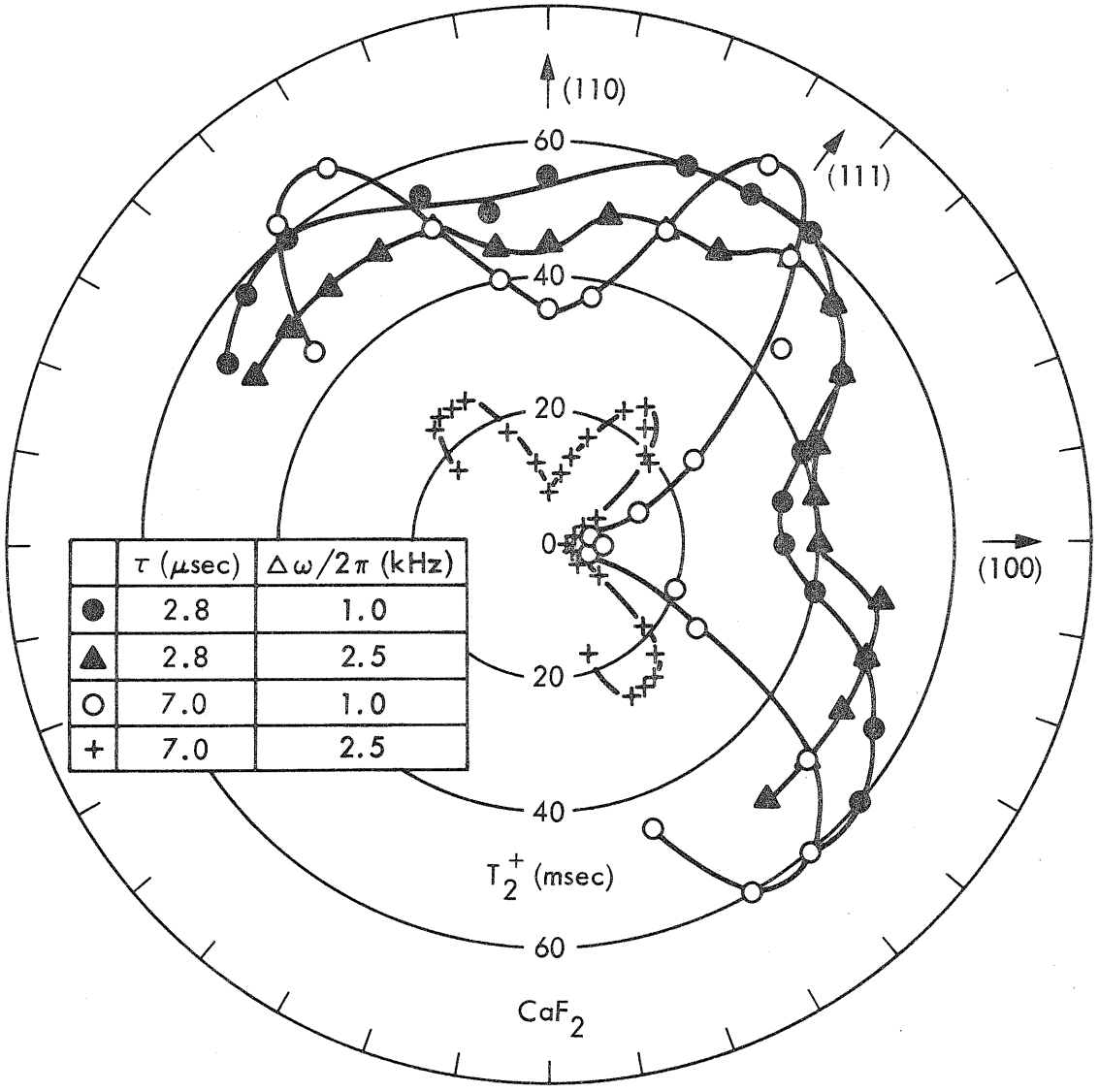
(110)
(111)
(100)
60
40
20
0
20
40
60
T_2^+ (msec)
CaF_2
τ (μsec)
Δω/2π (kHz)
2.8
1.0
2.8
2.5
7.0
1.0
7.0
2.5

Fig. 4

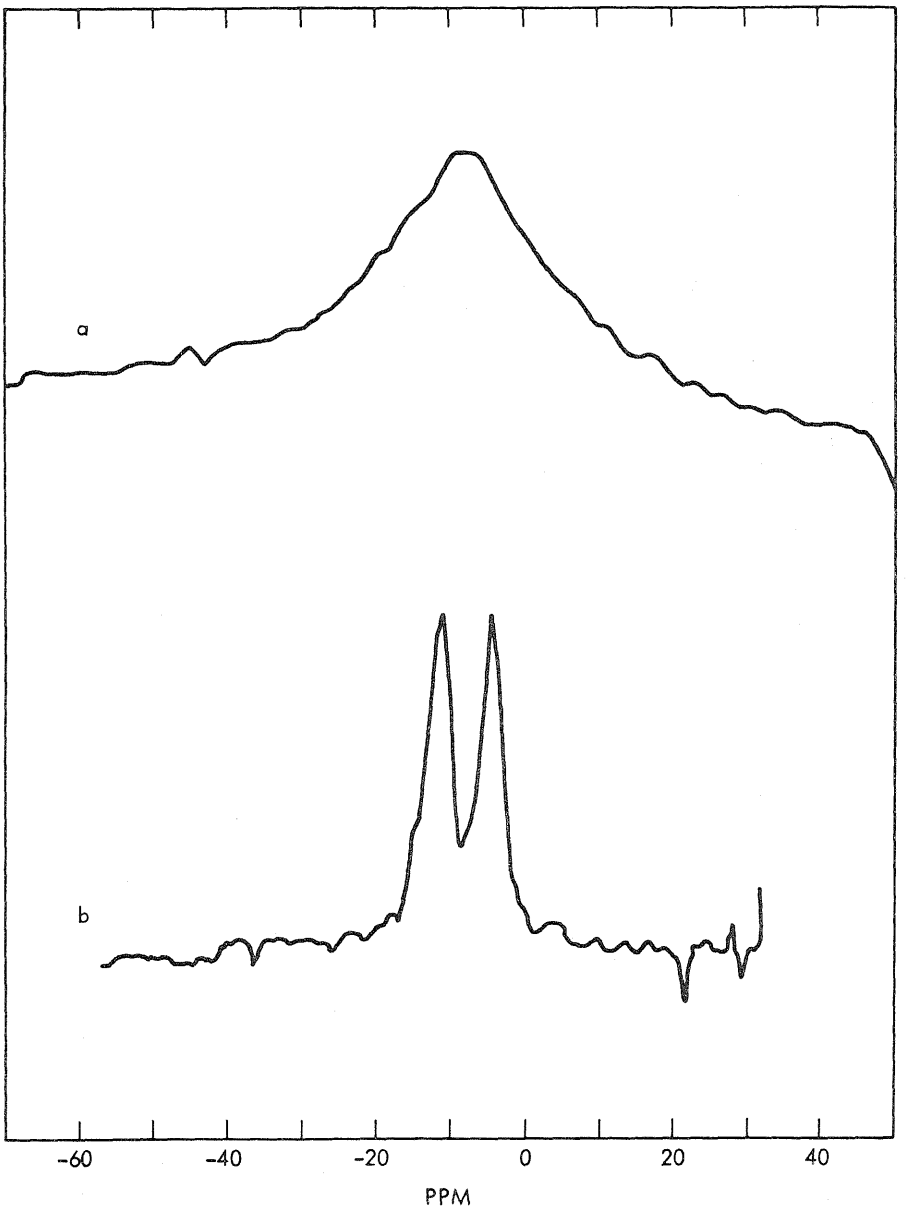

Fig. 5

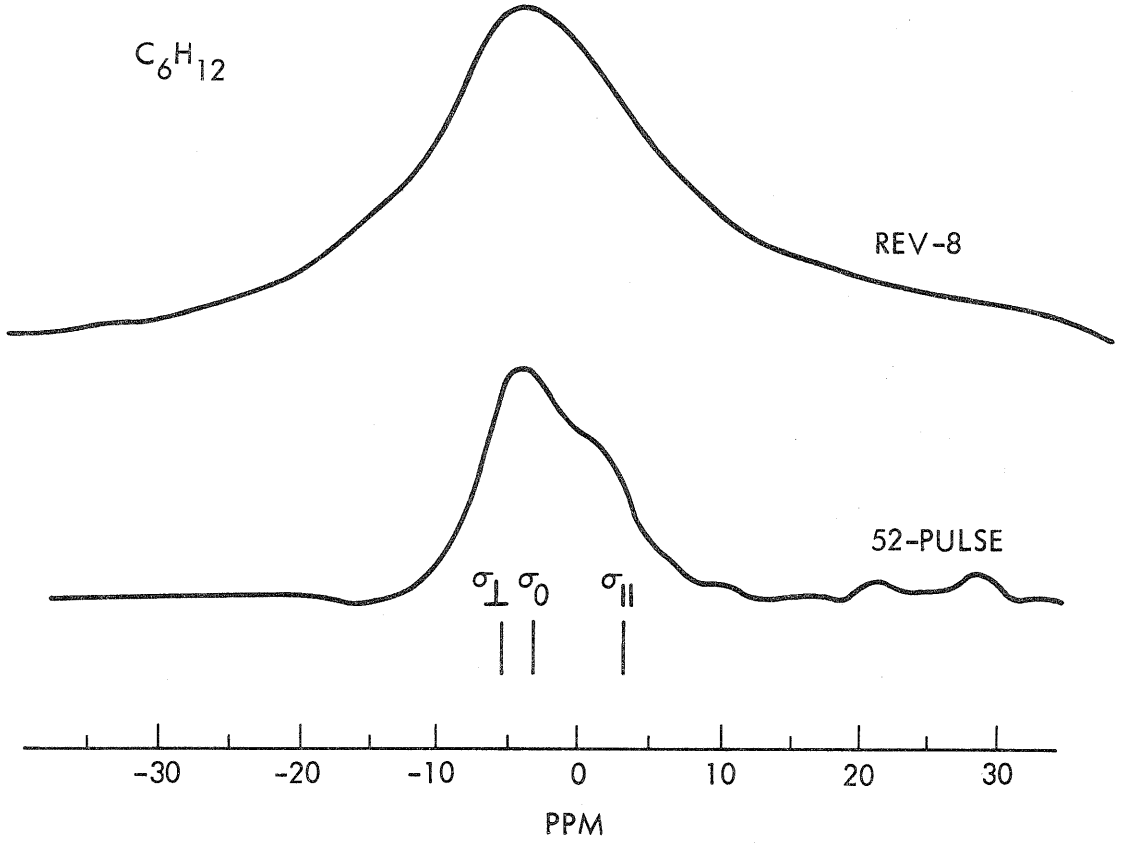
C_6H_{12}
REV-8
52-PULSE
$\sigma_\perp$ σ_0 $\sigma_\parallel$
-30
-20
-10
0
10
20
30
PPM

Fig. 6

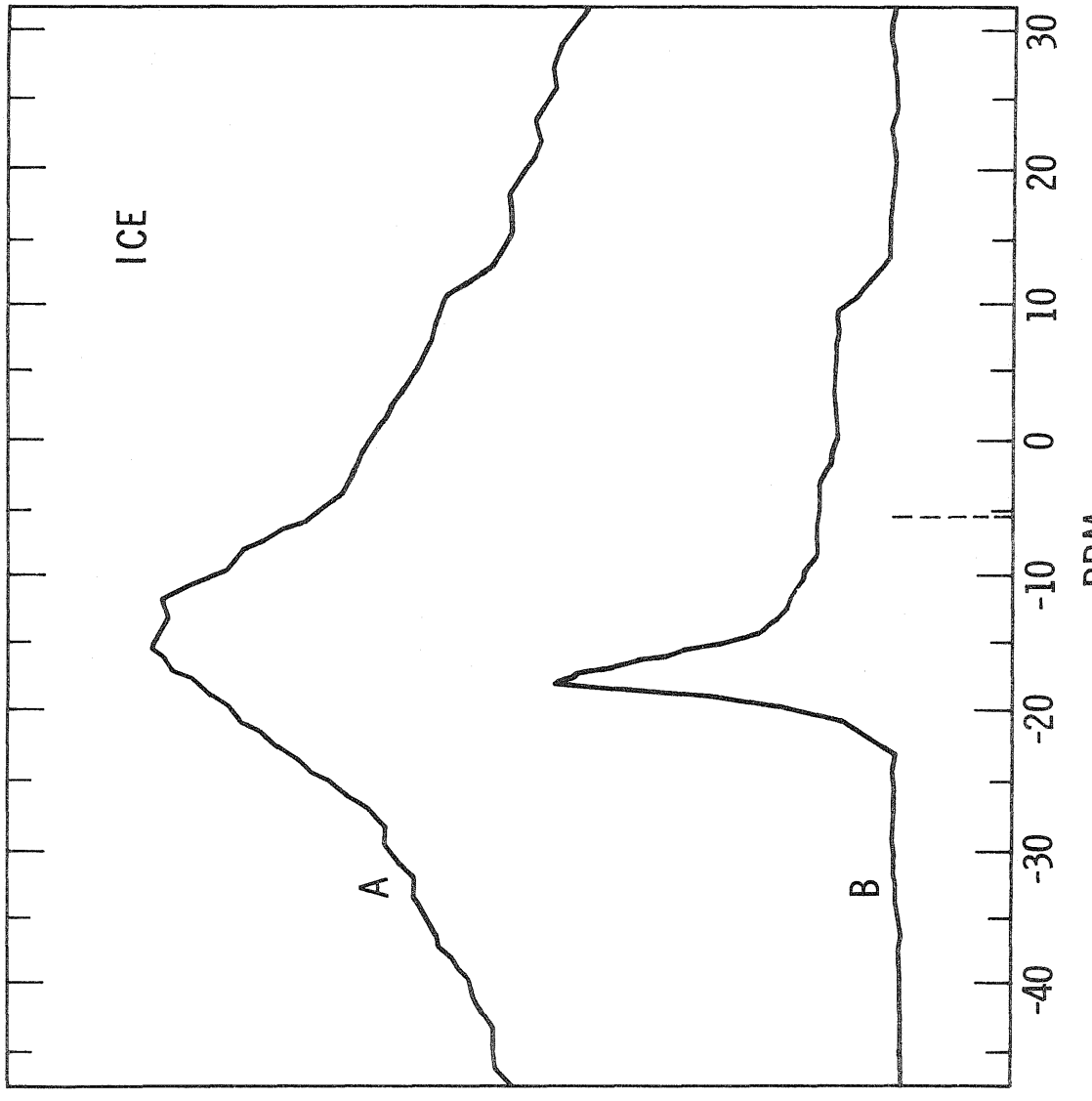

Fig. 7

Section 5

A Chemical Shift Study of Gypsum, $CaSO_4 \cdot 2H_2O$, Using the 52-Pulse Cycle

(This section is essentially an article by D. P. Burum and W. K. Rhim, "Proton NMR Study of Gypsum, $CaSO_4 \cdot 2H_2O$, Using an Improved Technique for Homonuclear Dipolar Decoupling in Solids" which has been submitted for Publication to The Journal of Magnetic Resonance.)

This section presents the results of a room temperature study of proton chemical shift anisotropy in gypsum, $CaSO_4 \cdot 2H_2O$, carried out using the 52-pulse sequence analyzed in section 4. Gypsum is of fundamental importance because of the simple, planar geometry of the water molecules and the presence of near linear O-H···O bonds. It is also appropriate because studies by neutron and X-ray diffraction[1,2] have made precise structural information available. Furthermore, the power of the new sequence to decouple the homonuclear dipolar interaction is demonstrated by its ability to produce well resolved chemical shift spectra for gypsum even at crystal orientations where the dipolar splitting is as great as 22 gauss.[3] The only other study of chemical shifts in gypsum was reported by McKnett et al.[4] who applied the REV-8 cycle at restricted crystal orientations, and their results are in substantial disagreement with this section.

Two gypsum crystals were used in this work. One crystal was rotated so that the external field remained in the plane perpendicular to the (010) axis (crystal A) while the other was rotated such that the external field swept out a plane containing the (010) axis (crystal B). The rotation device allowed the angle to be set within 1^{o}. All chemical shifts were corrected for bulk susceptibility using a value of -74×10^{-6} (cgs units) for the bulk susceptibility of gypsum and the tables of Osborn.[5] For this purpose it was assumed that the samples were roughly ellipsoidal with the following crystal axis ratios: for crystal A, (a,b,c) = (1.0,1.0,0.4); for crystal B, (a,b,c) = (1.0,0.75,0.75).

Figure 1 shows part of the unit cell of gypsum.[1-4] At room temperature

the protons in each water molecule rapidly exchange[4,6] so that only an average tensor is observed, which can be characterized in its principal coordinate frame by σ_{XX}, σ_{YY} and σ_{ZZ}. Because of the high symmetry of the crystal, the 8 water molecules in the unit cell occupy only two inequivalent positions in equal numbers, so that at room temperature one expects to observe at most two lines.

The improved resolution of the 52-pulse sequence made it possible to obtain complete and well defined chemical shift information for both crystals. The chemical shifts as a function of crystal rotation angle, along with theoretical fits to the data, are presented in figure 2 for crystal A and in figure 3 for crystal B. As expected from the crystal geometry, only one line was observed for crystal A, because the external field remained in a plane of mirror symmetry for the water molecules. For crystal B, comparison of the residual dipolar broadening of the two spectral lines allowed the two chemical shift curves to be readily assigned to the two inequivalent orientations of the water molecules.

Because all of the water molecules in gypsum lie in the plane containing the (100) and (010) crystal axes, the Z-axis of the principal coordinate frame can be taken to be perpendicular to this plane. With only this assumption, it was determined from the theoretical fits to the data shown in figures 2 and 3 that the X-axis makes an angle of 36.7^{o} with the (010) crystal axis, which agrees closely with the value of 38.8^{o} obtained by neutron diffraction[1] for the proton-proton vector of the water molecule. Of course, the Y-axis is perpendicular to the X-axis and lies in the plane of the water molecules. The principal tensor values in this coordinate

frame were determined to be σ_{XX} = 0.1 ± 0.5 ppm, σ_{YY} = -9.5 ± 0.5 ppm and σ_{ZZ} = -18.6 ± 0.5 ppm relative to TMS. The angle between the water molecule plane and the plane swept out by the external field in crystal B was also determined from the theoretical fits shown in figures 2 and 3.

These chemical shift results can be compared with the study done by McKnett et al.[4]. By using the REV-8 cycle, they were able to obtain data corresponding to most of the points in figure 2. However, they were able to obtain data corresponding to only a few of the points shown in figure 3. They began by assuming that the Z-axis of the principal coordinate frame was perpendicular to the water molecule plane and that the X-axis was along the proton-proton vector in the water molecule, and obtained the following results: σ_{XX} = -10.9 ± 1 ppm, σ_{YY} = -5.9 ± 1 ppm and σ_{ZZ} = -17.6 ± 1 ppm relative to TMS. The close agreement between the σ_{ZZ} values for the two studies is not surprising, when one realizes that this value can be obtained using only the data shown in figure 2. On the other hand, the reason for the considerable descrepancy between the values obtained in the two studies for σ_{XX} and σ_{YY} is not clear. It can only be conjectured that it is due in part to the difficulty of determining values for σ_{XX} and σ_{YY} accurately and unambiguously when most of the information shown in figure 3 is not available, as was the case for McKnett et al.

If one is willing to make the additional assumptions that the tensors for the two separate protons in the water molecule are equivalent and that their principal axes are oriented with the X-axis along the O-H bond, the Y-axis perpendicular to this in the plane of the water molecules and the Z-axis perpendicular to this plane, then the tensor values given above can be used to predict the tensor for an individual proton in the absence of

exchange. Using the value 105.6° given by neutron diffraction[1] for the H-O-H angle, the following principal tensor values are obtained: σ_{xx} = 13.2 ± 0.5 ppm, σ_{yy} = -22.5 ± 0.5 ppm and σ_{zz} = -18.6 ± 0.5 ppm relative to TMS.

The two gypsum crystals used for this study were the same ones that were used in the study made by McKnett et al.[4]

REFERENCES

1. M. Atoji and R. E. Rundle, J. Chem. Phys. 29, 1306 (1958).

2. W. F. Cole and C. J. Lancucki, Nature (London) Phys. Sci. 242, 104 (1973).

   W. F. Cole and C. J. Lancucki, Acta Cryst. B30, 921 (1974).

3. G. E. Pake, J. Chem. Phys. 16, 327 (1948).

4. C. L. McKnett, C. R. Dybowski and R. W. Vaughan, J. Chem. Phys. 63, 4578 (1975).

5. J. A. Osborn, Phys. Rev. 67, 351 (1945).

6. D. C. Look and I. J. Lowe, J. Chem. Phys. 44, 2995 (1966).

FIGURE CAPTIONS

1. Portion of the unit cell of gypsum. The principal axis system for a water molecule undergoing rapid proton exchange is indicated, and a key to the nuclear species and the fractional coordinates (± 0.05) is given.
2. Chemical shift relative to TMS vs. crystal rotation angle for gypsum crystal A. The crystal was rotated so that the external field remained in the (010) plane. The solid line is the theoretical fit to the data.
3. Chemical shifts relative to TMS vs. crystal rotation angle for gypsum crystal B. The crystal was rotated so that the external field swept out a plane containing the (010) axis and making an angle of 30.7^{o} with the plane containing the water molecules. The solid lines show the theoretical fit to the data.

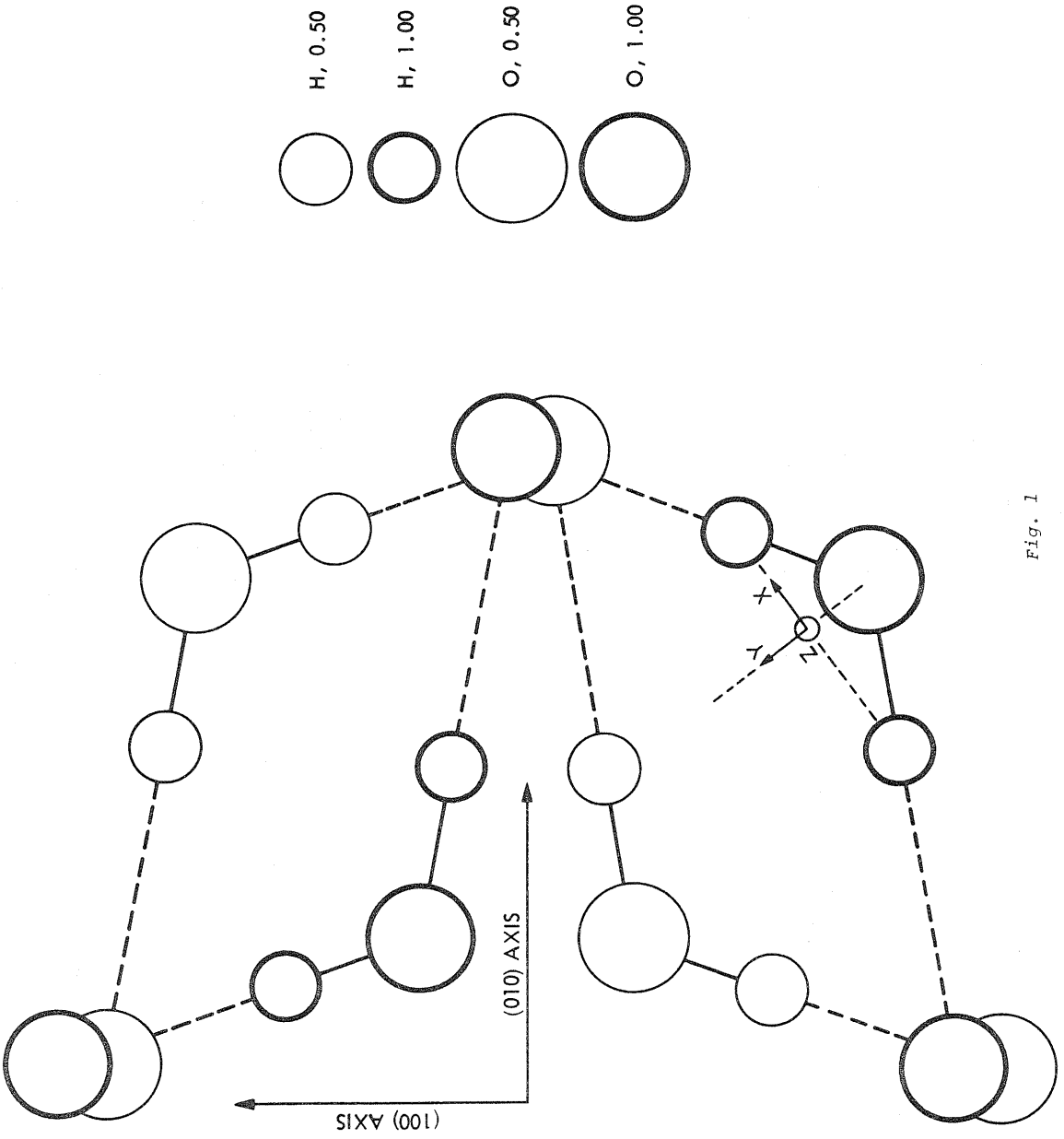

Fig. 1

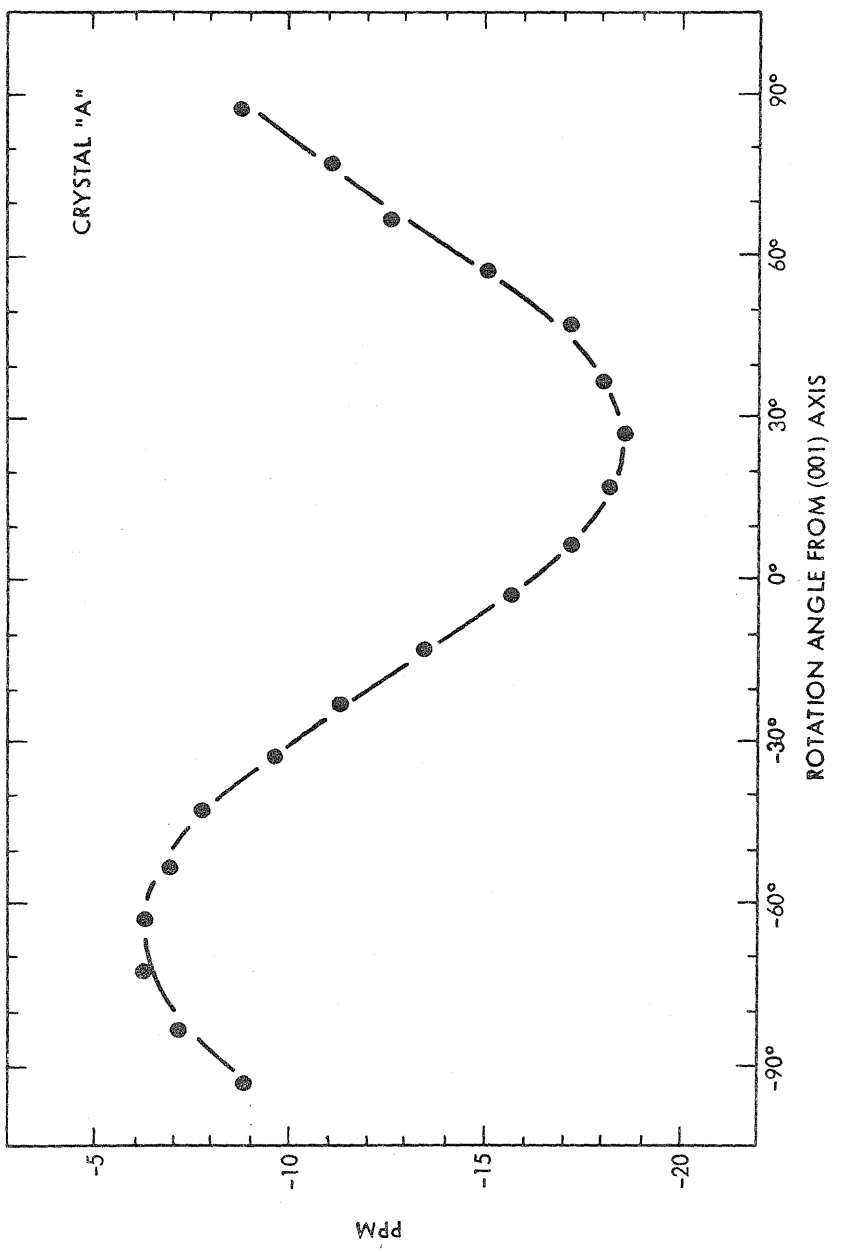
CRYSTAL "A"
-5
-10
-15
-20
ppm
-90°
-60°
-30°
0°
30°
60°
90°
ROTATION ANGLE FROM (001) AXIS

Fig. 2

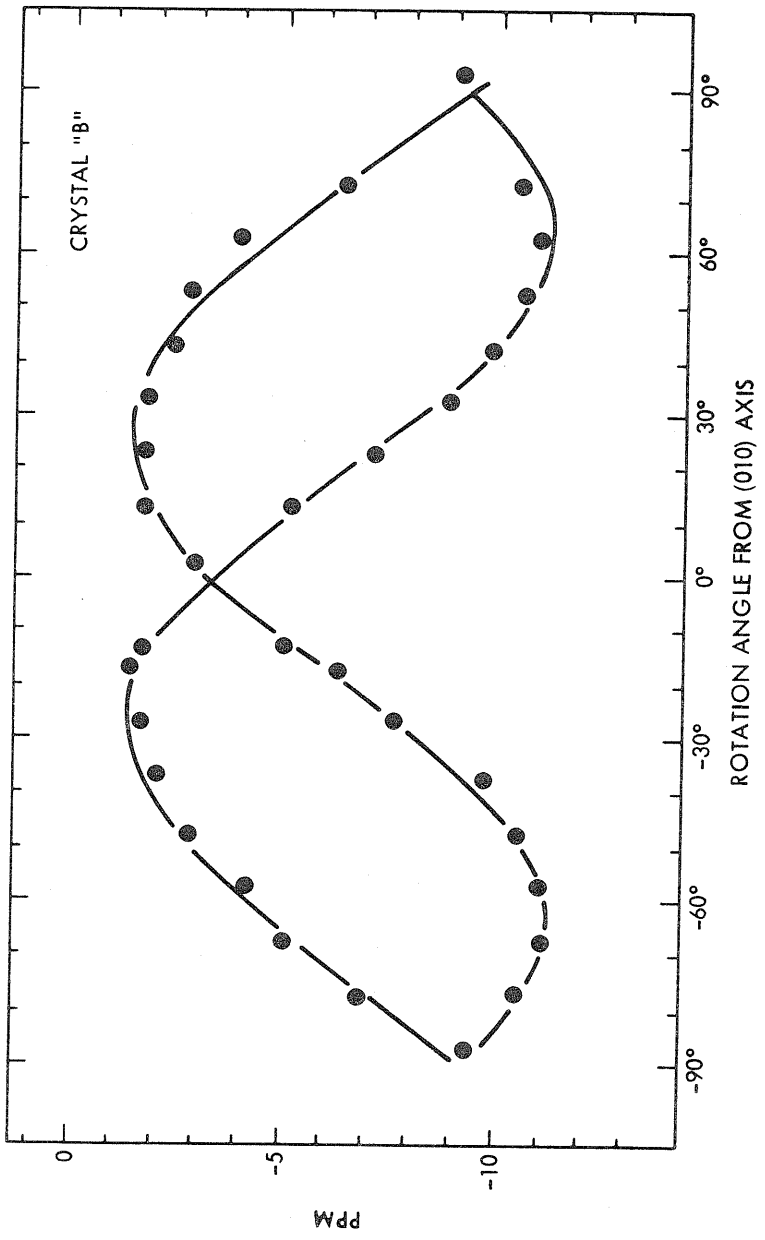
CRYSTAL "B"
ppm
0
-5
-10
-90°
-60°
-30°
0°
30°
60°
90°
ROTATION ANGLE FROM (010) AXIS

Fig. 3

Chapter III

Observation and Utilization of Thermodynamic Phenomena in Strongly Time Dependent Interaction Frames

Section 1

Introduction

In this chapter, the thermodynamic relaxation of the nuclear spin system due to coupling with the lattice is treated theoretically for several multiple pulse experiments. The applicability of the thermodynamic spin temperature hypothesis[1] in strongly time dependent interaction frames is demonstrated through the development of several pulse techniques which yield results predictable by thermodynamic arguments. These new techniques are important additions to NMR technology because they provide tremendously increased data rates ($\geq 10^2$ or 10^3) as compared to the cw techniques in use. This is because the transient response of the system can be measured in between pulses throughout the pulse train, whereas techniques involving cw irradiation only allow the magnetization to be sampled at the end of the experiment. Thus the cw experiment must be repeated many times, while the time development of the system can be characterized by a single application of the multiple pulse technique.

In Chapter II the time development of the nuclear spin system during various multiple pulse experiments was predicted and interpreted through the application of a coherent averaging theory based on the Magnus expansion[2] which was first applied to NMR by Evans.[3] This theory is very useful for analyzing the behavior of the system under many circumstances, but it cannot fully explain relaxation phenomena because it contains no information regarding the thermodynamic coupling of the spin system with its environment. For example, consider a train of identical, equally spaced ($\pi/2$), pulses applied to a dipolar solid. Four pulses make a cycle for which, assuming δ-function pulse shapes,[4]

$$\bar{\mathcal{H}}_D^{(0)} = -(1/2)\mathcal{H}_D^{(x)} \tag{1}$$

$$\bar{\mathcal{H}}_D^{(1)} = \phi \tag{2}$$

This result is also obtained for continuous irradiation with the same average amplitude. Therefore, one would expect similar behavior of the spin system during either form of rf irradiation. In particular, since

$$[I_x; \mathcal{H}_D^{(x)}] = \phi \qquad (3)$$

one would expect magnetization in the x-direction to remain "locked", i.e. to decay very slowly, during both experiments. However, this is not what is observed. Instead, the magnetization in the x direction decays much more rapidly for the pulsed case than for the cw experiment. This effect is called spin heating.

In the following sections the phenomenon of spin heating is shown to be caused by an interaction between the first Fourier component of the pulse train and the precession frequency of the magnetization in the rotating frame due to the average rf field. It is shown that this effect can be made arbitrarily small by reducing the neutation angle of the pulses. The thermodynamic behavior of the spin system during these "small angle" experiments is demonstrated by observing adiabatic demagnetization in the rotating frame (ADRF) during an amplitude modulated rf pulse train. The decay time of the magnetization during pulsed spin locking is calculated, and this calculation is verified by measurements performed on solid C_6F_6 and C_6F_{12}. A pulsed version of a method for determining the first moment of an NMR spectrum is introduced and is used to measure shifts in the resonance positions of CaF_2 and BaF_2 as a function of external pressure.

In the final section of this chapter, a single scan experiment for measuring the spin-lattice relaxation time of a solid is introduced and compared to the multiple scan method using a polycrystalline sample of frozen C_6F_6. This single scan technique utilizes the 2-pulse solid echo sequence[5] in

monitoring the time development of the system, thus minimizing the loss of magnitization during sampling. It is shown that the residual perturbation of the system due to the measurement process can be considered a form of thermodynamic spin heating, although caused by a different mechanism than the spin heating discussed above. By measuring the strength of the spin heating it is possible to obtain undistorted relaxation times using this technique.

References

1. M. Goldman, Spin Temperature and Nuclear Magnetic Resonance in Solids, Oxford Univ. Press (1970).

2. W. Magnus, Commun. Pure Appl. Math. 7, 649 (1954).

3. W. A. B. Evans, Ann. Phys. 48, 72 (1968).

4. See Chapter II, Section 2.

5. J. G. Powles and P. Mansfield, Phys. Lett. 2, 58 (1962).
J. G. Powles and J. H. Strange, Proc. Phys. Soc. 82, 6 (1963).
P. Mansfield, Phys. Rev. A137, 961 (1965).

Section 2

Elimination of Spin Heating in Multiple Pulse Experiments

(Most of the material in this section is drawn from the following articles:

W. K. Rhim, D. P. Burum and D. D. Elleman,
Phys. Rev. Lett. 37, 1764 (1976)

W. K. Rhim, D. P. Burum and D. D. Elleman,
Proc. XIXth Congress Ampere, 225 (1976)

W. K. Rhim, D. P. Burum and D. D. Elleman,
Phys. Lett. 62A, 507 (1977).)

This section is concerned with spin heating for the case in which a dipolar solid is irradiated by a string of identical rf pulses near resonance. In general the harmonics which are generated by such a pulse train will interact with the spin system in a complicated way. However, if the fundamental frequency Ω is much larger than the average rf strength $\gamma\bar{H}_1$, resonance offset frequency $\gamma\Delta H$ and local field γH_{loc}, all the higher harmonics can be safely neglected. The problem is then reduced to one in which the rf amplitude is sinusoidally modulated.[1]

The Hamiltonian for this case is given by

$$\mathcal{H}_R = -\Delta\omega I_z - \bar{\omega}_1(1 + \eta\cos\Omega t)I_x + \mathcal{H}_D^{(z)} \quad , \tag{1}$$

where $\bar{\omega}_1 = \gamma H_1$, $\Delta\omega$ is the resonance offset frequency and η in the modulation constant, which is ≈ 1. The explicit time dependence of the Zeeman term in eq. (1) can be transferred to the dipolar part if we move to an "oscillating frame" by the transformation

$$U_1 = \exp\left\{i\, I_x \frac{\eta\bar{\omega}_1}{\Omega}\ \sin\Omega t\right\} \tag{2}$$

The transformed Hamiltonian is given by

$$\mathcal{H}_{RU} = -\Delta\omega J_o\left(\frac{\eta\bar{\omega}_1}{\Omega}\right) I_z - \bar{\omega}_1\, I_x + \mathcal{H}_D^{(z)} + \mathcal{H}_\varepsilon(t) \tag{3}$$

$$\equiv -\vec{\omega}_e\cdot\vec{I} + \mathcal{H}_D^{(z)} + \mathcal{H}_\varepsilon(t), \tag{4}$$

where $\omega_e^2 = \left[\Delta\omega J_o\left(\frac{\eta\bar{\omega}_1}{\Omega}\right)\right]^2 + \bar{\omega}_1^2$, (5)

$$\mathcal{H}_\varepsilon(t) = -\Delta\omega \sum_{k=-\infty}^{\infty}{}' J_k\left(\frac{\eta\bar{\omega}_1}{\Omega}\right)(I_z \cos k\Omega t - I_y \sin k\Omega t) \tag{6}$$

$$+ \left[J_o\left(\frac{2\eta\bar{\omega}_1}{\Omega}\right) - 1\right](G_2 - G_{-2})$$

$$+ \sum_{k=-\infty}^{\infty}{}' J_k\left(\frac{2\eta\bar{\omega}_1}{\Omega}\right)\left(G_2 e^{i2k\Omega t} + G_{-2}e^{-i2k\Omega t}\right)$$

and $$G_{\pm 2} = (1/12)\left(\mathcal{H}_D^{(z)} - \mathcal{H}_D^{(y)} \mp \left[I_x, \mathcal{H}_D^{(z)}\right]\right) \tag{7}$$

In eq. (6), Σ' designates omission of the term for k=0 from the summation.

$\mathcal{H}_\varepsilon(t)$ can be made arbitrarily small for large Ω by reducing the pulse angle, and thus reducing the arguments of the Bessel functions in eq. (6). For instance, for 36^o rf pulses, $2\bar{\omega}_1/\Omega = .2$, $J_o(.2) = .99$, $J_1(.2) = .1$ and the higher order Bessel functions are even smaller. A similar argument was also given by Waugh and Wang[1] in their analysis of the generalized Ostroff-Waugh sequence, but they discussed only larger pulse angles. The major point of this discussion is that $\mathcal{H}_\varepsilon(t)$ can be made small enough to be treated by perturbation theory even when the Zeeman term and $\mathcal{H}_D^{(z)}$ in eq. (4) are comparable in size. $\mathcal{H}_{RU}$ in eq. (4) is essentially identical in form to the continuous irradiation case if $\mathcal{H}_E(t) \approx 0$. For $\omega_e \approx \|\mathcal{H}_D^{(z)}\|$, the system obtains a common spin temperature within a time of the order of T_2,[2,3] and the system can then be described by the spin temperature T_s, with the semi-equilibrium density matrix given by

$$\sigma_{RU} = 1 - \frac{\hbar}{kT_s}\left(-\vec{\omega}_e \cdot \vec{I} + \mathcal{H}_D^{(z)}\right) \tag{8}$$

The spin temperature hypothesis[3] can thus be used to explain various experiments performed during the time interval

$$T_2 << t << \|\mathcal{H}_\varepsilon(t)\|^{-1} \tag{9}$$

The above reasoning was tested experimentally using a CaF_2 single crystal oriented with its (111) direction approximately along the static magnetic field. Using discrete rf pulses, the spectrometer was adjusted at exact resonance to produce a conventional Ostroff-Waugh sequence[5] (i.e., $(90^\circ)_y[\tau\,(90^\circ)_x\tau\,]^n$) with $\tau = 10\ \mu$sec, and the decay time constant $T_{1e} = 29.5$ msec was observed. Under the same conditions, we reduced the pulse angle θ_x to $(45^\circ)_x$, the only effect of which was to reduce the arguments of the Bessel functions in eq. (6). The result was a considerable prolongation of $T_{1e} = 1.057$ sec. T_{1e} took on intermediate values at other pulse angles between these two.

Now, suppose only the spacing between the pulses is changed. Since $2\eta\bar{\omega}_1/\Omega = \eta\theta/\pi$ is independant of $\Omega = \pi/\tau$, increasing Ω will simply increase the frequency of the sinusoidal oscillations in $\mathcal{H}_\varepsilon(t)$, resulting in a better averaging effect. Fig. 2 shows this effect for three different pulse angles. The decay constant was recorded as a function of average rf field; i.e., $\bar{H}_1 = \theta\Omega/(2\pi\gamma)$, for three different values of θ. As can be seen in this figure, increasing Ω has a very strong averaging effect, increasingly so for smaller values of θ. The saturation of T_{1e} above the 1 second level is caused by the spin lattice interaction, which was confirmed by performing a separate cw locking experiment. Thus the saturated $T_{1e} = T_{1\rho}$.

Having seen that $\mathcal{H}_\varepsilon(t)$ can easily be made much smaller than the inverse cross relaxation time between the Zeeman and dipolar reservoirs, we can now test whether the system truly achieves a common spin temperature after a few θ_x pulses following the initiating $(90^\circ)_y$ pulse. If this is the case, the magnetization M_z of this semi-equilibrium state should obey the formula

$$\frac{M_z}{M_o} = \frac{\bar{H}_1^2}{\bar{H}_1^2 + H_{loc}^2} \quad , \tag{10}$$

which is identical in its form to the c.w. locking experiment with a 90^o prepulse. Here M_o is the equilibrium magnetization before the initiating $(90^o)_y$ pulse is applied and $H_{loc}^2 = Tr(\mathcal{H}_D^{(z)})^2/(\gamma^2 Tr(I_z^2))$. The actual variation of $\bar{H}_1$ was accomplished by changing the pulse angle as well as the pulse spacing. The measured magnetization is shown in Fig. 3, together with the theoretical curve from eq. (10) with $H_{loc} \approx$ 1.1 gauss. Considering the uncertainty in crystal orientation, this figure provides convincing evidence that the spin temperature hypothesis is well justified for this pulsed spin locking case.

A slow modulation can also be imposed on the values of θ_x in the same pulse sequence, thus causing the spin system to follow $\bar{H}_1$ isentropically, which is analogous to the c.w. case. By sampling the signal between rf pulses, we observed the adiabatic demagnetization and inverse remagnetization process almost instantly. Fig. 4a shows the slow amplitude modulation of the rf burst, and Fig. 4b is the result obtained during such an adiabatic process. In the remagnetization process the rf carrier phase was changed by 180^o compared to the demagnetization process, producing inverse remagnetization. In this experiment the magnetization was proportional to $\bar{H}_1/(\bar{H}_1^2 + H_{loc}^2)^{1/2}$ as expected for an adiabatic process.[3]

ADRF was also observed using pulse sequences for which θ is gradually varied past an integral multiple of π.

Figure 5 shows the rf pulse sequence used. After the spin system reached its thermal equilibrium polarization in a strong magnetic field, a $(\frac{\pi}{2})_x$ pulse initiated the pulse sequence. This was followed by a string of near $(n\pi)_y$ pulses which were separated by a time $\tau < T_2$. The amplitude of these pulses was slowly varied in such a way that the pulses started with angles slightly larger than $n\pi$ and gradually decreased in angle to below $n\pi$.

The NMR signal from a single crystal of CaF_2 as observed between the rf pulses is shown in Figure 6. Starting from a large initial polarization, it decreased to zero as the pulse angle approached $n\pi$. The polarization then continued to a negative value as the pulse angle decreased below $n\pi$. The nutation angle of the pulses used to obtain Figure 6 was near π. However, a similar effect was also observed using pulses near 2π.

The observed effect can be qualitatively explained using average Hamiltonian theory.[6] The Hamiltonian in the rotating frame is given by

$$\mathcal{H}_R = -\Delta\omega I_Z + \mathcal{H}_D + \mathcal{H}_{rf}(t) \tag{11}$$

where the first term is the off-resonance term, $\mathcal{H}_D$ is the secular part of dipolar interaction and $\mathcal{H}_{rf}(t)$ is due to the applied rf pulse sequence. $\mathcal{H}_{rf}(t)$ can be decomposed into two terms:

$$\mathcal{H}_{rf}(t) = \mathcal{H}_{rf}^{(1)}(t) + \mathcal{H}_{rf}^{(2)}(t) \tag{12}$$

where $\mathcal{H}_{rf}^{(1)}(t)$ is the term in which all the pulses are assumed to have nutation pulse angles exactly equal to $n\pi$ and $\mathcal{H}_{rf}^{(2)}(t)$ is made up of the small differences between $\mathcal{H}_{rf}(t)$ and $\mathcal{H}_{rf}^{(1)}(t)$. By moving to an interaction representation, assuming δ-function pulse shapes, we separate out the large time dependent term $\mathcal{H}_{rf}^{(1)}(t)$ from the rest of the terms, and then calculate the average Hamiltonian in this toggling frame. The average Hamiltonian so obtained is given by

$$\bar{\mathcal{H}}_{RT} = -\Delta\omega I_Z - \overline{\Delta\omega}_1 I_x + \mathcal{H}_D \qquad \text{for n even} \qquad (13)$$

$$= \qquad -\overline{\Delta\omega}_1 I_x + \mathcal{H}_D \qquad \text{for n odd}$$

where the off-resonance term disappears for n odd and $\overline{\Delta\omega}_1$ is due to the average of $\mathcal{H}_{rf}^{(2)}$ alone. In either case, the Hamiltonian has a form identical to that which would be obtained if a continuous rf irradiation were applied. Therefore, for $\Delta\omega << \overline{\Delta\omega}_1$, the nuclear polarization which was initially locked along the effective field ($\vec{\gamma H}_{eff} \simeq \overline{\Delta\omega}_1 \hat{x}$) can be adiabatically demagnetized as $\overline{\Delta\omega}$ gradually approaches zero and inversely repolarized as $\overline{\Delta\omega}$ changes its sign. This is exactly what is shown in Figure 6.

For solids with large dipolar interactions, the effect of n being even or odd could not be easily distinguished, even though the off-resonance term causes their effective Hamiltonians to be different. However, a definite distinction was easily observed in liquid samples due to the appearance of a rotary spin echo[7] only when n was even.

The experiment was performed at slightly off-resonance using the pulse sequence given in Figure 1 but without the initiating $(\frac{\pi}{2})_x$ pulse. In this case the signal was observed along the x-direction instead of the y-direction. Since rf inhomogeneity was present, we initially expected the signal to decay in an ordinary way. In fact, for odd n, the signal decayed and no echo was observed. However, when n was even, a strong rotary echo appeared. Figure 7 shows a typical example of the echo phenomenon, where in this case n = 2. The explanation for the appearance of an echo should be clear when one notes that the magnetization changes its sign due to the adiabatic process, while the rf inhomogeneity remains unchanged throughout the pulse string.

It is important to note that near $n\pi$ pulse strings with $|n| > 0$ provide alternate methods of achieving the large values of $\overline{H}_1$ which are required in many $T_{1\rho}$ experiments.[8]

References

1. J. S. Waugh and C. H. Wang, Phys. Rev. 162, 209 (1967).

2. A. Abragam, The Principles of Nuclear Magnetism, Oxford Univ. Press (1961).

3. M. Goldman, Spin Temperature and Nuclear Magnetic Resonance in Solids, Oxford Univ. Press (1970).

4. S. R. Hartman and E. L. Hahn, Phys. Rev. 128, 2042 (1962).

5. E. D. Ostroff and J. S. Waugh, Phys. Rev. Letters 16, 1097 (1966). P. Mansfield and D. Ware, Phys. Lett. 22, 133 (1966).

6. Chapter II, Section 2.

7. I. Solomon, Phys. Rev. Lett. 2, 301 (1959).

8. Section 3.

FIGURE CAPTIONS

Figure 1. Decay curves for two different pulse angles. The pulse spacing was the same for each and the decays showed good exponential behavior after a few T_2's. Note the large increase in decay constant in going from 90^o to 45^o. The sample was a single crystal of CaF_2 with its (111) axis approximately aligned along H_o.

Figure 2. The decay constant T_{1e} as a function of average rf field $\bar{H}_1$ for three different values of pulse angle. The data points are smoothly connected by dashed lines. A CaF_2 single crystal with its (111) axis oriented approximately along H_o was used as the sample.

Figure 3. Initial semi-equilibrium values of the magnetization as a function of average rf field strength. The dotted line is the theoretical curve (eq. (10)), with H_{loc} = 1.1 gauss. Various $\bar{H}_1$ values were achieved by changing both the spacing and the angles of the pulses. A CaF_2 single crystal with its (111) axis oriented approximately along H_o was used as the sample.

Figure 4. Demonstration of adiabatic demagnetization in the rotating frame: (a) the modulation envelope of the rf burst; (b) the corresponding signal sampled between rf pulses. The maximum $\bar{H}_1 \approx 2$ gauss and the horizontal scale is 5 msec/cm. In the remagnetization process the rf phase was changed by 180^o, producing inverse remagnetization.

Figure Captions

Figure 5: rf pulse sequence to observe ADRF using near $n\pi$ pulses. τ = 20 μsec, rf pulse width ≃ 8 μsec.

Figure 6: Adiabatic demagnetization and inverse repolarization process in a CaF_2 crystal near the (111) direction. The maximum signal amplitude is about half of the fid signal amplitude, and the maximum pulse angle was ≃ 210°. (Horizontal scale: 2 msec/cm).

Figure 7: Rotary spin echo signal observed in liquid C_6F_6 when n = 2. The pulse sequence in Figure 5 was used with the $(\frac{\pi}{2})_x$ prepulse omitted and the signal was detected along the x-direction. (Horizontal scale: 2 msec/cm).

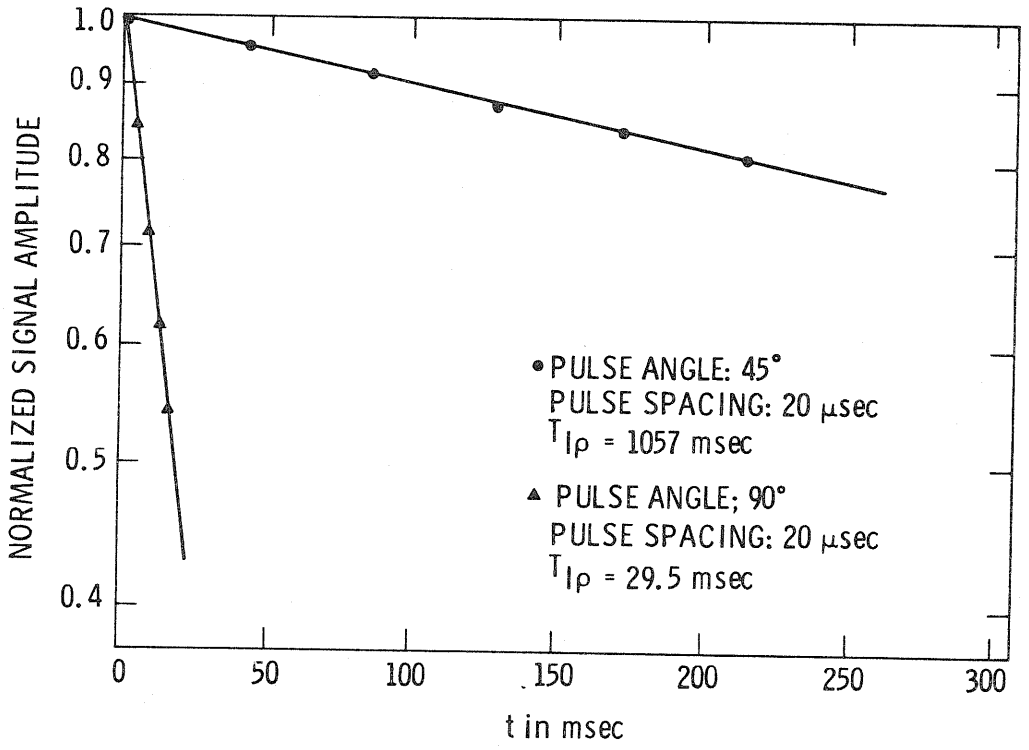
NORMALIZED SIGNAL AMPLITUDE
1.0
0.9
0.8
0.7
0.6
0.5
0.4
0
50
100
150
200
250
300
t in msec
• PULSE ANGLE: 45°
PULSE SPACING: 20 μsec
$T_{1\rho}$ = 1057 msec
▲ PULSE ANGLE; 90°
PULSE SPACING: 20 μsec
$T_{1\rho}$ = 29.5 msec

Fig. 1

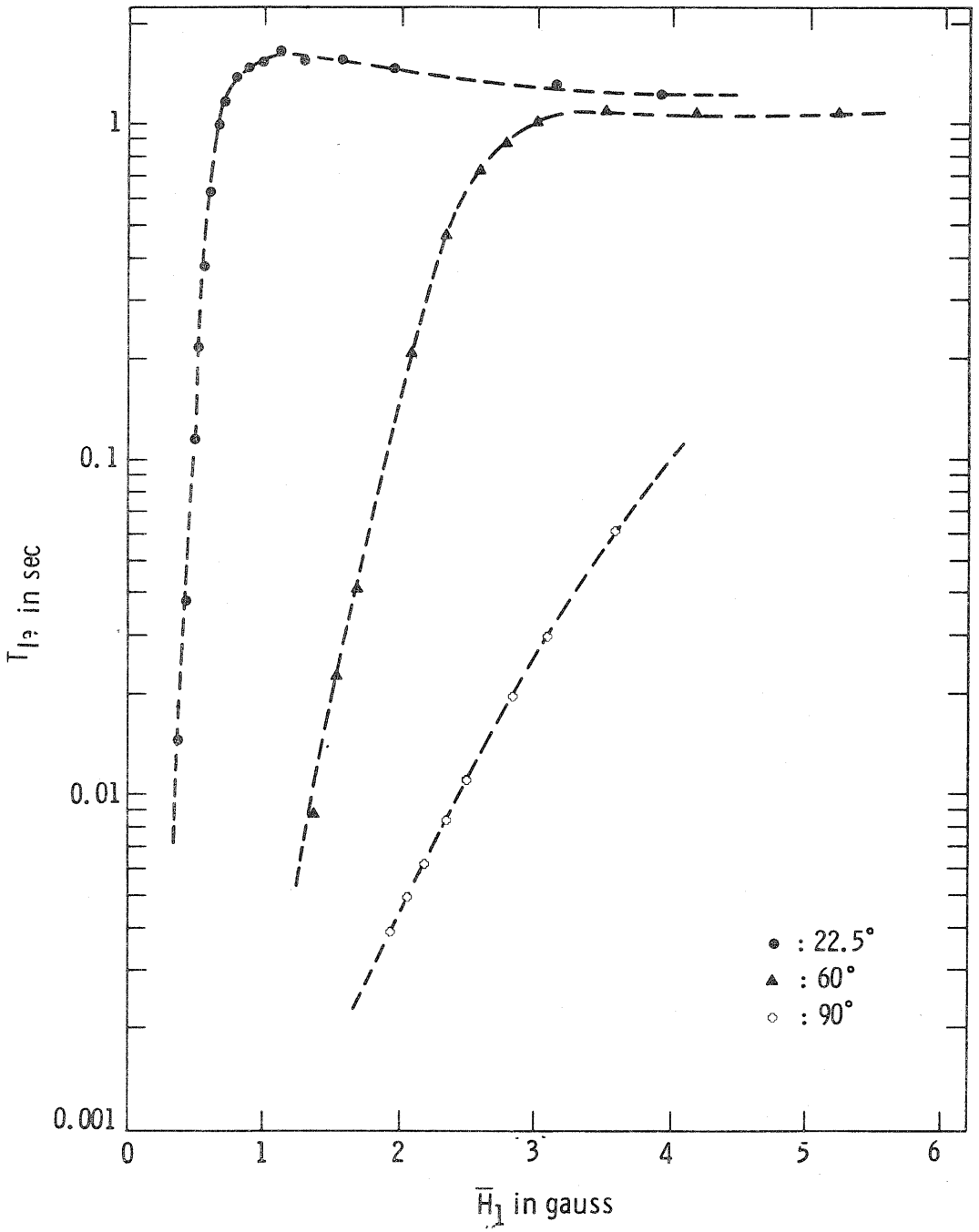
1
0.1
0.01
0.001
$T_{1\rho}$ in sec
0
1
2
3
4
5
6
$\overline{H}_1$ in gauss
● : 22.5°
▲ : 60°
○ : 90°

Fig. 2

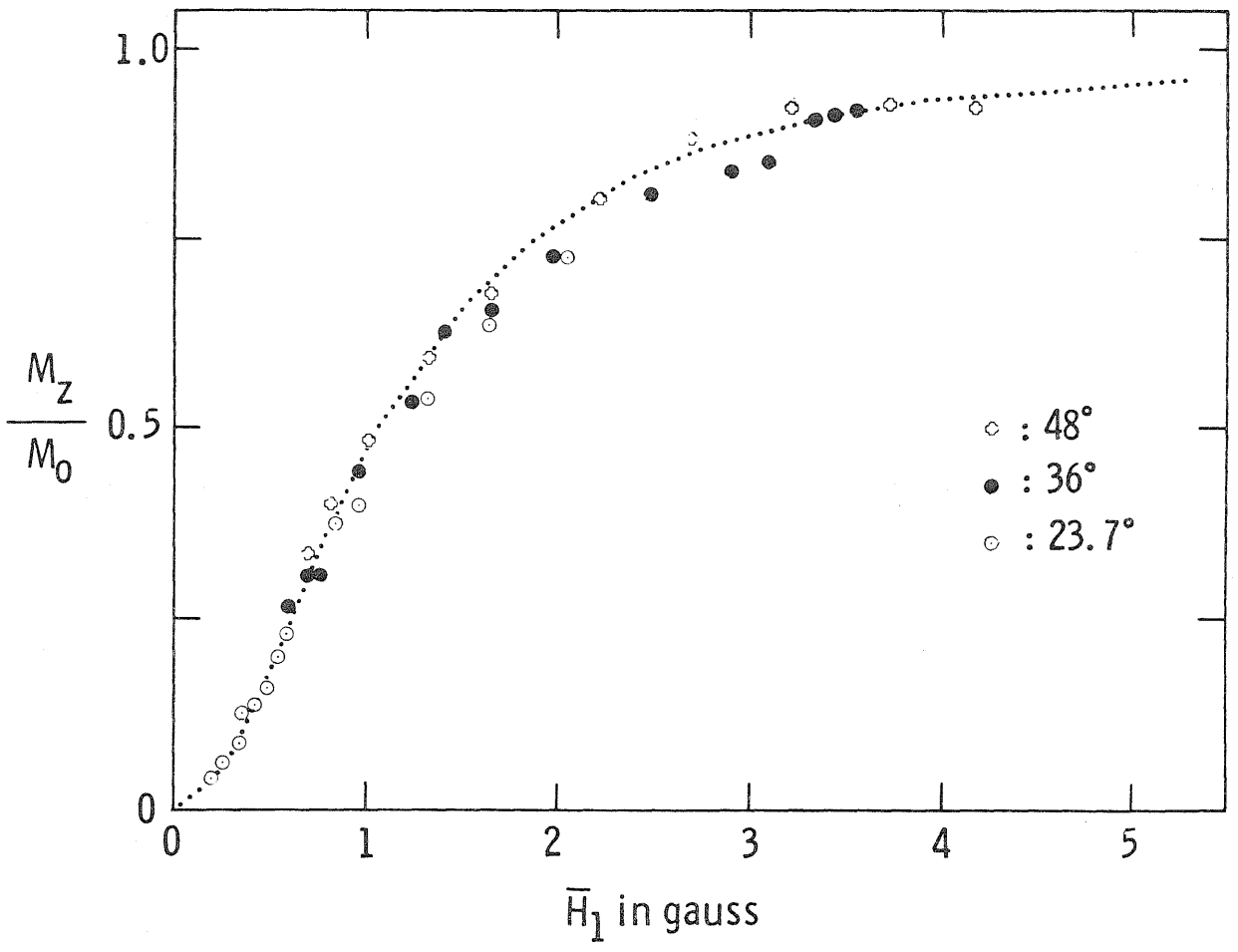

Fig. 3

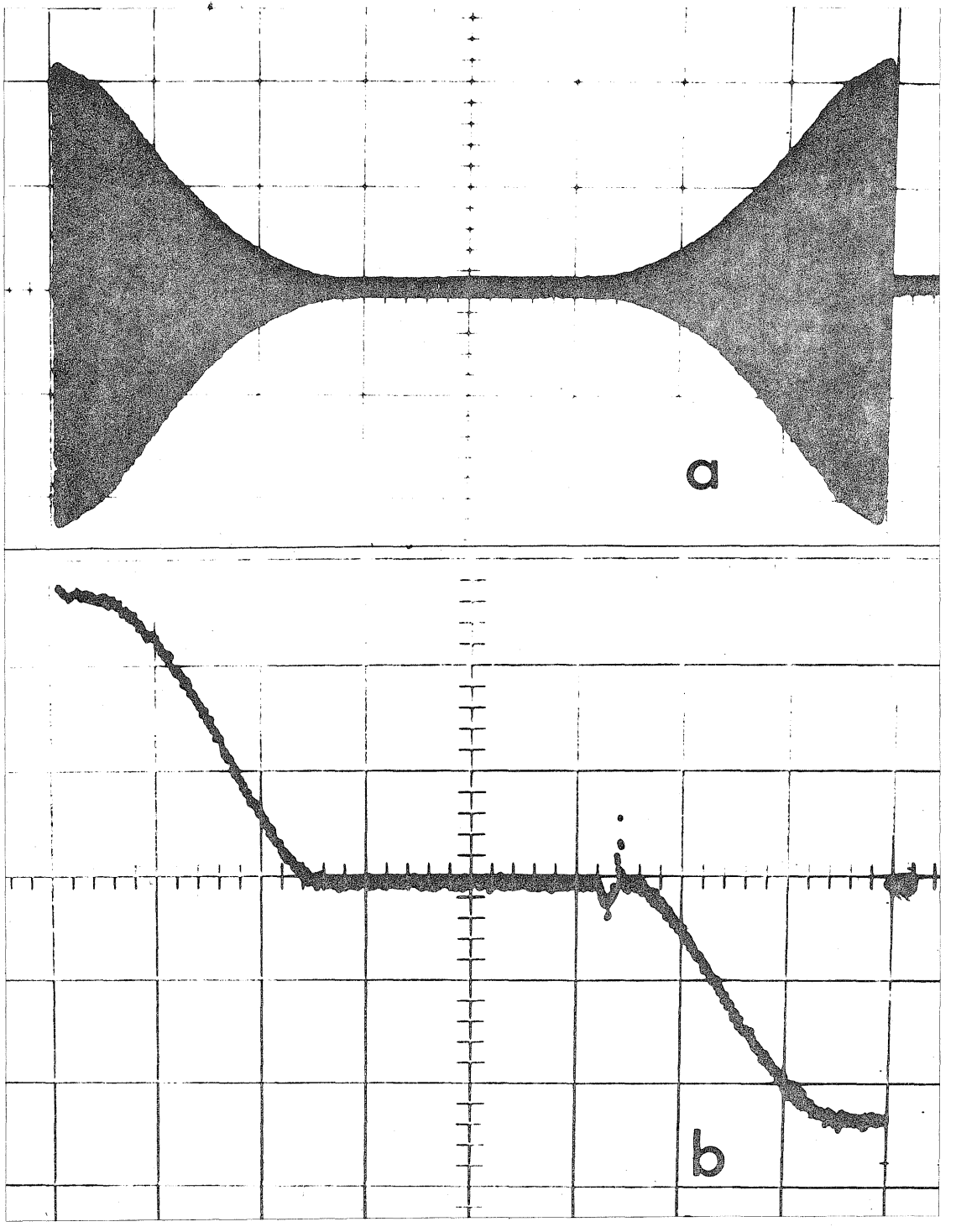

Fig. 4

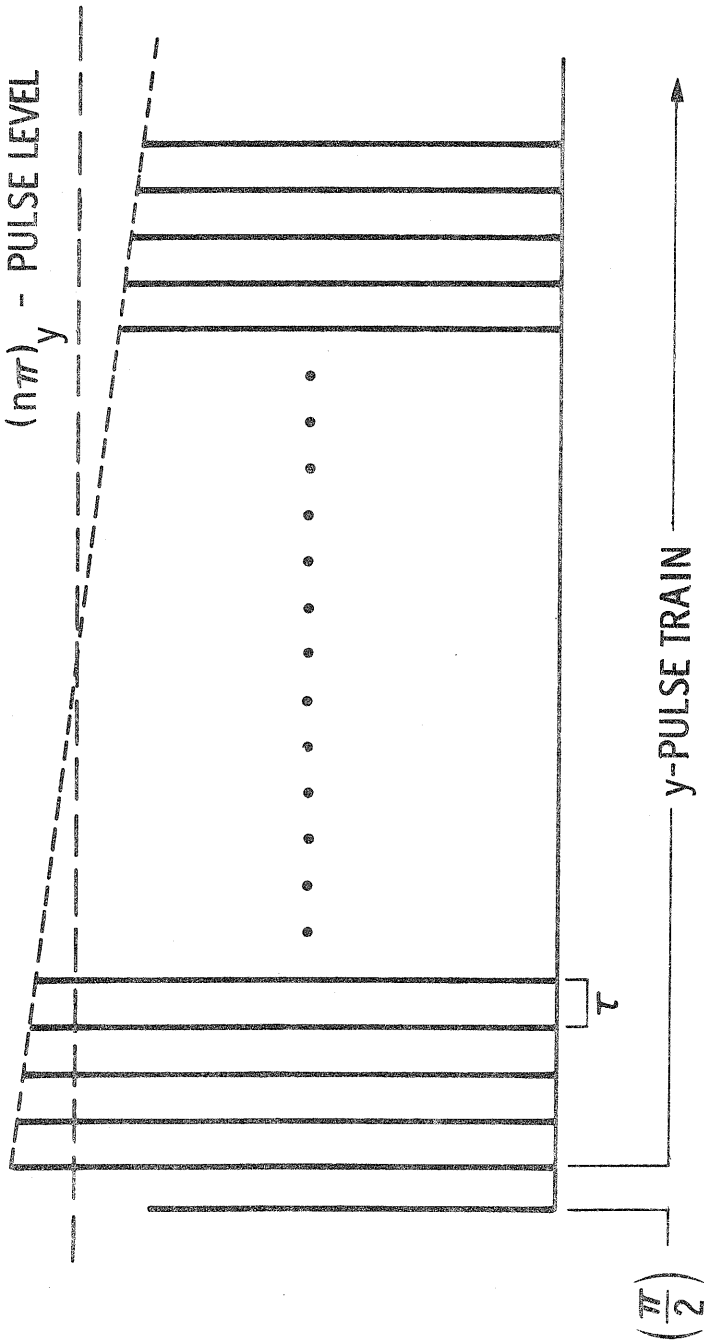

Fig. 5

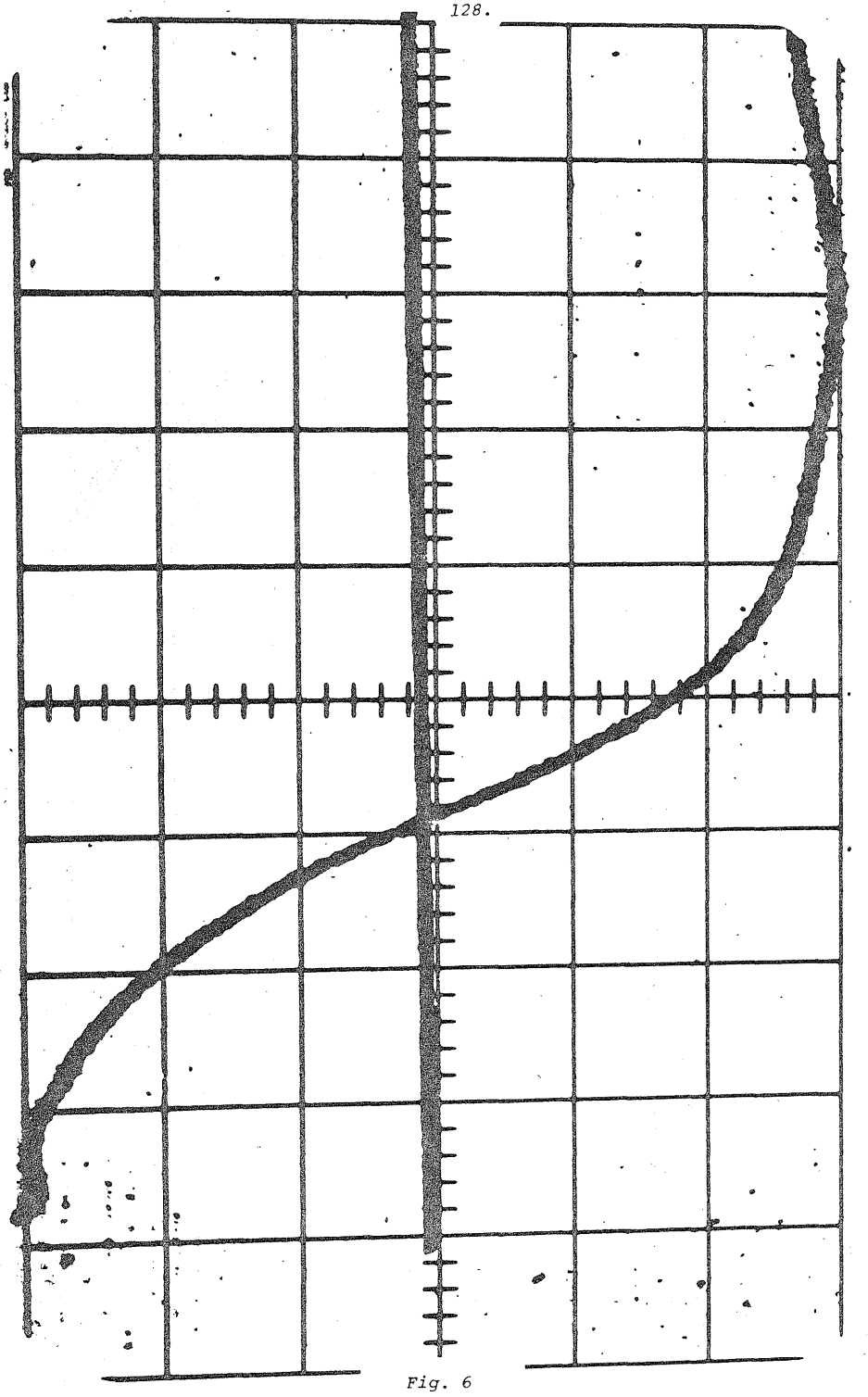

Fig. 6

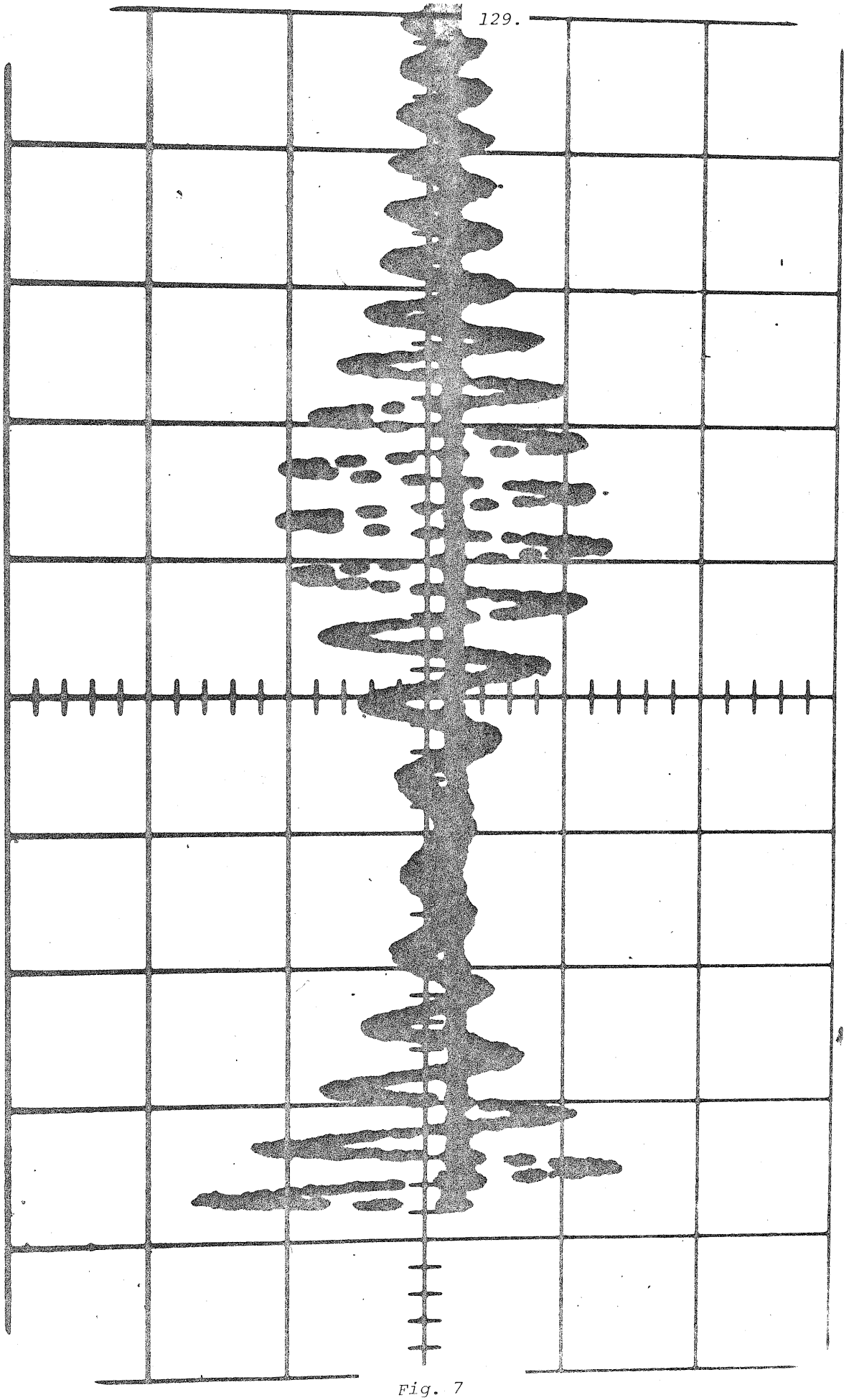

Fig. 7

Section 3

Calculation of Spin-Lattice Relaxation During Pulsed Spin Locking in Solids

(Most of this section is an article by W. K. Rhim, D. P. Burum and D. D. Elleman, J. Chem. Phys. 68, 692 (1978)).

A. INTRODUCTION

The calculation made in the previous section assumed that the string of rf pulses was applied with a repetition rate, or fundamental frequency Ω, which was much greater than the average rf strength $\gamma\bar{H}_1$, the resonance offset $\gamma\Delta H$ and the local field γH_{loc}. The more general case is analyzed in this section. It is assumed that the direct spin heating effect can be neglected, and a calculation is presented of the spin lattice relaxation time due to molecular motion in a dipolar solid when it is irradiated by a train of identical rf pulses with arbitrary nutation angle and finite width. From the resulting formula it is easy to obtain the results which have been previously derived for special cases using $\pi/2$ pulses.[1] For heteronuclear spin systems the relaxation time has been calculated only for δ-function pulses of arbitrary angle. Finally, experimental confirmation is given for a homonuclear dipolar system (C_6F_{12}) which establishes the validity of the general relaxation time formula.

B. THEORY

In this sub-section, a calculation is made of the spin lattice relaxation time, T_{1e}, of a dipolar solid when it is irradiated by a train of identical, rectangular x-pulses. Each of the pulses has nutation angle θ and pulse width t_w, as shown in figure 1, and the time between pulses, 2τ, is assumed to be much shorter than T_2. The procedure for our calculation is essentially similar to that of Gründer *et al*.[1]

At exact resonance, the Hamiltonian of the spin system in the rotating frame is given by

$$\mathcal{H}(t) = \mathcal{H}_D(t) - \omega_1 I_x g(t) \tag{1}$$

where g(t) is the rf amplitude modulation function, which alternates between 1 and 0 for the pulse sequence under consideration, and $\mathcal{H}_D(t)$ is the secular part of the homo- and heteronuclear dipolar interactions given by

$$\mathcal{H}_D(t) = \sum_{i<j} B_{ij}(t)(\vec{I}_i \cdot \vec{I}_j - 3 I_{zi} I_{zj}) + \sum_{i,j} C_{ij}(t) I_{zi} S_{zj} . \tag{2}$$

The normalized signal along the x-axis is given by

$$I_x(t) = \frac{\mathrm{Tr}\{U(t)\ I_x\ U^{-1}(t)\ I_x\}}{\mathrm{Tr}\{I_x^2\}} \tag{3}$$

where U(t) can be expressed using the time ordering operator, T, as

$$U(t) = \mathrm{Texp}\{-i\int_0^t \mathcal{H}(t')dt'\} \quad . \tag{4}$$

By separating out the coherent rf part of U(t), one obtains

$$U(t) = U_{rf}(t)U_{int}(t) \tag{5}$$

where

$$U_{rf}(t) = \mathrm{Texp}\{i\int_0^t \omega_1 g(t') I_x dt'\} \tag{6}$$

and

$$U_{int}(t) = \mathrm{Texp}\{-i\int_0^t \tilde{\mathcal{H}}_D(t')dt'\} \tag{7}$$

with

$$\tilde{\mathcal{H}}_D(t) = U_{rf}^{-1}(t)\mathcal{H}_D(t)U_{rf}(t) \quad . \tag{8}$$

Since $U_{rf}(t)$ commutes with I_x, eq. (3) can be rewritten as

$$\langle I_x(t)\rangle = \frac{\mathrm{Tr}\{U_{int}(t)\ I_x\ U_{int}^{-1}(t)\ I_x\}}{\mathrm{Tr}\{I_x^2\}} \tag{9}$$

By applying the Magnus expansion to eq.(7), one obtains

$$U_{int}(t) = \exp\{-i\sum_{n=0}^{\infty} F_n(t)\} \tag{10}$$

where

$$F_o(t) = \int_0^t \tilde{\mathcal{H}}_D(t_1)dt_1 \tag{11}$$

$$F_1(t) = -\frac{i}{2}\int_0^t dt_1 \int_0^{t_1} dt_2 [\tilde{\mathcal{H}}_D(t_1), \tilde{\mathcal{H}}_D(t_2)] \tag{12}$$

etc. Taking only the first term in eq.(10), and assuming a Gauss-Markoff process, eq.(9) can be written as

$$\langle I_x(t)\rangle = \exp\left\{\frac{\langle \mathrm{Tr}\{[F_o(t), I_x]^2\}\rangle_{av}}{2\,\mathrm{Tr}\{I_x^2\}}\right\} \tag{13}$$

where $\langle\ \rangle_{av}$ designates the ensemble average. Calculation of the spin lattice relaxation time, T_{1e}, is therefore reduced to the calculation of the exponent in eq.(13). For many specialized pulse sequences, such as the cw or $\theta = \pi/2$ cases, the calculation is simple and straightforward. For the more generalized pulse sequence, however, one must go through some tedious algebra.

(1) Homonuclear Case

Assuming an exponential correlation function defined by

$$\overline{B_{ij}(t_1)B_{ij}(t_2)} \equiv \overline{B_{ij}^2(0)}\exp\left\{\frac{-|t_1 - t_2|}{\tau_c}\right\}, \tag{14}$$

eq.(13) can be expressed for $t \gg \tau_c$ as

$$\langle I_x(t)\rangle = \exp\{-t/T_{1e}\}\ . \tag{15}$$

The full expression for T_{1e} in this case is given by

$$\frac{1}{T_{1e}} = \frac{M_2^{II}\tau}{2\alpha^2}\{[2\alpha_1 - \sinh(2\alpha_1) + D\sinh(2\alpha)]$$

$$+ \frac{1}{A_+}[\beta + 2\sinh(2\alpha_1) - 2D(\sinh(2\alpha) - \omega_1\tau_c\sin(2\theta))]$$

$$- \frac{A_-}{A_+^2}[\sinh(2\alpha_1) - D(\sinh(2\alpha) - 2\omega_1\tau_c\sin(2\theta))]\} \tag{16}$$

where M_2^{II} is the second moment of the homonuclear dipolar interaction, and the following definitions are made for other parameters:

$$\alpha = \tau/\tau_c$$

$$\alpha_1 = \tau_1/\tau_c$$

$$\beta = t_w/\tau_c$$

$$A_{\pm} = 1 \pm 4\omega_1^2\tau_c^2$$

and

$$D \equiv \frac{\cosh(2\alpha_1) - 1}{\cosh(2\alpha) - \cos(2\theta)} \quad . \tag{17}$$

Eq.(16a) can be expressed more compactly in the following way:

$$\frac{1}{T_{1e}} = \frac{M_2^{II}\tau}{2\alpha^2}\left\{2\alpha_1 + \frac{\beta}{A_+}\right.$$

$$- \frac{(2\omega_1\tau_c)^2}{A_+^2(\cosh 2\alpha - \cos 2\theta)}\,[A_-(\sinh\beta - \sinh 2\alpha + \sinh 2\alpha_1 \cos 2\theta)$$

$$\left. - 4\omega_1\tau_c(\cosh 2\alpha_1 - 1)\sin 2\theta]\right\}. \tag{16b}$$

A result which agrees with these expressions has also been obtained by Vega and Vaughan using the stochastic Liouville equation[2].

From eq.(16) the formulas for the following special cases can be immediately deduced, ie.

(i) For the Ostroff-Waugh[3] sequence, in which $\theta = \pi/2$, eq. (16) reduces to

$$\frac{1}{T_{1e}} = \frac{M_2^{II}\tau}{2\alpha^2}\{[2\alpha - \beta + \sinh\beta - (1 + \cosh\beta)\tanh\alpha]$$

$$+ \frac{1}{A_+}[\beta - 2\sinh\beta + 2(1 + \cosh\beta)\tanh\alpha]$$

$$- \frac{A_-}{A_+^2}[(1 + \cosh\beta)\tanh\alpha - \sinh\beta]\} \quad . \tag{18}$$

This is identical to the result obtained by Gründer et al.[1] It can be further simplified if we assume δ-function pulses:

$$\frac{1}{T_{1e}} = M_2^{II}\tau \frac{1}{\alpha}\left[1 - \frac{\tanh\alpha}{\alpha}\right] \quad . \tag{19}$$

(ii) Eq.(16) approaches the more familiar cw case as $\tau_1 \longrightarrow 0$, which implies that $2\alpha \longrightarrow \beta$, ie.

$$\frac{1}{T_{1e}} = \frac{M_2^{II}\tau_c}{1+4\omega_1^2\tau_c^2} \tag{20}$$

This is identical to the result obtained by Jones[4] and Look and Lowe[5].

(iii) For the case of δ-function pulses of angle θ, which we will find has a wider applicability, $A_{\pm} \rightarrow \pm\infty$, and T_{1e} is given by the following:

$$\frac{1}{T_{1e}} = M_2^{II}\tau_c \quad \{1 - \frac{\sinh(2\alpha)(1 - \cos 2\theta)}{2\alpha(\cosh(2\alpha) - \cos(2\theta))}\} \ . \tag{21}$$

Figure 2 is a graph of $T_{1e}M_2^{II}\tau$ as a function of τ_c/τ_1 which was obtained from eq. (16) for several values of θ and t_w/τ_1. The overall behavior of equation (16) can be seen more clearly if we observe the minimum values of $T_{1e}M_2^{II}\tau$ and the corresponding values of τ_c/τ as a function of t_w/τ_1 for different values of θ, as shown in Figures 3 and 4. From these figures we note the following behavior:

(i) For $t_w/\tau_1 < .1$, T_{1e} is essentially given by the formula for a δ-function pulse train, equation (21). Also, notice that the minimum values for θ and π-θ converge to the same value in this region.

(ii) For $t_w/\tau_1 > 10$, T_{1e} can be approximated by equation (20), which is valid in the cw rf irradiation case. In this region the values for θ and π-θ are distinctly different, as expected.

(iii) For $.1 < t_w/\tau_1 < 10$, a smooth transition takes place between the (i) and (ii) cases. For smaller values of θ we observe smaller changes between these two extremes. At $\theta = \pi/6$, for instance, the overall difference in $(T_{1e}M_2^{II}\tau)_{min}$ between $t_w/\tau_1 = .01$ and $t_w/\tau_1 = 100$ is about 9.1 %, and for $\theta = \pi/9$ the difference is only 4.3%. For $\theta = \pi/2$, however, the difference is 17.4%.

The above observations clearly show the advantage of using small values of θ. Namely, for small θ the direct spin heating effect is greatly reduced, as was realized in the previous section, while the spin lattice relaxation time, T_{1e}, closely approaches the value $T_{1\rho}$ which would be obtained in a continuous rf spin locking experiment.

(2) Heteronuclear Case

When a heteronuclear dipolar interaction is involved, equation (2) can be written

$$\mathcal{H}_D = \mathcal{H}_D^{II} + \mathcal{H}_D^{IS}. \tag{22}$$

The contributions of the homo- and heteronuclear parts of $\mathcal{H}_D$ to $\langle I_x(t)\rangle$ are separable, so that one can write

$$\langle I_x(t)\rangle = \langle I_x(t)\rangle^{II} \langle I_x(t)\rangle^{IS}, \tag{23}$$

where the II and IS terms are obtained from equation (13) when $\mathcal{H}_D$ in equation (8) is replaced by $\mathcal{H}_D^{II}$ and $\mathcal{H}_D^{IS}$, respectively. The result is that

$$\frac{1}{T_{1e}} = \frac{1}{T_{1e}^{II}} + \frac{1}{T_{1e}^{IS}}. \tag{24}$$

We have calculated the expression for T_{1e}^{IS} in the δ-function pulse limit. Our result is:

$$\frac{1}{T_{1e}^{IS}} = M_2^{IS}\tau_c \left\{ 1 - \frac{\sinh 2\alpha\ (1 - \cos\theta)}{2\alpha(\cosh 2\alpha - \cos\theta)} \right\}. \tag{25}$$

If $\theta = \pi/2$,

$$\frac{1}{T_{1e}^{IS}} = M_2^{IS}\tau_c \left\{ 1 - \frac{\tanh 2\alpha}{2\alpha} \right\}, \tag{26}$$

which again agrees with the result obtained by Gründer et al.[1,6]

C. EXPERIMENT

The experimental verification of equation (16) was carried out using commerical grade perfluorocyclohexane (C_6F_{12}) with unknown impurity content. Instead of the graphical representation shown in Figures 3 and 4, it was found to be more convenient for experimental verification to re-plot equation (16) as a function of θ for a number of different values of t_w/τ_1, as shown in Figures 5 and 6. It is clear from these figures that $(T_{1e}\tilde{M}_2^{II}\tau)_{min}$ is periodic with period π for the δ-function case, and gradually becomes a straight line as it approaches the cw case. Also, in Figure 5 we observe a region of θ in which the minimum value for the discrete pulse case exceeds the cw value. The experimental points in these figures were closely fit to the theoretical curves by assuming a value of .40 G^2 for M_2^{II}. This agrees reasonably well with the value .44 G^2 obtained by Fratiello and Douglass,[7] who assumed translational diffusion in addition to the fast rotational motion of the molecules. The values of τ_c/τ which correspond to the T_{1e} minimum points shown in Figure 5 are plotted in Figure 6. These experimental points were closely fit to the theoretical curve by assuming an activation energy of 12.35 Kcal/mole. This agrees well with the value of 12.5 Kcal/mole obtained by Roeder and Douglass.[8]

It should be clear from this section and the previous section that the spin-lattice relaxation time in the rotating frame during the application of the pulse sequence shown in figure 1 will be equal to the relaxation time for cw spin locking, $T_{1\rho}$, if $\theta_x/\pi \ll 1$. As an example, figure 6 compares values of $T_{1\rho}$ for frozen C_6F_6 obtained using the multiple pulse technique with measurements made by Albert et al.[9] using cw spin locking. The differences between the $T_{1\rho}$ curves at low temperature agree with the thermodynamic prediction according to the difference in average spin locking field strength. For example, the ratio of the two minima at 170°K is 1.82, which compares well with the predicted value 2.0. For the pulsed experiment $\theta_x = 30^\circ$ and $2\tau = 15$ μsec. It should be noted that the two $T_{1\rho}$ experiments yielded equivalent data, as can be seen in figure 6, but the data rate for the multiple pulse technique was roughly 10^3 greater than for the cw method.

REFERENCES

1. W. Gründer, H. Schmiedel and D. Freude, Ann. Phys. 27, 409 (1971).
W. Gründer, Wiss. Zeit Karl-Marx Univ., Leipzig 23, 466 (1974).

2. A. J. Vega and R. W. Vaughan, J. Chem. Phys. 68, 1958 (1968).

3. E. D. Ostroff and J. S. Waugh, Phys. Rev. Lett. 16, 1097 (1966).
P. Mansfield and D. Ware, Phys. Lett. 22, 133 (1966).

4. G. P. Jones, Phys. Rev. 148, 332 (1966).

5. D. C. Look and I. J. Lowe, J. Chem. Phys. 44, 2995 (1966).

6. Apparently, there is a typographical error in Gründer's expression for $\theta = \pi/2$ in reference 1 (1974). Our equation (26) agrees with his limiting cases for $\tau_c \gg \tau$ and $\tau_c \ll \tau$.

7. A. Fratiello and D. C. Douglass, J. Chem. Phys. 41, 974 (1964).

8. S. B. W. Roeder and D. C. Douglass, J. Chem. Phys. 52, 5525 (1970).

9. S. Albert,H. S. Gutowski and J. A. Ripmeester, J. Chem. Phys. 56, 2844 (1972).

FIGURE CAPTIONS

1. The rf pulse sequence analyzed in this paper. The initiating $(\pi/2)_y$ pulse is followed by a string of identical θ_x pulses.
2. Graphical representation of equation (16) as a function of τ_c/τ_l for different values of θ_x and t_w/τ_1.
3. $(T_{1e}M_2^{II}\tau)_{min}$ as a function of t_w/τ_1 for different values of θ_x.
4. τ_c/τ corresponding to $(T_{1e}M_2^{II}\tau)_{min}$ as a function of t_w/τ_1 for different values of θ_x.
5. $(T_{1e}M_2^{II}\tau)_{min}$ as a function of θ_x for different values of t_w/τ_1. Experimental values obtained using solid C_6F_{12} are also indicated.
6. Theoretical and experimental values of τ_c/τ corresponding to $(T_{1e}M_2^{II}\tau)_{min}$ as a function of θ_x for different values of t_w/τ_1.
7. $T_{1\rho}$ as a function of temperature for frozen C_6F_6. Data obtained using the pulsed spin locking technique shown in figure 1 are compared with results obtained by Albert et al. using cw spin locking. The average strength of the locking field is indicated for each curve. For the pulsed experiment $\theta = 30^o$ and $2\tau = 15$ μsec.

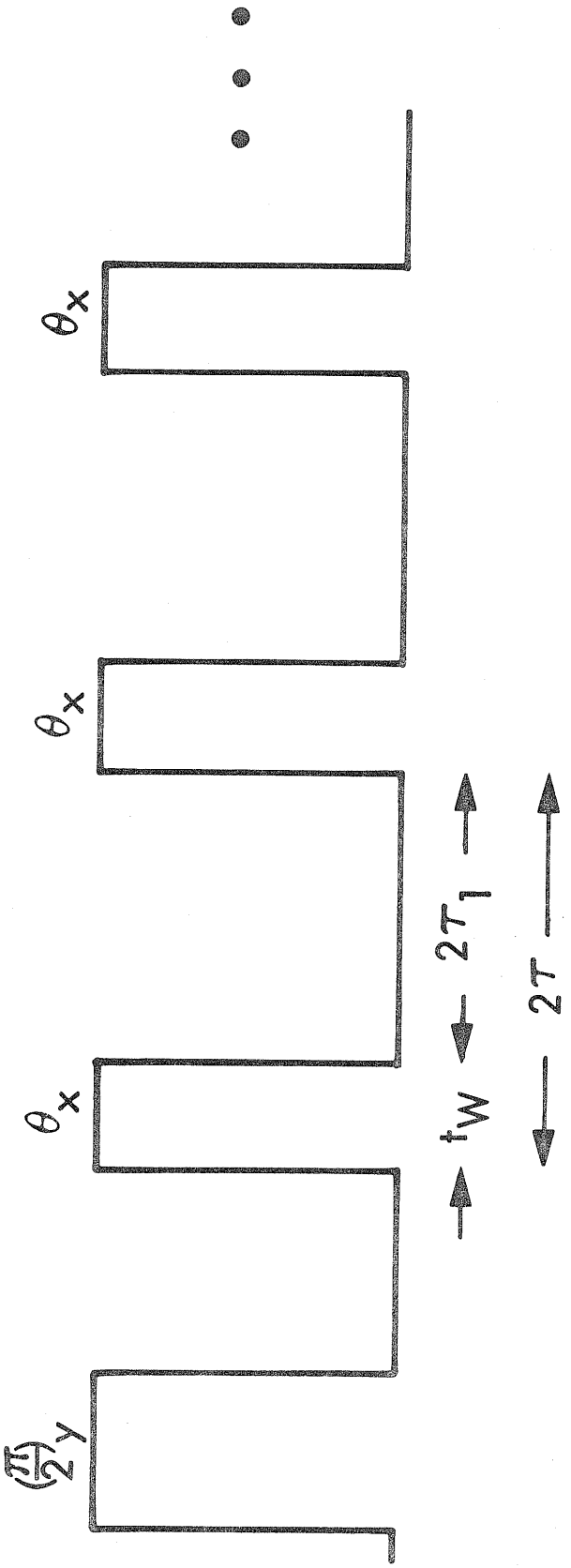

Fig. 1

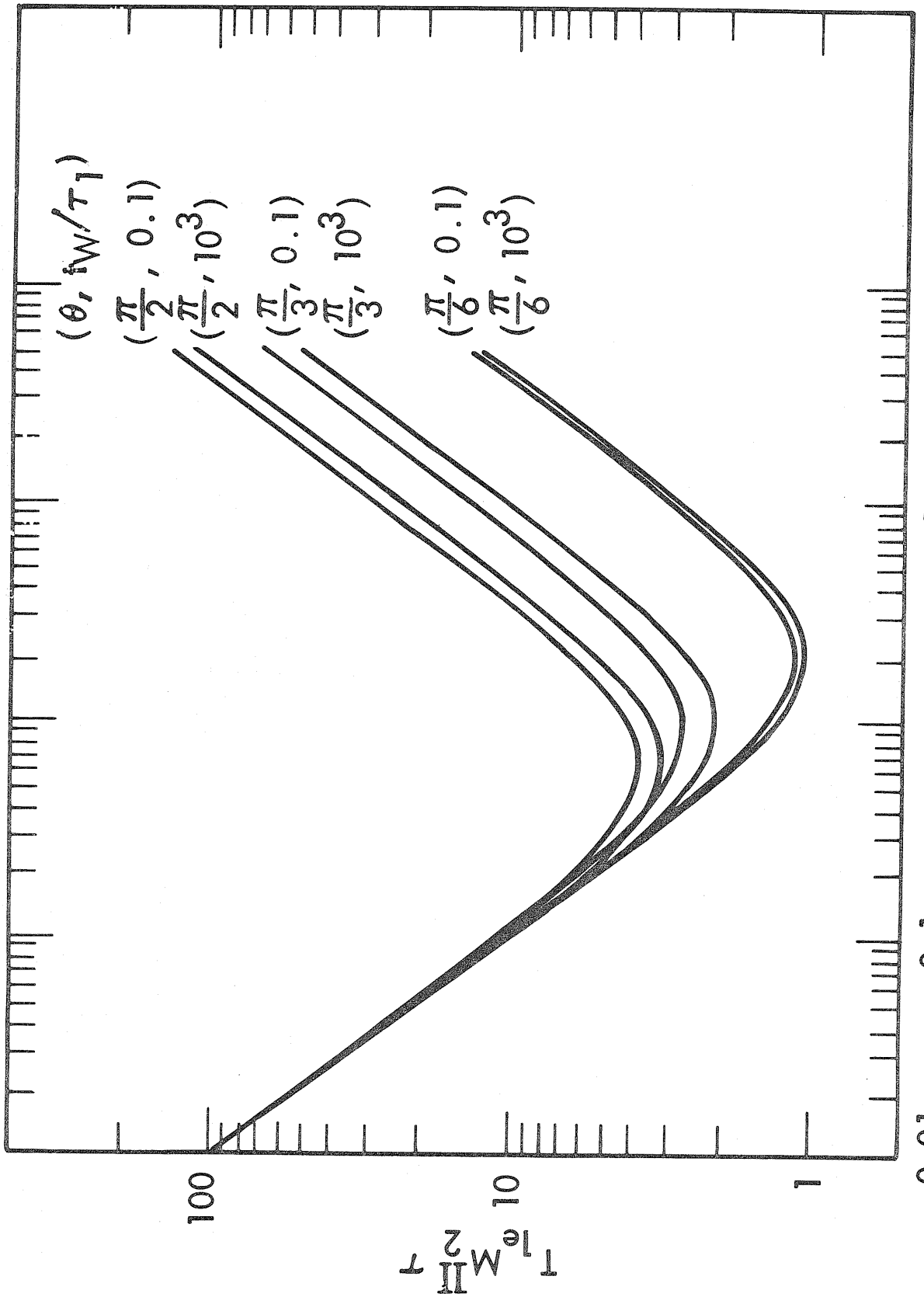
$T_{1e}M_2^{II}T$
100
10
1
0.01
0.1
1
10
100
τ_c / τ_1
$(\theta, f_W/\tau_1)$
$(\frac{\pi}{2}, 0.1)$
$(\frac{\pi}{2}, 10^3)$
$(\frac{\pi}{3}, 0.1)$
$(\frac{\pi}{3}, 10^3)$
$(\frac{\pi}{6}, 0.1)$
$(\frac{\pi}{6}, 10^3)$

Fig. 2

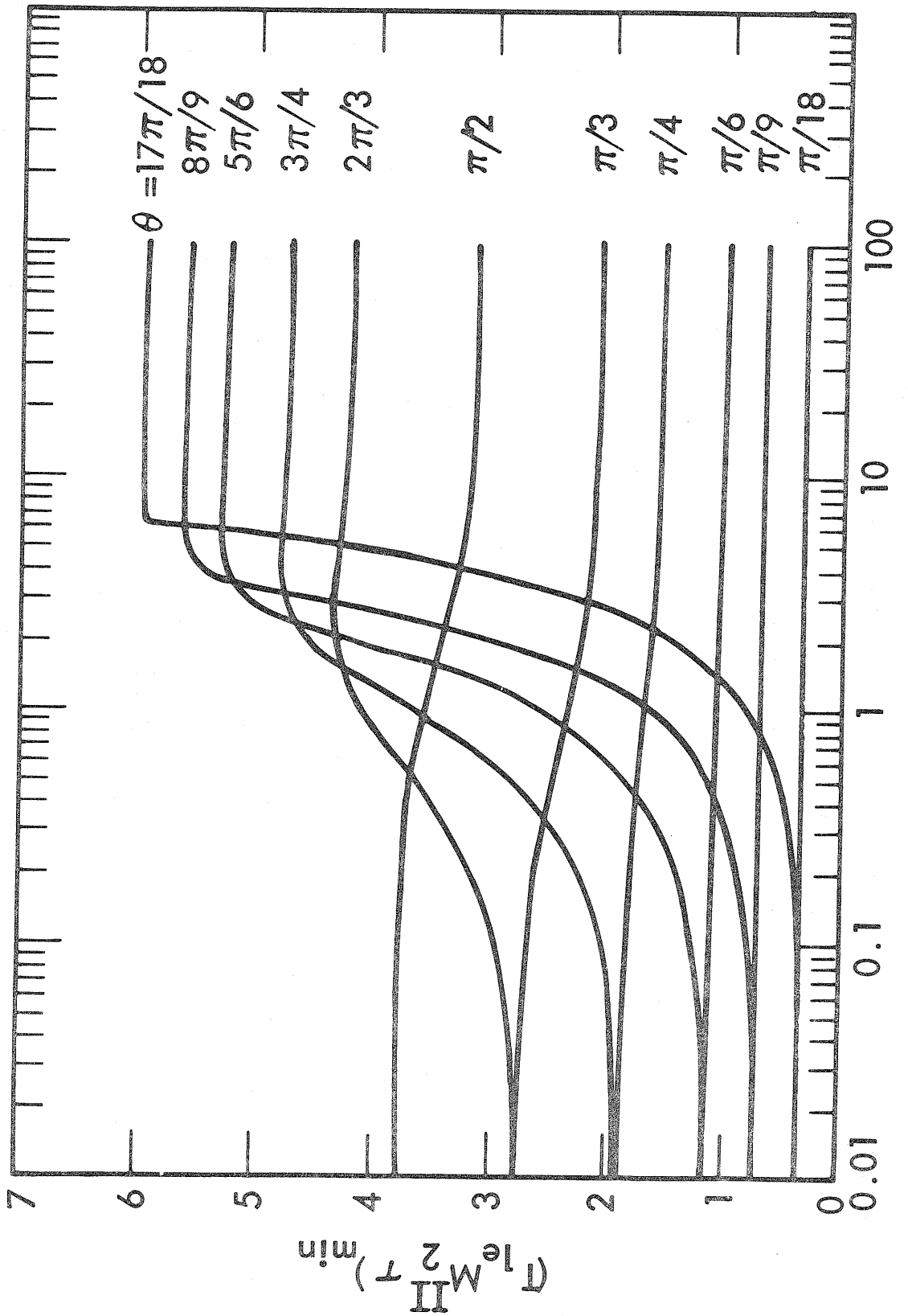
$(\Gamma_{1e}M_2^{II}\tau)_{min}$
t_w/τ_1
$\theta = 17\pi/18$
$8\pi/9$
$5\pi/6$
$3\pi/4$
$2\pi/3$
$\pi/2$
$\pi/3$
$\pi/4$
$\pi/6$
$\pi/9$
$\pi/18$
0.01
0.1
1
10
100
1
2
3
4
5
6
7

Fig. 3

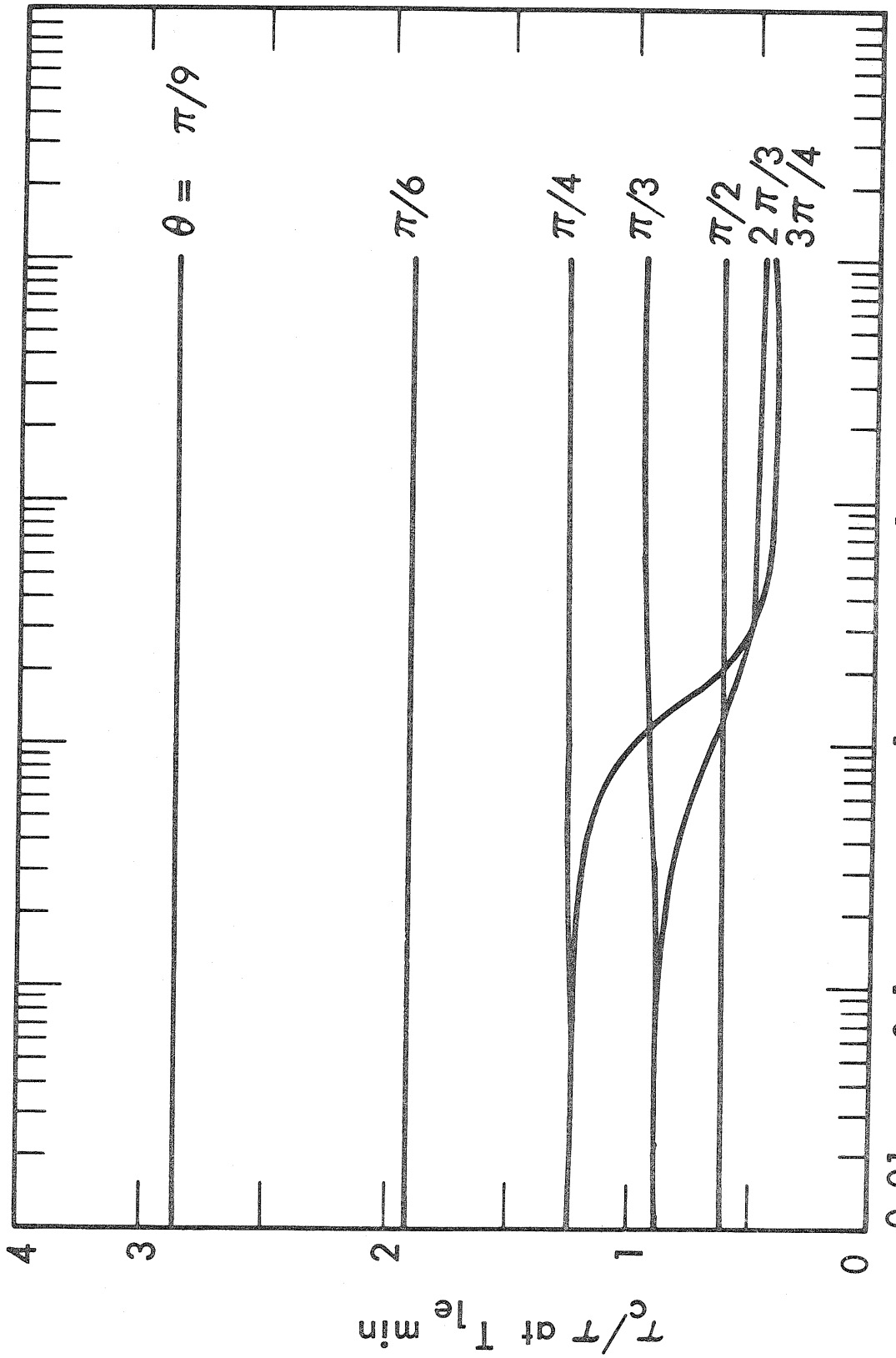
τ_c/τ at T_{le} min
0
1
2
3
4
0.01
0.1
1
10
100
t_w/τ_1
$\theta = \pi/9$
$\pi/6$
$\pi/4$
$\pi/3$
$\pi/2$
$2\pi/3$
$3\pi/4$

Fig. 4

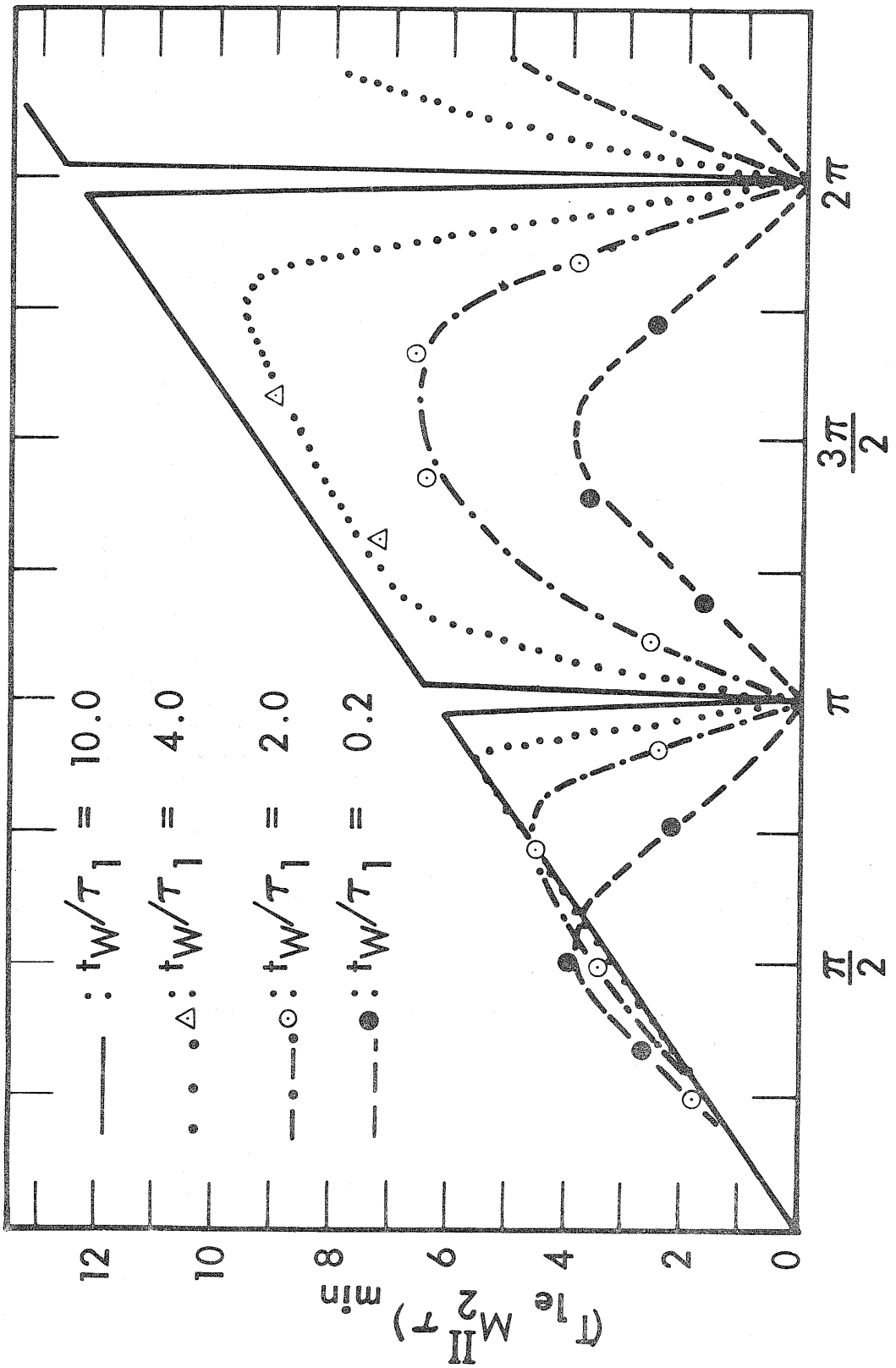
$(\Gamma_{1e}\ M_2^{II}\ T)_{min}$
0
2
4
6
8
10
12
$\frac{\pi}{2}$
π
$\frac{3\pi}{2}$
2π
θ in rad
t_W/T_1 = 10.0
t_W/T_1 = 4.0
t_W/T_1 = 2.0
t_W/T_1 = 0.2

Fig. 5

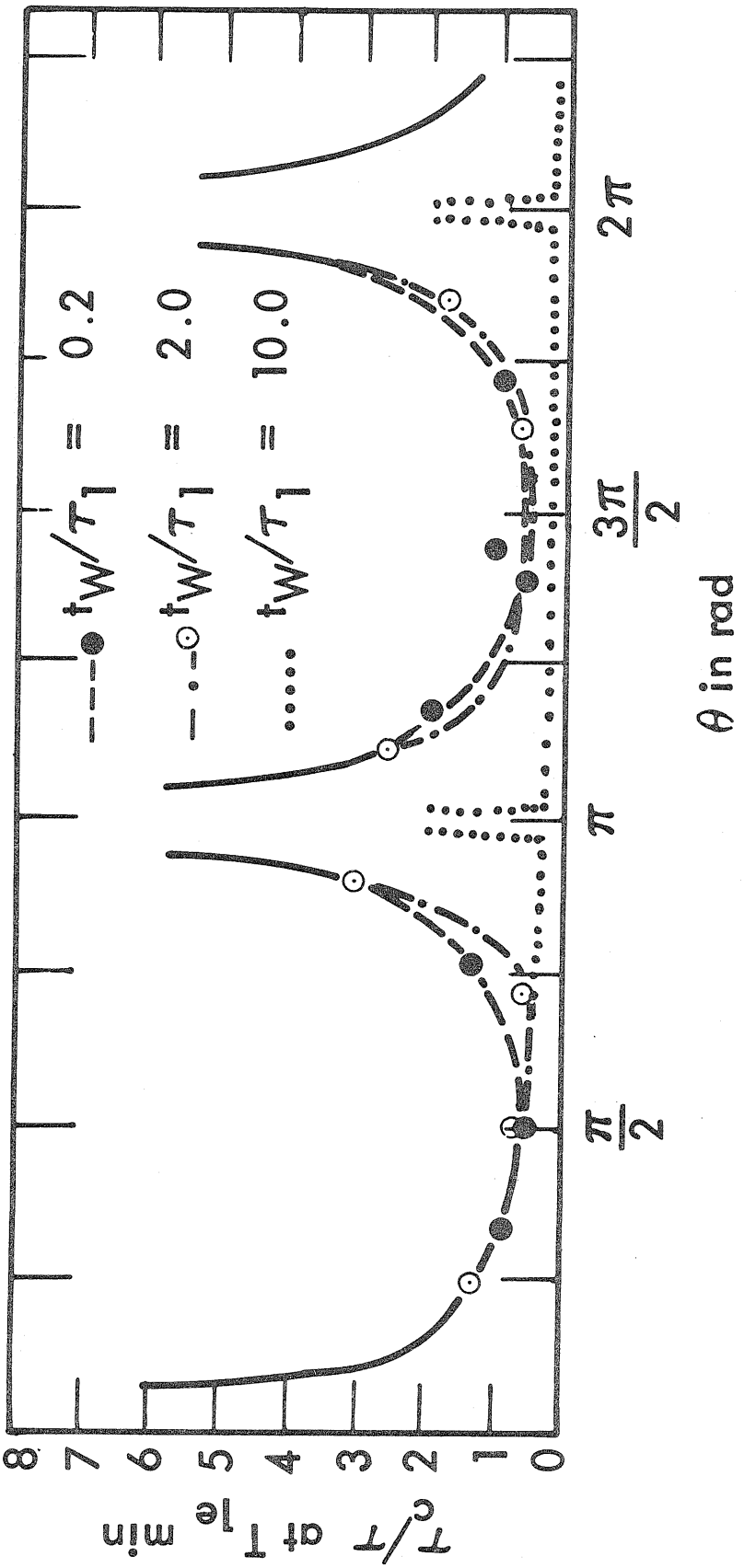
T_c/T at T_{le} min
0
1
2
3
4
5
6
7
8
$\pi/2$
π
$3\pi/2$
2π
θ in rad
t_w/τ_1 = 0.2
t_w/τ_1 = 2.0
t_w/τ_1 = 10.0

Fig. 6

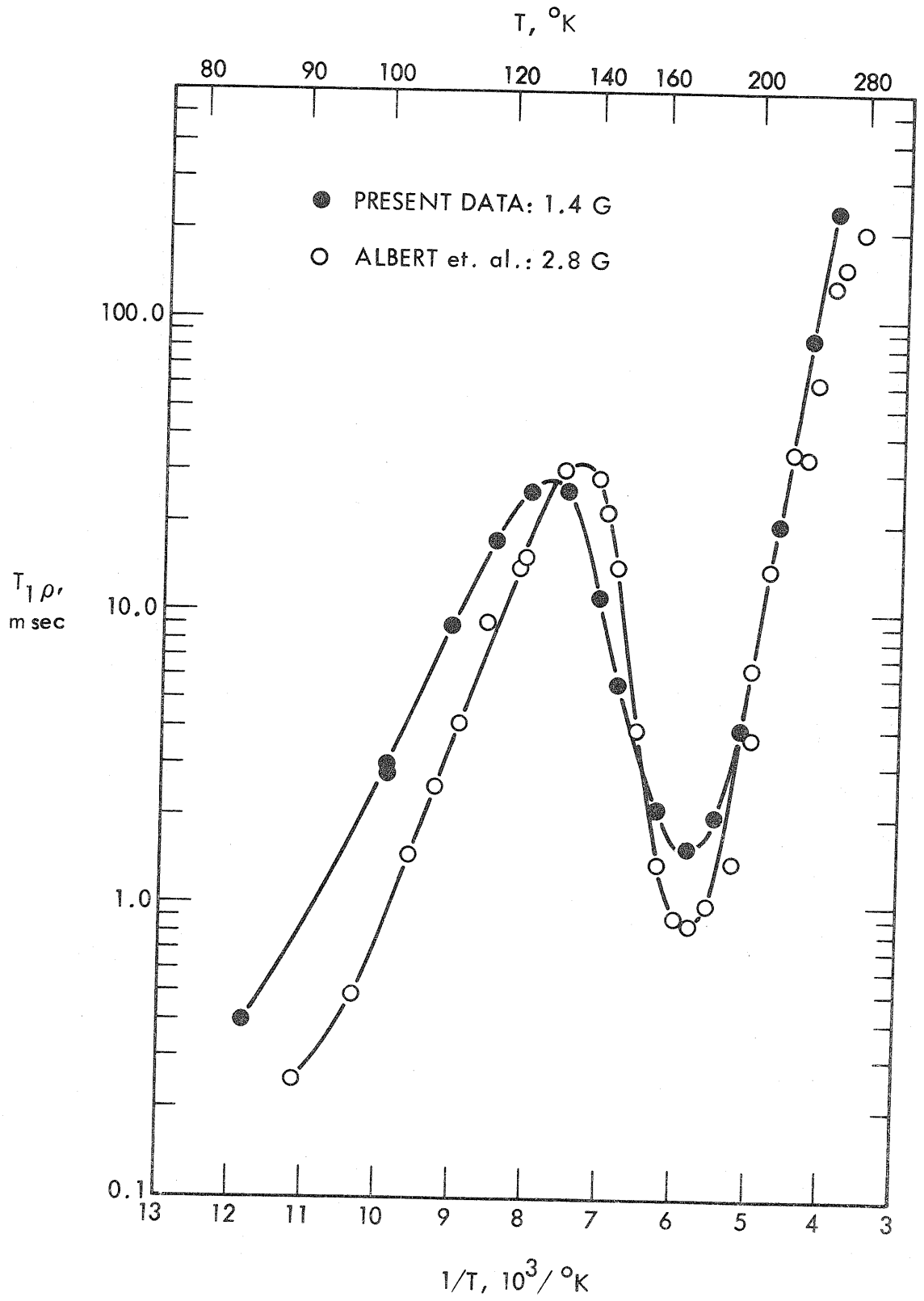
T, °K
80
90
100
120
140
160
200
280
PRESENT DATA: 1.4 G
ALBERT et. al.: 2.8 G
100.0
10.0
1.0
0.1
$T_{1\rho}$, m sec
13
12
11
10
9
8
7
6
5
4
3
1/T, 10^3/ °K

Fig. 7

Section 4

A Multiple Pulse Technique for Accurately Determining the First Moment of an NMR Spectrum

(This section is essentially an article by D. P. Burum, D. D. Elleman and W. K. Rhim, J. Chem. Phys. 68, 1164 (1978)).

A. INTRODUCTION

It was demonstrated in sections 2 and 3 that the spin temperature assumption can be applied to a dipolar solid when excited by a string of identical, discrete rf pulses, and that the Hamiltonian of a system irradiated by such a pulse train rapidly converges to the Hamiltonian describing continuous rf irradiation when the condition

$$\bar{\omega}_1/\Omega \ll 1 \tag{1}$$

is met. Here $\bar{\omega}_1 = \gamma \bar{H}_1 = \frac{\Theta\Omega}{2\pi}$ is the average precession frequency in the rotating frame due to the rf pulses applied with repetition frequency $\Omega/2\pi$, and Θ is the pulse angle. Hence, it is possible in principle to replace cw irradiation by a string of identical, small angle pulses without changing the physics involved as long as condition (1) is satisfied. This was demonstrated for adiabatic demagnetization in the rotating frame (ADRF), sudden spin locking and $T_{1\rho}$ measurements.[1] The advantage of using pulsed irradiation is that the signal can be observed between pulses, thus allowing the time development of the system to be monitored during a single pulse train.

In this section the validity of the multiple pulse correspondence principle is further demonstrated by applying it to a technique for accurately determining the resonance point of a dipolar broadened NMR line. This "zero crossing" technique has long been known in solid state NMR.[1,2] However, because it utilizes cw rf irradiation, this conventional technique only allows the signal to be observed at the end of a scan. By replacing this cw irradiation by a multiple pulse train, a technique is developed which,

because of its extremely high data rate, is typically several orders of magnitude more sensitive than the corresponding cw technique. (The accuracy which can be expected is usually better than $\pm$ 0.5 ppm.) The multiple pulse method is also easy to apply, and is relatively insensitive to pulse errors and probe detuning, which makes it particularly well suited for use under varying conditions of temperature and pressure. This is in contrast to multiple pulse line narrowing techniques, which are highly susceptible to these sources of error.[3]

In the following sub-sections the theoretical expressions which characterize the multiple pulse zero crossing technique in its various forms, as shown in Figure 1 are discussed and compared. The theoretical expressions which describe the cw method also describe the multiple pulse technique when condition (1) is satisfied, as is required by the multiple pulse correspondence principle. The more general case of a polycrystalline sample is also considered, and conditions are presented under which the first moment of the chemical shift powder pattern for such a sample can be determined. Experimental procedures are discussed next, including several modifications of the multiple pulse sequence which are useful for determining the baseline of every scan. This allows one to eliminate errors due to baseline fluctuations and distortions. As a demonstration of the technique, the ^{19}F chemical shifts at ambient temperature and pressure are reported for a number of compounds, and are compared with literature values where available. Finally, chemical shift data for CaF_2 and BaF_2 as a function of pressure up to 5 kbar are presented and compared with the results obtained by Lau and Vaughan using multiple pulse line narrowing techniques.[4]

B. THEORY

In this sub-section two versions of the zero crossing technique are discussed, each of which can be applied in either a cw or a multiple pulse form. Consider a system of N spins in a static field H_o which are in thermal contact with each other through the dipolar interaction, so that a single spin temperature applies. Figure 1A illustrates the cw form of what is called the "sudden" version of the zero crossing technique. In this approach, a burst of cw irradiation of frequency ω and strength H_1 lasting several T_2's is applied suddenly to the sample, and the initial amplitude, M_x, of the free induction decay which immediately follows is recorded. This initial amplitude is given by[5]

$$\left(\frac{M_x}{M_o}\right)_{\text{sudden}} = \frac{hH_1}{h^2 + H_L^2 + H_1^2} \quad . \tag{2}$$

Here M_o is the equilibrium magnetization, and H_L is the local dipolar field defined by

$$H_L^2 \equiv \mathrm{Tr}(\mathcal{H}_D^{(z)})^2 \; / \; [\gamma^2 \, \mathrm{Tr}(I_z)^2]. \tag{3}$$

The off resonance term, h, is given by

$$h = N^{-1} \sum_j [H_o(1-\sigma_{zzj}) - \omega/\gamma] \tag{4}$$

where σ_{zzj} is the chemical shift of the j'th spin. Note that (2), which is linear in h for $h^2 \ll H_1^2 + H_L^2$, crosses zero at "exact resonance," which can be defined as the point where h = 0. When condition (1) is met, equation (2) also applies to the multiple pulse form of the "sudden" technique (Figure 1B) because of the multiple pulse correspondence principle

outlined in the introduction. This was confirmed experimentally, and the comparison between theory and experiment is shown in Figure 2. The details of the experiment are discussed in a later sub-section.

From equations (2)-(4) we see that the "sudden" zero crossing technique will determine the average value of σ_{zz} for a system of spins in thermal contact with one another. For the special case in which all the spins in a single crystal are equivalent, both chemically and crystallographically, the full chemical shift tensor can be determined by measuring σ_{zz} for various crystal orientations. If the same technique is applied to a polycrystalline sample, then each of the crystallites will obey equations (2)-(4) separately. The resulting signal is given by

$$\left(\frac{M_x}{M_o}\right)_{\text{sudden}} = N^{-1}\sum_i \frac{h_i H_1 N_i}{h_i^2 + H_{L_i}^2 + H_1^2} \tag{5}$$

where N_i is the number of spins in the i^{th} crystallite. Of course, if h is independent of crystallite orientation, as is the case for CaF_2, then (5) will cross zero at h = 0.

The zero crossing point of equation (5) can be expressed rather simply if the dependence on the subscript i in the denominator can be neglected. This is the case if the local field, H_L, is isotropic, and if H_1 can be made large enough so that, near the zero crossing point,

$$H_L^2 + H_1^2 \gg h_i^2 \tag{6}$$

for all values of i. In this case (5) crosses zero when

$$\frac{H_1}{N(H_L^2 + H_1^2)} \sum_i h_i N_i = 0 \quad . \tag{7}$$

If equation (4) is rewritten as

$$\begin{aligned} h_i &= N_i^{-1} \sum_j [H_o(1 - \sigma_{zz_{ij}}) - \omega/\gamma] \\ &\equiv N_i^{-1} \sum_j [H_{ij} - \omega/\gamma] \end{aligned} \tag{8}$$

then (7) becomes

$$N^{-1} \sum_i h_i N_i = N^{-1} \sum_{i,j} (H_{ij}) - \omega/\gamma = 0 \tag{9}$$

or

$$\omega = \gamma N^{-1} \sum_{i,j} H_{ij} = \gamma \langle H \rangle \quad . \tag{10}$$

Thus the zero crossing point determines the first moment of the chemical shift pattern. Condition (6) can be clarified by writing h_i in yet another form:

$$\begin{aligned} h_i &= (H_o - \omega/\gamma) - N_i^{-1} \sum_j H_o \, \sigma_{zz_{ij}} \\ &\equiv h_o - H_o \langle \sigma_{zz} \rangle_i \quad . \end{aligned} \tag{11}$$

Near the zero crossing point, the extreme values of $H_o \langle \sigma_{zz} \rangle_i$ are on the same order of magnitude as the largest h_i. Therefore, condition (6) can be written

$$H_L^2 + H_1^2 \gg (H_o \langle \sigma_{zz} \rangle_i)^2 \quad . \tag{12}$$

In most cases H_L is orientation dependent. Nevertheless, H_1 can often be made large enough so that the anisotropy of H_L can be neglected. If the average of the local field over all crystallites, $\overline{H_L}$, is large compared to the anisotropic part, h_{L_i}, for all i, condition (12) can be replaced by

$$\bar{H}_L^2 + H_1^2 \gg (H_o \langle \sigma_{zz} \rangle_i)^2 + 2\bar{H}_L h_{L_i} \quad . \tag{13}$$

When this condition is satisfied, equations (7) - (10) are again valid. Therefore, if H_1 can be made large enough to satisfy (13), the sudden zero crossing technique can be used to determine the first moment of a chemical shift powder pattern. One should note that (13) is particularly easy to satisfy for proton spectra, because of the relatively small values of $\langle \sigma_{zz} \rangle_i$ that are encountered.

The multiple pulse correspondence principle can also be applied to the version of the zero crossing technique shown in Figure 1C. This approach, which we call the "adiabatic" technique, was introduced by Kunitomo [2] and was used to measure chemical shifts by Terao and Hashi.[6] Initially, a low level rf field, H_{1i}, is suddenly turned on. After thermal equilibrium is established, the rf field is adiabatically increased to a much larger final value, H_{1f}, in order to rotate the magnetization onto the x-axis. The cw irradiation is then turned off, and the initial magnitude, M_x, of the free induction decay which follows is observed. If this technique is applied to a sample in which all the spins are in thermal contact, such as a single crystal, the result is given by [5]

$$\left(\frac{M_x}{M_o}\right)_{\text{adiabatic}} = \frac{h\, H_{1f}}{(h^2 + H_L^2 + H_{1i}^2)^{\frac{1}{2}} (h^2 + H_L^2 + H_{1f}^2)^{\frac{1}{2}}} \quad . \tag{14}$$

Of course, (14) also applies to the multiple pulse form shown in Figure 1D if condition (1) is met. Note that the "sudden" technique is a special case of this "adiabatic" method, so that substituting $H_{1i} = H_{1f} \equiv H_1$ in (14) yields (2).

The sensitivities of the sudden and adiabatic techniques can be

compared by comparing the slopes of (2) and (14) at h = 0. The slope of (2) is maximum when $H_1 = H_L$, and is given by

$$\frac{\partial}{\partial h}\left(\frac{M_x}{M_o}\right)_{\text{sudden}}\Bigg|_{\substack{h=0 \\ H_1=H_L}} = \frac{1}{2H_L} \quad . \tag{15}$$

The slope of (14) at h=0 increases as $H_{1i} \to 0$ and $H_{1f} \to \infty$. The maximum value is given by

$$\frac{\partial}{\partial h}\left(\frac{M_x}{M_o}\right)_{\text{adiabatic}}\Bigg|_{\substack{h=0 \\ H_{1i} \to 0 \\ H_{1f} \to \infty}} = \frac{1}{H_L} \quad . \tag{16}$$

Thus, at most, the sensitivity of the adiabatic method can be twice the maximum sensitivity of the sudden technique.

When the adiabatic technique is applied to a polycrystalline sample, each of the crystallites obeys equation (14) separately. In order to determine the first moment of a chemical shift powder pattern, however, it is H_{1i} that must be large enough to satisfy the condition that was imposed on H_1 in equation (13). In practice, this reduces the advantage in sensitivity of the adiabatic technique over the sudden technique to a factor of roughly $\sqrt{2}$. Therefore, there is little reason to apply the more complicated adiabatic technique to a polycrystalline sample.

The high data rate of the multiple pulse zero crossing technique gives it an advantage in signal-to-noise ratio over the corresponding cw technique on the order of $(T_{1\rho}/\ T_2)^{\frac{1}{2}}$. Care should be taken, however, to avoid errors caused by anisotropy in $T_{1\rho}$. For relatively pure, rigid crystals $T_{1\rho}$ is usually long. However, in many molecular crystals $T_{1\rho}$

changes substantially with temperature. In such cases a temperature should be chosen, if possible, at which $T_{1\rho}$ is relatively long, and T_1 is short, in order to attain higher sensitivity. It is also important to use a value of $\overline{H_1}$ for which the signal amplitude will be greatest, taking care that condition (1) is satisfied by a suitable choice of pulse angle and repetition rate. It should be pointed out that if condition (1) is not satisfied a strong spin heating occurs which can cause the magnetization to decay much more rapidly than it otherwise would.[7] Nevertheless, as long as this effect does not cause the decay time to be shorter than the time needed to establish thermal equilibrium, the expressions presented in this paper remain valid and, in particular, the zero crossing point is not altered. Therefore, the zero crossing technique can be used without misleading results even when condition (1) is not met, but considerable sensitivity may be sacrificed.

C. EXPERIMENTAL PROCEDURE

The "sudden" multiple pulse technique (Figure 1B) was used to obtain all the data reported in this paper because it was more convenient, and because the increase of roughly $\sqrt{2}$ in signal-to-noise ratio which could have been gained in some cases by using the adiabatic method was not needed. The rf pulse angle was usually about 30°, and the pulse spacing was 20 μsec. This provided an $\overline{H_1}$ of about 1 gauss, which was roughly equal to H_L for the samples we used. The magnetic field was stabilized during the experiment by using an NMR locking system with a separate probe.

The signal observed between pulses during the rf irradiation was integrated in order to improve the signal-to-noise ratio. However,

any error in baseline level was also amplified by this procedure. Therefore, it was important to determine the baseline of every scan very accurately, so that it could be subtracted from the signal before integration. If the shape of the baseline was not distorted, then only its dc level was needed. This was automatically determined if $T_{1\rho}$ was so short that the signal decayed to baseline level before the end of the scan. If $T_{1\rho}$ was long, the signal was forced to decay abruptly near the end of the scan either by inserting a gap several T_2's wide in the pulse train, as illustrated in Figure 3A, or by using a $(\pi/2)_y$ pulse to rotate the magnetization away from the locking direction, as shown in Figure 3B.

If it was necessary to correct for baseline shape imperfections, the results from a separate baseline scan were subtracted from the data. This baseline scan was identical in all respects to the scan used to obtain the data, except that a $(\pi/2)_y$ pulse was applied several T_2's earlier than the Θ_x pulse train in order to remove the initial magnetization.

The direct result of applying the pulse sequence illustrated in Figure 3A at 56.5 MHz to a CaF_2 crystal 1KHz above resonance is shown in Figure 4A, and in Figure 4B these data have been integrated. Figure 5 compares the results obtained by this same procedure at exact resonance and at $\pm$50 Hz.

Sufficient accuracy was achieved for all the data reported in this paper by simply varying the synthesizer frequency until the zero point was obtained. A more accurate method, however, would be to plot several points above and below resonance and determine the zero crossing point graphically.

When the resonance points of various compounds were being compared, either $T_{1\rho}$ or the method of Figure 3A was used to set the electronic baseline, and the signal was observed without integration.

For the high pressure measurements, the apparatus previously described by Lau and Vaughan was used without modification[4], and the two scan method was used to correct the baseline. In order to insure that there were no detectable effects due to probe detuning or changes in the hydraulic oil as a function of pressure, the resonance point of a CaF_2 crystal which was kept at one atmosphere pressure within a glass capsule was monitored as a function of hydraulic pressure. The zero crossing point remained constant to within 0.1 ppm.

D. EXPERIMENTAL RESULTS

The experimental points shown in Figure 2 were obtained by applying the "sudden" multiple pulse zero crossing technique with a pulse spacing of 15 μsec. and a pulse angle of 29° to a single crystal of CaF_2 oriented with its (111) axis parallel to H_o. They are in close agreement with the theoretical curve, which was obtained from equation (2) with H_L = 1.0 gauss. Because equation (2) was originally derived from the cw technique shown in Figure 1A, Figure 2 also demonstrates the validity of the multiple pulse correspondence principle and the validity of the thermodynamic spin temperature assumption.

Table I presents the results of ^{19}F chemical shift measurements made on a number of compounds at room temperature and pressure, along with previously reported data where available. With the exception of CdF_2, the data presented here agree very well with the literature. In particular, our value for KPF_6 is indistinguishable from that obtained by Sears[14] using Kunitomo's approach, and our value for $LiPF_6$ agrees closely with the curve given by Sears for chemical shift as a function of cation radius if the radius of Li^{+2} is taken to be 0.60 Å. Single crystals of CaF_2,

CdF_2, and BaF_2 were used, although powder samples would have yielded the same results. The rest of the measurements were made on powder samples. The error estimate is smaller for the three single crystals because the data for these samples were integrated, whereas the data for the other samples were not.

Figure 6 presents the results obtained in measuring the chemical shifts of CaF_2 and BaF_2 as a function of applied pressure. The measured value of $-0.29 \pm .02$ ppm/kbar for CaF_2 is in good agreement with the theoretical prediction of -0.46 ppm/kbar given by Lau and Vaughan.[4] However, it is somewhat at variance with the experimental value of -1.7 ± 1 ppm/kbar which they obtained by using an 8-pulse cycle to remove the dipolar boadening of the CaF_2 resonance line. Although line narrowing techniques are very useful for determining the full structure of a complicated resonance pattern, they are very susceptible to pulse errors and probe detuning.[3] Therefore, the multiple pulse zero crossing technique is often a better choice when it is only necessary to accurately determine the first moment of a simple resonance spectrum, especially when this is to be done as a function of temperature or pressure.

Our result of $-0.62 \pm .05$ ppm/kbar for BaF_2, which is just over twice that for CaF_2, is consistent with the larger radius of the Ba^{+2} ion. The error bars for the BaF_2 data are larger than those for CaF_2 because T_1 was longer for the BaF_2 crystal. This allowed the long term electronic instabilities of our system to become more noticeable in the BaF_2 case. Also, the apparent hysteresis of the BaF_2 data at low pressures was actually caused by a slight drift in the magnetic field near the end of the data run. These last few points were therefore ignored in computing

the slope of the chemical shift vs. pressure curve.

Finally, note that the pressure data presented here for BaF_2 could not have been obtained using a standard multiple pulse line narrowing technique, because the pulse sequence would not have removed the heteronuclear dipolar broadening of the BaF_2 resonance line.

REFERENCES

1. I. Solomon and J. Ezratty, Phys. Rev. 127, 78 (1962).
2. M. Kunitomo, J. Phys. Soc. Japan 30, 1059 (1971).
3. W.-K. Rhim, D. D. Elleman, L. B. Schreiber and R. W. Vaughan, J. Chem. Phys. 60, 4595 (1974).
4. K.-F. Lau and R. W. Vaughan, J. Chem. Phys. 65, 4825 (1976).
5. A. Abragam, The Principles of Nuclear Magnetism, Oxford University Press, (1961), Chapt. 12.
6. T. Terao and T. Hashi, J. Phys. Soc. Japan 36, 989 (1974).
7. Section 2.
8. R. W. Vaughan, D. D. Elleman, W.-K. Rhim and L. M. Stacey, J. Chem. Phys. 57, 5383 (1972).
9. J. S. Waugh, L. M. Huber and U. Haeberlen, Phys. Rev. Lett. 20, 180 (1968).
10. L. M. Akhutsky, Yu. V. Gararinsky and S. A. Polyshchuk, Spectry. Letters 2, 75 (1969).
11. C. D. Cornwell, J. Chem. Phys. 44, 874 (1966).
12. Wang Yi-ch'iu, Dokl. Akad. Nauk SSSR 2, 317 (1961) [Soviet Phys. Doklady 6, 39 (1961)].
13. F. I. Skripov and I-Chu Wang, Wu Li Hsueh Pao 20, 41 (1964).
14. R. E. Sears, J. Chem. Phys. 59, 973 (1973).

TABLE I.

^{19}F CHEMICAL SHIFTS OF VARIOUS COMPOUNDS AT AMBIENT TEMPERATURE AND PRESSURE†

COMPOUND	σ_{zz} (ppm)	PREVIOUSLY REPORTED DATA
NaF	62.0 ±1.	
KF	-36.6 ±1.	
CaF_2	-56.6 ±0.5	-55.6 ±0.5 [a]
		-61 ±1 [b]
		-58 ±2 [c]
		-53 ±8 [d]
		-64 [e]
SrF_2	-78. ±1.	-82 ±1 [b]
		-67 ±8 [d]
CdF_2	24.8 ±0.5	33 ±1 [b]
		39 ±8 [d]
BaF_2	-153.5 ±0.5	-154 ±1 [b]
		-138 ±8 [d]
		-108 ±15 [f]
		-113 ±20 [g]
TiF_3	-13.1 ±1.	
$LiBF_4$	-1.1 ±1.	
$NaBF_4$	-3.2 ±1.	
$K BF_4$	-13.1 ±1.	
$RbBF_4$	-16.3 ±1.	
$KSiF_6$	-32.5 ±1.	
$BaSiF_6$	-57. ±5.	
$LiPF_6$	-74.2 ±1.	
$K PF_6$	-91.5 ±1.	-91.3 ±1 [h]

† All values are relative to C_6F_6.

a. Reference 6
b. Reference 8
c. Reference 9
d. Reference 10
e. From Figure 1 of reference 11
f. From Figure 1 of reference 12
g. From Figure 3 of reference 13
h. Reference 14

FIGURE CAPTIONS

1. The "sudden" (A and B), and "adiabatic" (C and D) versions of the zero crossing technique in both their cw and multiple pulse forms.
2. Result of applying the sudden multiple pulse zero crossing technique (Figure 1B) to a CaF_2 single crystal with $\overline{H_1} = 1.35$ gauss. The theoretical curve (equation 2) was fit to the data by assuming a value of $H_L = 1.0$ gauss. The pulse angle was 29^o and the spacing between pulses was 15 μsec. Part B is a magnification of part A near the zero crossing point.
3. Two modifications of Figure 1B which can be used to determine the baseline level of the scan. In part A, a gap in the pulse train allows the magnetization to decay to zero in a few T_2 . In part B, a $(\pi/2)_y$ pulse rotates the magnetization away from the spin locking direction, so that $M_x = 0$.
4. Result of applying the pulse sequence shown in Figure 3A to a CaF_2 crystal 1 KHz above resonance. Part A shows the signal as it was observed between pulses. Note the effectiveness of the baseline determining method. In part B the data from part A have been integrated for the purpose of signal averaging.
5. The procedure of Figure 4B applied at three frequencies near resonance: (A) +50 Hz; (B) exact resonance; (C) -50 Hz.
6. ^{19}F chemical shift vs. pressure curves for CaF_2 and BaF_2. The slopes of the curves are CaF_2: -0.29 ±.02 ppm/kbar, and BaF_2: -0.62 ±.05 ppm/kbar. Arrows pointing up or down indicate data taken as the pressure was being raised or lowered, respectively. The apparent hysteresis in the BaF_2 curve near zero pressure was caused by a drift in the magnetic field near the end of the data run. The chemical shifts for each curve are

given relative to the value at zero pressure. The shift between CaF_2 and BaF_2 is not shown.

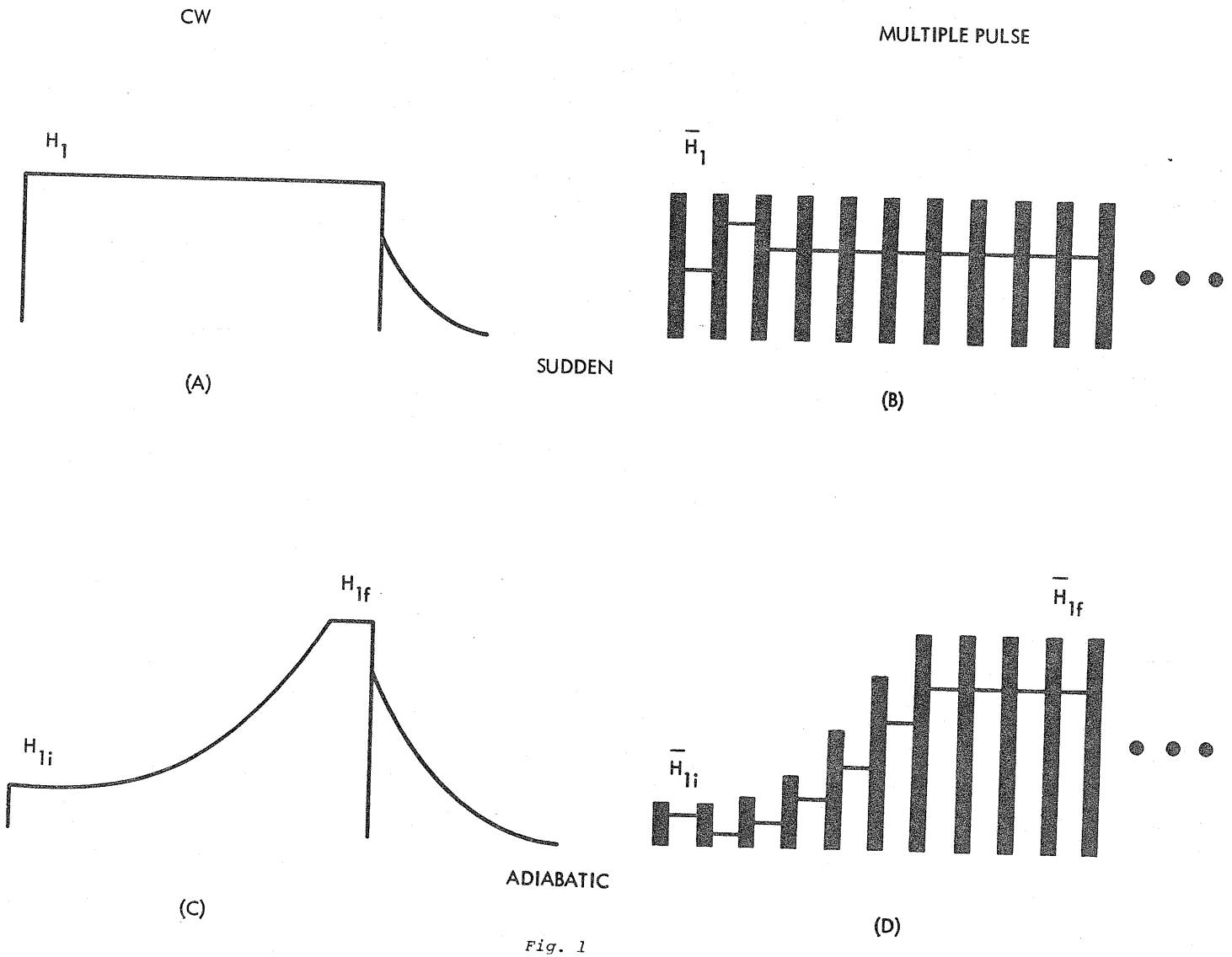
CW
MULTIPLE PULSE
H_1
$\bar{H}_1$
SUDDEN
(A)
(B)
H_{1f}
$\bar{H}_{1f}$
H_{1i}
$\bar{H}_{1i}$
ADIABATIC
(C)
(D)

Fig. 1

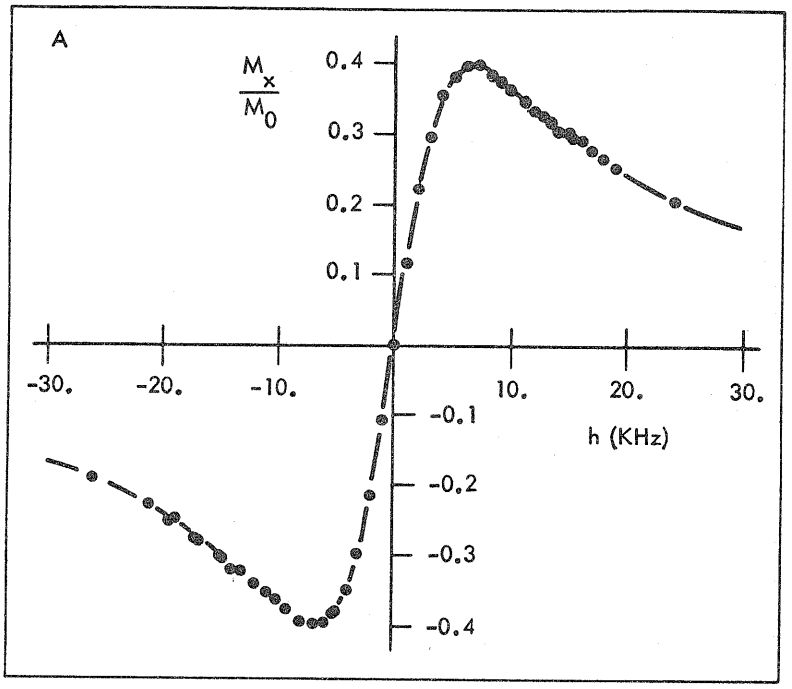
A
$\frac{M_x}{M_0}$
0.4
0.3
0.2
0.1
-30.
-20.
-10.
10.
20.
30.
h (KHz)
-0.1
-0.2
-0.3
-0.4

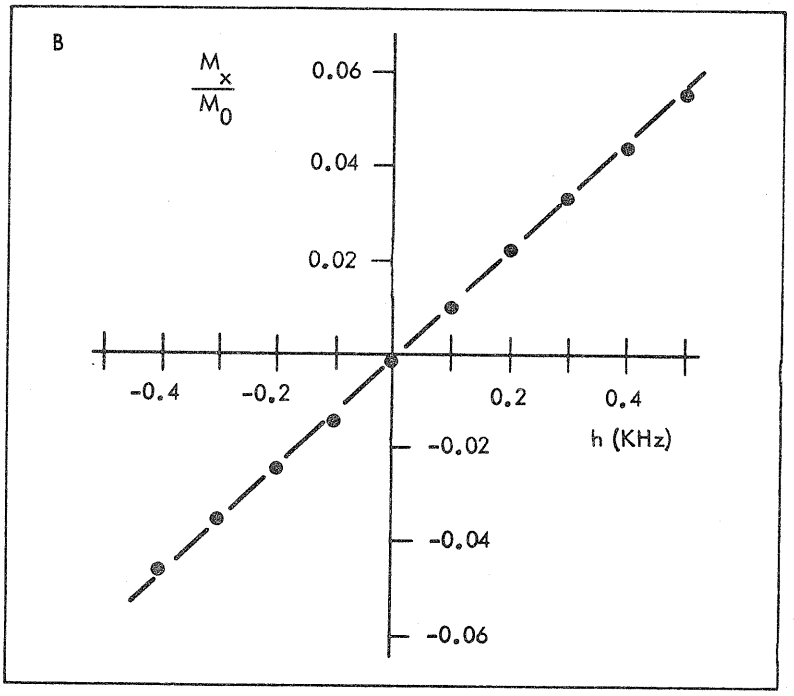
B
$\frac{M_x}{M_0}$
0.06
0.04
0.02
-0.4
-0.2
0.2
0.4
h (KHz)
-0.02
-0.04
-0.06

Fig. 2

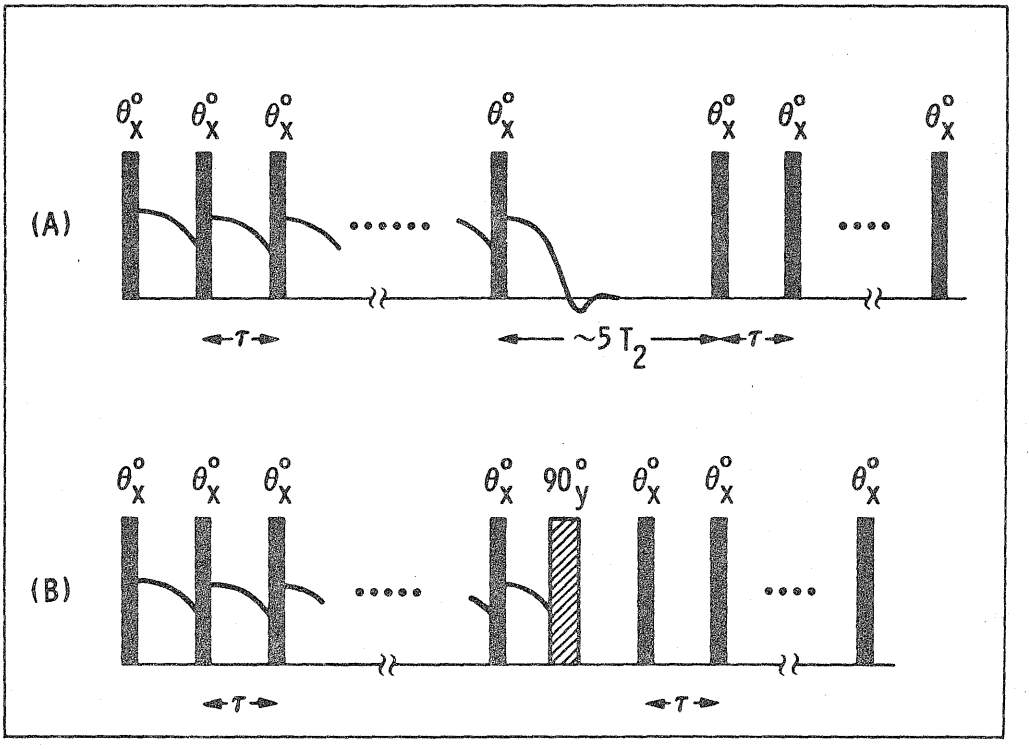
(A)
θ°_x θ°_x θ°_x θ°_x θ°_x θ°_x θ°_x
τ
~5 T_2
τ
(B)
θ°_x θ°_x θ°_x θ°_x 90°_y θ°_x θ°_x θ°_x
τ
τ

Fig. 3

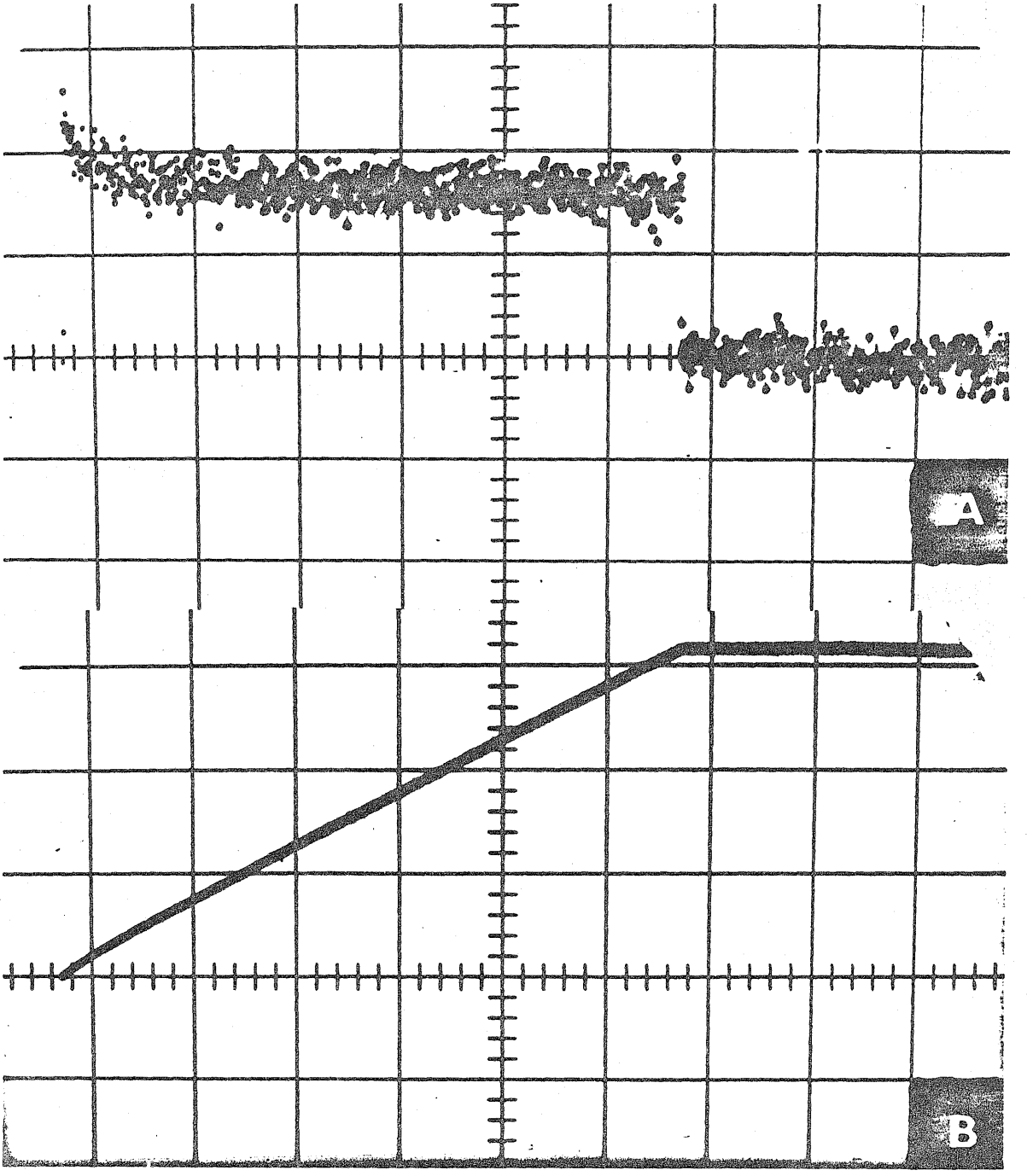

Fig. 4

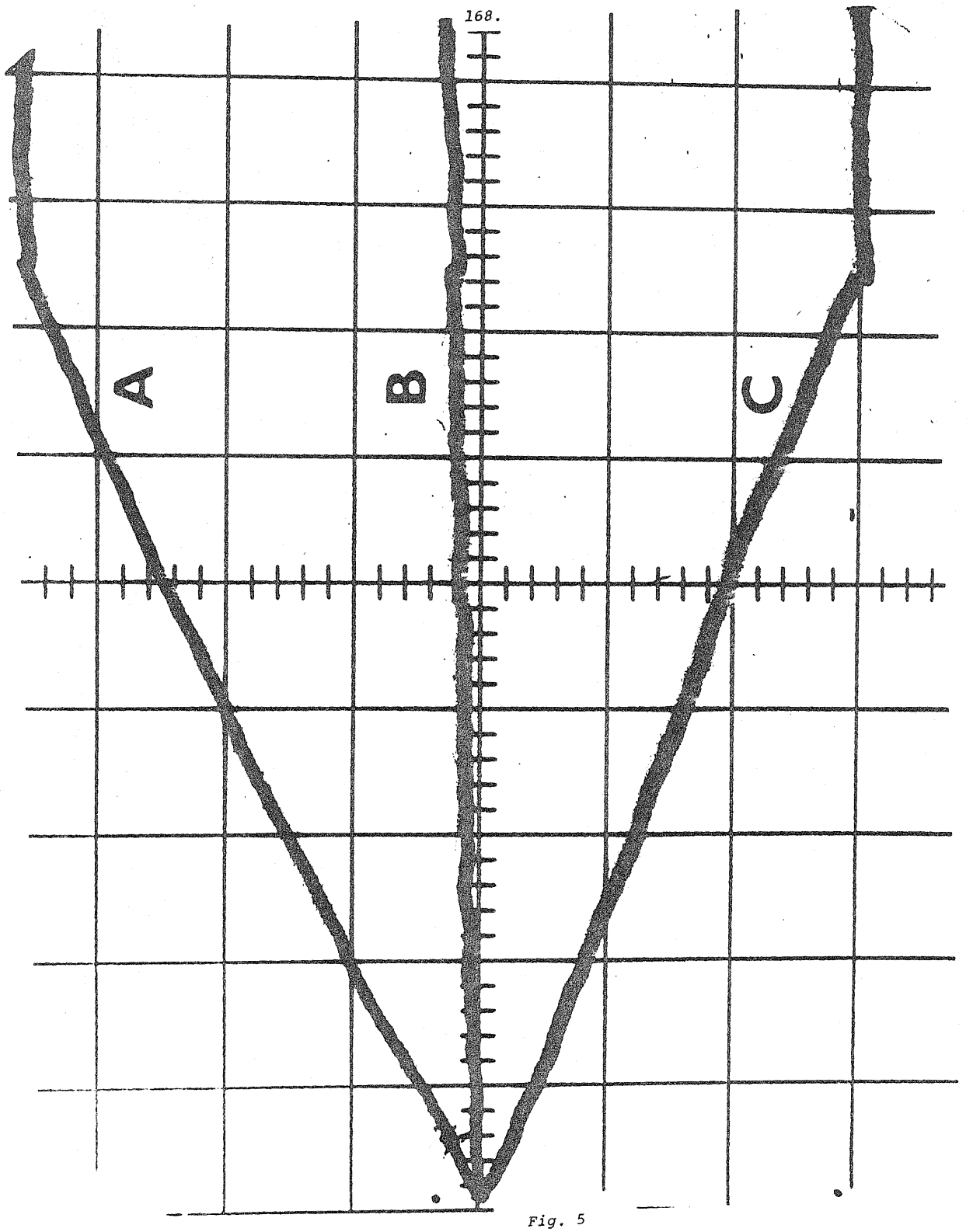

Fig. 5

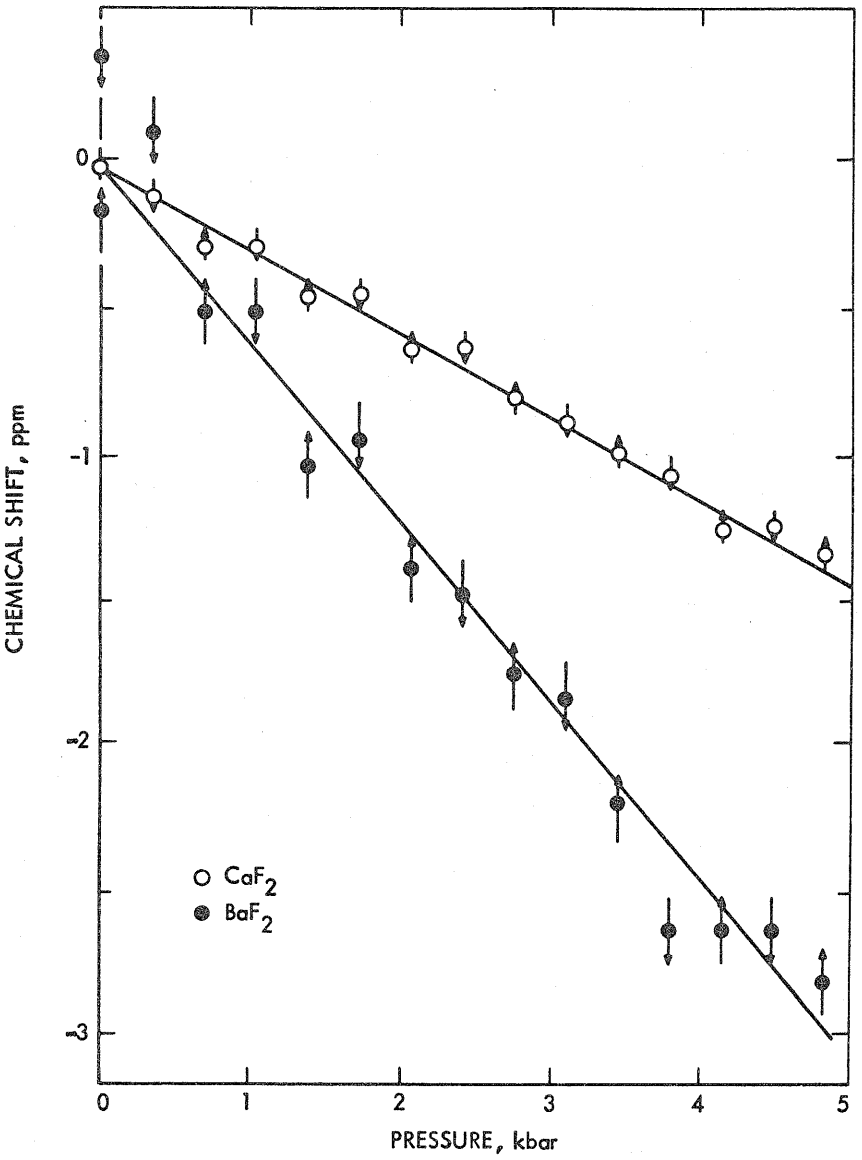

Fig. 6

Section 5

A Single Scan Technique for Measuring Spin-Lattice Relaxation Times in Solids

(This section is essentially an article by D. P. Burum, D. D. Elleman and W. K. Rhim, Rev. Sci. Instrum. 49, 1169 (1978).)

A. INTRODUCTION

In the previous three sections it was demonstrated that thermodynamic properties of a spin system in a solid could be measured using one kind of multiple pulse experiment, namely spin locking by a train of identical θ_x pulses. In this section it is shown that thermodynamics can also be applied in analyzing a pulsed experiment applicable to solids for measuring the spin-lattice relaxation time in the laboratory frame, T_1, in a single data scan.

The only difference between the two thermodynamic spin-lattice relaxation times, $T_{1\rho}$ in the rotating frame and T_1 in the laboratory frame, is the difference in the strength of the spin locking fields. As was seen in section 3, $T_{1\rho}$ involves spin locking of an applied rf field which is typically between 0.5 and 10 gauss. On the other hand, T_1 is the characteristic relaxation time for magnetization locked along the Zeeman field, H_o, which can easily range from 10 to 75 kilogauss.

The usual method for measuring T_1 is to use one of the following pulse sequences: $\{(\pi/2)_x - \tau - (\pi/2)_x\}$ or $\{(\pi)_x - \tau - (\pi/2)_x\}$. In either case, the first pulse perturbs the equilibrium state of the spin system, and the second pulse allows one to observe the progress that the system has made toward returning to equilibrium during the time interval τ. Thus the experiment must be repeated many times with various values of τ in order to fully characterize the time development of the magnetization.

The technique discussed in this section allows the magnetization of a solid to be observed many times as it returns to its equilibrium state. It is shown that the perturbation of the system by the measurement process can be treated thermodynamically as a source of spin heating, which should not be confused with the spin heating effect discussed in section 2. By measuring

the strength of the spin heating, it is possible to extract T_1 from the relaxation curve during the experiment. The assumption is made throughout this section that the entire system can be described at all times by a common spin temperature.

There have been several other attempts to develop techniques for measuring T_1 in a single scan. For example, the z-restoring pulse sequence[1] $\{\pi - \tau - [(\pi/2)_x - \tau - (\pi)_y - \tau - (\pi/2)_{-x} - \tau' -]_n\}$ has been particularly successful for measuring T_1 in liquids. This technique produces a virtually undistorted spin-lattice decay curve by utilizing Hahn's inhomogeneity echo to refocus the magnetization before restoring it parallel to the H_o field. However, the single scan T_1 measuring techniques for solids have not been as successful in avoiding signal decay caused by the sampling process. Some of these methods, such as the small angle pulse sequence $(\pi - \tau - (\theta - \tau' -)_n : \theta < \frac{\pi}{2})$ introduced by Look and Locker,[2] can reduce this effect only by sacrificing signal amplitude. Others, such as the "flip-flop" sequence $(\pi - \tau - ((\frac{\pi}{2})_x - \tau - (\frac{\pi}{2})_{-x} - \tau' -)_n)$ proposed by Demco et al.,[3] attempt to avoid this signal decay by returning the magnetization to its alignment with the H_o field immediately after sampling. However, the sampling window must be larger than the recovery time of the receiver, and in solids a significant loss of magnetization usually occurs during this time. None of the single scan techniques for solids which have been proposed so far have made any attempt to refocus the magnetization after sampling, in analogy with the z-restoring technique for liquids.

This section introduces a pulse sequence for single scan T_1 measurements in solids (see Figure 1) which utilizes the so-called "solid echo"[4-6] to refocus most of the magnetization which would otherwise be lost during sampling. The effective spin heating is thereby considerably reduced, allowing more sampling during a scan with a corresponding increase in sensitivity. The residual spin heating which is caused by the incompleteness of the solid echoes is taken into account in determining the actual value of T_1 by applying the analysis of Look and Locker.[2,7,8] This analysis does not require a detailed knowledge of the various sources of spin heating. Therefore, the technique tends to be insensitive to spectrometer misadjustments since these errors appear in the form of spin heating, and are automatically corrected along with the spin heating due to incomplete echoes. The only exception is misadjustment of the initiating π-pulse (if it is used), which causes an error in the initial amplitude of the decay curve. The data rate of the technique can be further increased by repeating the scans in a time much less than the $6\ T_1$ required for the magnetization to fully recover.

In the following sections the theoretical expressions which describe the solid echo and the method developed by Look and Locker for taking spin heating into account are reviewed. The analysis of Look and Locker is then extended to apply to scans of any length which are repeated at an arbitrary rate. Experimental procedures and methods of data analysis are next discussed, and various experimental results using a single crystal of CaF_2 are reported which demonstrate our technique and compare it with more conventional techniques. The applicability of our method to liquids is then illustrated using C_6F_6. Finally, several other possible "echo" single scan T_1 techniques for solids are discussed, along with our reasons for concluding that the sequence presented in this paper is the most advantageous.

B. THEORY

The dipolar "solid echo" which is utilized in this paper was analyzed for the case of an isolated dipole pair by Powles and Mansfield,[4] and then for the more general case by Powles and Strange[5] and by Mansfield.[6] The expression for the echo amplitude, M_E, generated by the pulse sequence $((\frac{\pi}{2})_x - \tau - (\frac{\pi}{2})_y - \tau)$ applied to a sample with initial magnetization M_o is[5]

$$M_E = M_o \{1 - \frac{6\tau^4}{4!} M_{4x} + \ldots\} \tag{1}$$

where

$$M_{4x} = T_r \{[H_D^{(z)} + H_D^{(x)}, [H_D^{(z)}, I_y]]$$
$$[H_D^{(z)}, [H_D^{(z)}, I_y]]\}/T_r \{I_y^2\}$$

$$H_D^{(z)} = \sum_{i<j} A_{ij}(\underset{\sim}{I}_i \cdot \underset{\sim}{I}_j - 3 I_{zi} I_{zj})$$

$$H_D^{(x)} = \sum_{i<j} A_{ij}(\underset{\sim}{I}_i \cdot \underset{\sim}{I}_j - 3 I_{xi} I_{xj})$$

and

$$A_{ij} = -\frac{1}{2}\gamma^2\hbar(1 - 3\cos^2\theta_{ij})/r_{ij}^3 . \tag{2}$$

It is clear from equation (1) that M_E approaches M_o very rapidly as $\tau/T_2 \to 0$. In fact, for small τ the factor governing the incompleteness of the echo will be[5,6] (τ^4/T_2^4).

The T_1 measuring sequence which we wish to present in this paper is illustrated in Figure 1. The scan begins with a π pre-pulse which inverts the magnetization. (This pulse is omitted in some cases. See the discussion in the Experimental Procedure section.) Then the relaxation of the spin system is observed periodically using a group of three pulses which generates

a solid echo and then returns the refocused magnetization to the z-axis. In solids it is impossible to avoid a slight loss of magnetization due to the last term in equation (1). However, this can be taken into account in calculating T_1 by applying the analysis of Look and Locker.[2,7,8]

If M_n and M_n^+ are the magnetizations before and after the n'th sampling pulse group, respectively, n = 0, 1, 2,..., then the loss of magnetization during sampling can be described in terms of the invariance factor, X, by

$$M_n^+ = M_n(1 - X) \quad . \tag{3}$$

For all n, assuming exponential decay between samplings,

$$\begin{aligned} M_{n+1} &= (M_n(1-X) - M_{eq}) \exp(-\tau'/T_1) + M_{eq} \\ &= M_n(1-X) \exp(-\tau'/T_1) + M_{eq}(1 - \exp(-\tau'/T_1)), \end{aligned} \tag{4}$$

where M_{eq} is the value of the magnetization when it is in thermal equilibrium with the lattice. After many samplings, the magnetization will arrive at a steady state value, M_∞, which can be obtained from equation (4):

$$M_\infty = M_\infty(1-X) \exp(-\tau'/T_1) + M_{eq}(1 - \exp(-\tau'/T_1)) \quad . \tag{5}$$

This yields

$$M_\infty = M_{eq}[1 - \exp(-\tau'/T_1)][1 - (1-X) \exp(-\tau'/T_1)]^{-1} \quad . \tag{6}$$

Subtracting (5) from (4) gives

$$M_{n+1} - M_\infty = (M_n - M_\infty)(1-X) \exp(-\tau'/T_1) \quad . \tag{7}$$

From this recursion relation one obtains

$$M_n - M_\infty = (M_o - M_\infty)[(1-X) \exp(-\tau'/T_1)]^n \quad . \tag{8}$$

Substituting (5) in (8) gives

$$\begin{aligned} M_n - M_\infty &= (M_o - M_\infty)\left[1 - \frac{M_{eq}}{M_\infty}(1 - \exp(-\tau'/T_1))\right]^n \\ &\equiv (M_o - M_\infty) \exp(-t/T_H) \quad , \end{aligned} \tag{9}$$

where the last term expresses the fact that the observed decay shape will be a single exponential with decay constant T_H. Since $t = n(\tau' + 2\tau) \simeq n\tau'$, this implies that

$$\exp(-\tau'/T_H) = 1 - \frac{M_{eq}}{M_\infty}[(1 - \exp(-\tau'/T_1)], \tag{10}$$

which yields

$$\tau'/T_1 = -\ell n \left[1 - (1 - \exp(-\tau'/T_H)\frac{M_\infty}{M_{eq}})\right]. \tag{11}$$

Thus, the parameters which must be determined experimentally in order to solve for T_1 are T_H, M_∞ and M_{eq}. Note that equation (11) places no restrictions on the initial state of the magnetization, M_o. As can be seen from equation (9), the three parameters which are determined experimentally are T_H, M_∞ and M_o. Therefore, it is necessary to perform the

experiment in a way that will allow M_{eq} to be determined from M_o and the other measurable parameters. The most straightforward way of accomplishing this is to allow the system to fully recover before the start of each scan, so that $M_o = - M_{eq}$ or $+ M_{eq}$ depending on whether or not the initiating π-pulse is included.

It is possible to determine T_1 even if the measuring scans are being repeated so frequently that the magnetization cannot fully recover in between, as long as all the scans are identical and the time between the end of one scan and the beginning of the next, T, is held constant. After the first few scans are applied, the system will reach a steady state, and the value of M_o will be the same for all the decay curves which are obtained thereafter. The approach of M_o to its steady state value can be characterized by a time constant, T_o. If each scan contains N sampling groups and the initial magnetization of the j'th scan is $M_o^{(j)}$ (j = 0, 1, 2,...), then the time between $M_o^{(j)}$ and $M_o^{(j+1)}$ will be $N\tau' + T$. If we assume that the initiating π-pulse is not being applied, and that

$$(1 - X) \gg \exp\ (- N\tau'/T_H)\ , \tag{12}$$

then we obtain an equation relating $M_o^{(j+1)}$ to $M_o^{(j)}$ which is similar to equation (4):

$$M_o^{(j+1)} = [M_o^{(j)}\ e^{-N\tau'/T_H} + M_\infty\ (1 - e^{-N\tau'/T_H})\ ]\ e^{-T/T_1}$$

$$+ M_{eq}\ (1 - e^{-T/T_1})\ . \tag{13}$$

If the steady state value of M_o is given by $M_o^{(\infty)}$, then by replacing $M_o^{(j)}$ and $M_o^{(j+1)}$ by $M_o^{(\infty)}$ in equation (13) an expression can be obtained which is similar to equation (5). Then, in analogy with equations (8) and (9)

we obtain

$$M_o^{(j)} - M_o^{(\infty)} = (M_o^{(o)} - M_o^{(\infty)})[e^{-N\tau'/T_H} e^{-T/T_1}]^j$$

$$\equiv (M_o^{(o)} - M_o^{(\infty)}) e^{-j(N\tau' + T)/T_o} \qquad (14)$$

This yields

$$T_o = \frac{T_1 T_H}{N\tau' T_1 + T T_H} (N\tau' + T) . \qquad (15)$$

A similar analysis shows that (15) also applies when the initiating π-pulse is included in each scan. Table 1 gives several representative examples of the approach of $M_o^{(j)}$ to its steady state value. As can be seen from the Table, only a few scans are required to reach steady state when $N\tau' \geq T_H$ and $T \geq T_1$.

Once the system has reached steady state, signal averaging can begin. It is then possible to determine T_1 by considering the detailed behavior of the magnetization. The magnetization at the end of each scan, M, will be given by

$$M = M_{N-1} (1 - X)$$

$$= [(M_o - M_\infty) e^{-(N-1)\tau'/T_H} + M_\infty](1 - X) , \qquad (16)$$

where equation (9) has been used to expand M_{N-1}. By comparing equations (8) and (9), we see that

$$(1 - X) = e^{\tau'/T_1} e^{-\tau'/T_H} , \qquad (17)$$

which can be combined with (6) to give

$$M_\infty = M_{eq}(1 - e^{-\tau'/T_1})[1 - e^{-\tau'/T_H}]^{-1} \quad . \tag{18}$$

At this point, the analysis must be divided into two cases. If the scan is not initiated by a π-pulse, M_o is given in terms of M by

$$M_o = (M - M_{eq})\, e^{-T/T_1} + M_{eq} \quad . \tag{19a}$$

If the π-pulse is included, it inverts the sign, giving

$$M_o = -(M - M_{eq})\, e^{-T/T_1} - M_{eq} \quad . \tag{19b}$$

Equations (1) and (16)-(19) can be combined to give the following results: For the case of no π-pulse,

$$e^{-\tau'/T_1} = 1 - (1 - e^{-\tau'/T_H})\frac{M_\infty}{M_o}[1 - e^{-T/T_1} A_o]$$

$$A_o = \frac{(1 - e^{-N\tau'/T_H})(1 - e^{-\tau'/T_H} e^{\tau'/T_1})}{(1 - e^{-\tau'/T_H})(1 - e^{-T/T_1} e^{-N\tau'/T_H} e^{\tau'/T_1})} \quad ; \tag{20a}$$

if the π-pulse is included,

$$e^{-\tau'/T_1} = 1 - (1 - e^{-\tau'/T_H})\frac{M_\infty}{M_o}[-1 + e^{-T/T_1} A_\pi]$$

$$A_\pi = \frac{(1 - e^{-N\tau'/T_H})(1 - e^{-\tau'/T_H} e^{\tau'/T_1}) + 2\, e^{-N\tau'/T_H} e^{\tau'/T_1}(1 - e^{-\tau'/T_H})}{(1 - e^{-\tau'/T_H})(1 + e^{-T/T_1} e^{-N\tau'/T_H} e^{\tau'/T_1})} \quad . \tag{20b}$$

In either case the last term, A, is clearly a correction term, and equation (20) can be solved by iteration. In all the practical examples we encountered

($T \geq T_1$, $N\tau' \geq T_H$) this iteration process converged to within .1% in less than 6 cycles.

In the limiting case

$$N\tau' \gg T_H \ , \tag{21}$$

only one scan is required for M_o to reach steady state, and equations (20a) and (20b) reduce to a common expression,

$$e^{-\tau'/T_1} = 1 - (1 - e^{-\tau'/T_H}) \frac{M_\infty}{|M_o|} \left[1 - e^{-T/T_1} \ \frac{1 - e^{-\tau'/T_H} e^{\tau'/T_1}}{1 - e^{-\tau'/T_H}}\right], \tag{22}$$

which agrees with the expression derived by Look and Locker.[8] Of course, if $T \gg T_1$, then $|M_o| = M_{eq}$ and equation (22) reduces to equation (10). It is interesting to note that under the added condition

$$\tau'/T_H \ll 1 \ , \tag{23}$$

which is equivalent to assuming that the spin heating process is evenly distributed over the entire scan, equation (10) reduces to a much simpler form:

$$T_1 = \frac{M_{eq}}{M_\infty} T_H \ . \tag{24}$$

If, for example, $M_{eq}/M_\infty = 2$, the fractional error generated by this distributed heating assumption is given by τ'/T_H. Therefore, when this level of accuracy is acceptable, the analysis of the data can be greatly simplified by using equation (24).

C. EXPERIMENTAL PROCEDURE

In order to extract all of the parameters from a single scan which are required for calculating T_1, it is necessary to record the baseline along with the exponential decay of the magnetization. This usually presents no problems, because the baseline can be sampled between the triplet pulse groups. Sometimes it is more convenient, however, to employ a two-scan approach in order to avoid the need to measure the baseline directly. In this scheme the magnetization is allowed to return to equilibrium before the start of each scan. The first scan is applied as shown in Figure 1, yielding

$$M(t) = (-M_{eq} - M_{\infty}) \exp(-t/T_H) + M_{\infty} \quad , \tag{25}$$

while in the second scan the initiating π-pulse is omitted, giving

$$M(t) = (M_{eq} - M_{\infty}) \exp(-t/T_H) + M_{\infty} \quad . \tag{26}$$

One can then add and subtract the data from these two scans to obtain

$$M_{+} = (-2\, M_{\infty})\, e^{-t/T_H} + 2\, M_{\infty} \tag{27}$$

and

$$M_{-} = (2\, M_{eq})\, e^{-t/T_H} \quad . \tag{28}$$

By extracting the amplitudes and decay constants of these two curves, the required parameters can be determined without directly measuring the electronic baseline level.

Because of the design of the pulse spectrometer, it was convenient to direct the initial π-pulse along the -y direction. Also, the recovery time of our receiver was about 8 μsec, so τ was set to 10 μsec and the signal was sampled near the peaks of the solid echoes, i.e., just before the $(\frac{\pi}{2})_{-x}$ pulses.

For analyzing exponential decays, the exponential least squares fit[9] was found to be much more satisfactory than the logarithmic fit which is more commonly used. The logarithmic fit involves taking the logarithm of each point and then extracting the slope and y-intercept from the resulting straight line. This method requires that the baseline, M_∞, be determined very accurately before the logarithms of the points are calculated. Also, taking the logarithms of the points in the exponential tail tends to amplify the noise in that region tremendously, thereby reducing the accuracy of the fit.

The least squares fit, on the other hand, requires no independent determination of the baseline. In fact, it automatically yields the best fit to the baseline as well as the amplitude and decay constant, and it utilizes the full curve. Although the calculations for this least squares fit are more complicated than those for the logarithmic method, and although some iteration is involved in their solution, they are easily handled by a minicomputer or programmable calculator. In our case the data were analyzed by a DEC PDP 11/10 minicomputer interfaced to a Fabri-Tek 1070 signal averaging computer.

D. EXPERIMENTAL ANALYSIS

In order to test the solid echo technique and compare it with other single scan and multiple scan techniques, a number of measurements of T_1 were made at ambient temperature and pressure using single crystals of uranium-doped CaF_2.

The result of a typical T_1 measurement is shown in Figure 2. The lower trace in the figure was obtained using the full sequence shown in Figure 1, while the π-pulse was omitted for the upper trace. Also, the magnetization was allowed to return to thermal equilibrium before the start of each scan so that M_{eq} could be obtained directly from M_o.

The data shown in figure 2 are analyzed in Table 2. The T_1 values shown in the first column of the table were calculated using equation (11), while the results in the second column are from equation (24). A comparison of the T_1 calculations therefore measures the validity of the distributed spin heating assumption. The ratio M_{eq}/M_∞ is also listed in each case as a measure of the strength of the spin heating.

A measurement of T_1 was also made using the inversion-recovery multiple scan technique under conditions identical with those of Table 2. The result obtained, T_1=2.48 sec., is indistinguishable from the results in the table. Also, the flip-flop method was compared with our single scan technique. The results of the two methods agreed well, but the uncertainty for the flip-flop method was greater by a factor of 3, and the spin-heating ratio was larger by a factor of 3.6. This illustrates the clear advantage of our technique over the flip-flop method.

The effect of varying τ' in our solid echo pulse sequence is shown in Table 3. There is good agreement between all the T_1 values in the table, and the ratios M_{eq}/M_∞ show the decreasing trend of the spin heating with increasing τ'. The two scan method was used to obtain all the data in the table.

The validity of equation (20) for determining T_1 when the scans are repeated rapidly was demonstrated experimentally with and without the initiating π-pulse for values of $N\tau'/T_H$ between 2 and 7 and T/T_1 between 1 and 6. (The CaF_2 single crystal which was used to obtain the data in Tables 2 and 3 was also used in this case, but the crystal orientation was different than it was for either table.) The result, T_1=2.35 sec, was obtained consistently, but the repeatability of the measurements was somewhat reduced for the smaller values of $N\tau'/T_H$ and T/T_1, because in these cases the noise led to greater errors in exponential curve fitting. In order to characterize the repeatability which can be expected when applying our experimental procedure, over 5,000 computer simulated decay curves were analyzed for a wide range of noise levels and other experimental conditions. The results are discussed in sub-section F along with formulae and characteristic curves which relate the experimental parameters to the expected uncertainty of the results.

As a more practical test of our method, T_1 was measured for a different CaF_2 single crystal with a relatively long spin lattice relaxation time. A single scan with an initiating π-pulse and with τ' = 5 sec was used. The resulting values of T_1 = 107.3 sec and M_{eq}/M_∞ = 1.75 were found to be repeatable within 1.0%. Only about 20 min were required to obtain a 250 point decay curve using our method, while a curve of only 50 points using a multiple scan technique such as inversion-recovery would have required almost 9 hours.

The solid echo method was also used to measure T_1 for powder samples of several other solids, including NaF, KBF_4, $C_{10}F_8$ and C_6F_{12}. The repeatability of these measurements and the spin heating ratios were found to be comparable to the CaF_2 case.

Figure 3 compares T_1 measurements for frozen C_6F_6 made using the technique described in this section with measurements made by Boden et al.[10]

using the $\{(\pi/2)_x - \tau - (\pi/2)_x\}$ sequence. The differences between the two curves agree well with the thermodynamic prediction according to the Zeeman field strengths. For example, the ratios of the T_1 values for the two curves at the minima are 1.13 and 1.14, which can be compared with the predicted value 1.06. Notice also that the overall shapes of these curves are the same as the shapes of the $T_{1\rho}$ curves for C_6F_6 given in figure 6 of section 3, except that the T_1 curves are shifted considerably toward higher temperature. This is expected, since the Zeeman field H_o is much stronger than the rf spin-locking field, $\overline{H}_1$, used in measuring $T_{1\rho}$.

Although the technique described in this section was designed for use with solid samples, it is also applicable to liquids. This is illustrated in Figure 4, which was obtained using C_6F_6. As in Figure 2, the lower trace was generated using an initiating π-pulse while in the upper trace this pulse was omitted, and the magnetization was allowed to recover completely before each scan. The value of T_1 obtained from the lower trace is 1.88 sec, and the spin heating ratio, $M_{eq}/M_\infty = 1.09$, shows that there was almost no spin heating. Even though the pulse sequence does not refocus the magnetization in the liquid case, there is still very little spin heating because, for liquids, τ can be made much smaller than T_2. When our technique is applied to liquids, however, all of the effects due to spectrometer misadjustments will not be in the form of spin heating, as they are in the case of solids. Therefore, accurate determination of T_1 in the liquid case requires more careful tuning of the spectrometer. There are methods which have a slight advantage over our technique in the liquid case, such as the z-restoring sequence, which was discussed in the Introduction, but they are restricted more or less to liquids. Our technique eliminates the need to use separate pulse sequences for solids and liquids.

E. OTHER POSSIBLE SEQUENCES

Several other pulse sequences were considered as possible alternatives to the solid echo technique presented in this section. One idea was to use a "magic" echo [11] in place of the solid echo. Such a sequence might be expected to produce even less spin heating than the solid echo method, because the "magic" echo causes a more complete refocussing of the magnetization, especially when the initial free induction decay and its echo are separated by more than T_2. However, the solid echo is nearly as efficient as the magic echo for the small τ which are used in the T_1 sequence. Also, the magic echo involves a more complicated pulse sequence, which means that a magic echo T_1 sequence would be more complicated to produce than the solid echo sequence, and would be more sensitive to pulse imperfections.

Another possibility was to use a single cycle of either the 4- or 8-pulse line narrowing sequence [12] as the sampling pulse group. However, it was found that these T_1 sequences are more sensitive to resonance misadjustment than the present method. In one experiment the 4-pulse T_1 sequence showed a strong systematic error in T_1 at 1 KHz off resonance and the 8-pulse T_1 sequence showed a similar effect at 2 KHz while the present solid echo technique gave accurate T_1 results under the same conditions, although the resonance misadjustments caused some increases in spin heating.

T_1 measuring sequences which utilize the 4- or 8-pulse cycle may be more convenient to produce on some spectrometers which have already implemented these cycles for measuring the high resolution chemical shift spectra of solids. Otherwise, the basic solid echo technique introduced in this paper is clearly a better choice.

F. REPEATABILITY OF MEASUREMENTS

In order to determine the repeatability which can be expected from the experimental procedure outlined in this section, over 5,000 computer generated decay curves representing a wide range of experimental conditions were analyzed. In order to simulate the results of an experimental measurement, M_∞ was obtained in each case from equation (18) and M_o was calculated using equation (20). For convenience, it was assumed that $T_H = 1/2\ T_1$. Random noise with a gaussian envelope of the form

$$f(r) = \exp\left(-\frac{1}{2}\ r^2/a^2\right) \tag{29}$$

was superimposed on each decay curve, and the simulated spectrum was analyzed using the exponential least squares fit as described in the Experimental Procedure section. Equation (20) was then solved by iteration to obtain T_1.

It was found that y, the root-mean-square of the error, in percent, of the T_1 determinations, was directly proportional to the inverse noise ratio, x, defined by

$$x = a/M_{eq} \tag{30}$$

where a is the standard deviation of the noise as defined in equation (29), for any given values of $N\tau'/T_H$ and T/T_1: i.e.,

$$y/x = B \quad . \tag{31}$$

Furthermore, the dependence of B on $N\tau'/T_H$ and T/T_1 was found to be of a simple, exponential form:

$$B = C_1 + C_2\, e^{-N\tau'/T_H} + C_3\, e^{-T/T_1} + C_4\, e^{-N\tau'/T_H}\, e^{-T/T_1} \qquad (32)$$

where C_1-C_4 are constants. Thus it is possible to characterize the dependence of the RMS error in T_1 on the noise ratio under all experimental conditions by specifying the four constants C_1 through C_4. The values which were extracted from the simulated data are given in Table 4 for both when the π-pulse is included and when it is not.

The characteristic curves in Figures 5 and 6, which were generated using equations (29) - (32) and Table 4, can be very useful for selecting experimental parameters which will provide the required accuracy in T_1. For example, assume that the noise ratio (1/x) is 100, and it is required that T_1 for a certain sample be determined within 2%. Then y/x=200, and it can be seen from Figure 5 that if the initiating π-pulse is included in the measuring sequence, and if the signal is allowed to decay for 2 time constants ($N\tau'/T_H = 2$), then the time between scans need only be about $2T_1$. However, it can be seen from Figure 6 that if the initiating π-pulse is not included, then a measurement using these same parameters ($T/T_1=2$, $N\tau'/T_H=2$) will produce data which are only accurate within 10% ($y/x \approx 1000$).

REFERENCES

1. A. Csaki and G. Bene, Compt. Rend. Acad. Sci. 251, 228 (1960).

   R. L. Streever and H. Y. Carr, Phys. Rev. 121, 20 (1961).

2. D. C. Look and D. R. Locker, J. Chem. Phys. 50, 2269, (1969).

3. D. E. Demco and V. Simplaceanu, Rev. Roum. Phys. 18, 623 (1973).

   D. E. Demco, V. Simplaceanu and I. Ursu, J. Magn. Res. 15, 166 (1974).

4. J. G. Powles and P. Mansfield, Phys. Lett. 2, 58 (1962).

5. J. G. Powles and J. H. Strange, Proc. Phys. Soc. 82, 6 (1963).

6. P. Mansfield, Phys. Rev. A 137, 961 (1965).

7. D. C. Look and D. R. Locker, Phys. Rev. Lett. 20, 987, (1968).

8. D. C. Look and D. R. Locker, Rev. Sci. Instrum. 41, 250 (1970).

9. M. Sass and D. Ziessow, J. Magn. Res. 25, 263 (1977).

10. N. Boden, P. P. Davis, C. H. Stam and G. A. Wesslink, Mol. Phys. 25, 87 (1973).

11. W. K. Rhim, A. Pines and J. S. Waugh, Phys. Rev. Lett. 25, 218 (1970.

12. W. K. Rhim, A. Pines and J. W. Waugh, Phys. Rev. B 3, 684 (1971).

    U. Haeberlen and J. S. Waugh, Phys. Rev. 175, 453 (1968).

    W. K. Rhim, D. D. Elleman and R. W. Vaughan, J. Chem. Phys. 59, 3740 (1973).

TABLE I

EXAMPLES OF THE APPROACH OF

M_o TO ITS STEADY STATE VALUE (SEE EQUATION (14))

$\frac{N\tau'}{T_H}$	$\frac{T}{T_1}$	Scan No. (j)	$[M_o^{(j)} - M_o^{(\infty)}]/[M_o^{(o)} - M_o^{(\infty)}]$	
			Without π - Pulse	With π - Pulse
1	1	0	1.0000	1.0000
		1	0.1353	-0.1353
		2	0.0183	0.0183
		3	0.0025	-0.0025
		4	0.0003	0.0003
2	1	1	0.0498	-0.0498
		2	0.0025	0.0025
		3	0.0001	-0.0001
2	2	1	0.0183	-0.0183
		2	0.0003	0.0003
3	2	1	0.0067	-0.0067
		2	0.0000	0.0000

TABLE II

ANALYSIS OF FIGURE 2 (τ' = 80 msec.)

METHOD OF ANALYSIS	T_1 (sec) No Assumptions	T_1 (sec) Distributed spin Heating Assumption	M_{eq}/M_o
Single Scan with π-pulse	2.47	2.46	1.25
without π-pulse	2.44	2.43	1.25
2 - Scan	2.48	2.47	1.26

TABLE III

EFFECT OF VARYING τ' ON THE PRESENT METHOD

τ' (msec.)	T_1 (sec.)	M_{eq}/M_∞
20	1.76	2.71
40	1.72	1.85
60	1.75	1.55
80	1.73	1.45
100	1.70	1.33

TABLE IV

CONSTANTS FOR EQUATION (32)

	With π-pulse	Without π-pulse
C_1	24.	100.
C_2	620.	1370.
C_3	215.	353.
C_4	3060.	32,700.

FIGURE CAPTIONS

1. The solid echo pulse sequence for single scan T_1 measurements in solids. The initiating π-pulse may be applied along any direction, and is sometimes omitted.

2. Spin-Lattice decay curves obtained by applying the pulse sequence of Figure 1 to a CaF_2 single crystal. For the upper trace the initiating π-pulse was omitted. The data rate was 80 msec./point.

3. T_1 as a function of temperature for frozen C_6F_6. Results obtained using the solid echo technique are compared with measurements made by Boden et al. using a multiple scan method. The strength of the Zeeman field is indicated for each curve.

4. Spin-Lattice decay curves obtained from a liquid sample (C_6F_6) by applying the pulse sequence of Figure 1. The initiating π-pulse was omitted for the upper trace. The data rate was 40 msec./point.

5. The anticipated RMS error in T_1 due to inaccurate exponential curve fitting. It is assumed that the initiating π-pulse is included in the pulse sequence, and that the scans are of length $N\tau'$ and are repeated with separation time T. It is also assumed that the noise is gaussian with standard deviation = a, and that the non-linear least squares method is used to fit the data. $x \equiv a/M_{eq}$, and y is the root-mean-square of the error in the experimentally determined value of T_1.

6. The anticipated RMS error in T_1 due to inaccurate exponential curve fitting. It is assumed that the initiating π-pulse is not included in the pulse sequence, and that the scans are of length $N\tau'$ and are repeated with separation time T. It is also assumed that the noise is gaussian with standard deviation = a, and that the non-linear least squares method is used to fit the data. $x \equiv a/M_{eq}$, and y is the root-mean-square of the error in the experimentally determined value of T_1.

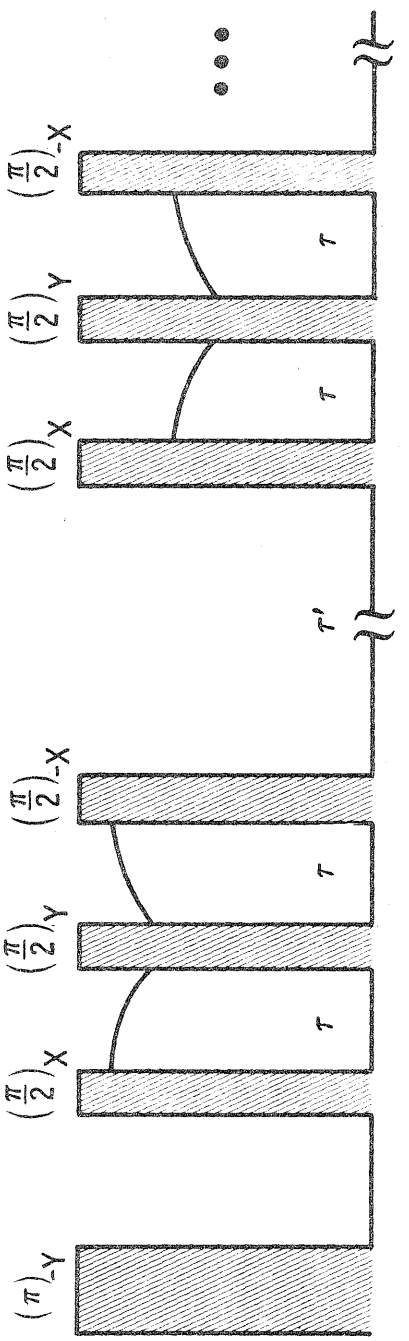
$(\pi)_{-Y}$
$(\frac{\pi}{2})_X$
$(\frac{\pi}{2})_Y$
$(\frac{\pi}{2})_{-X}$
τ
τ
τ
τ'
$(\frac{\pi}{2})_X$
$(\frac{\pi}{2})_Y$
$(\frac{\pi}{2})_{-X}$
τ
τ
τ

Fig. 1

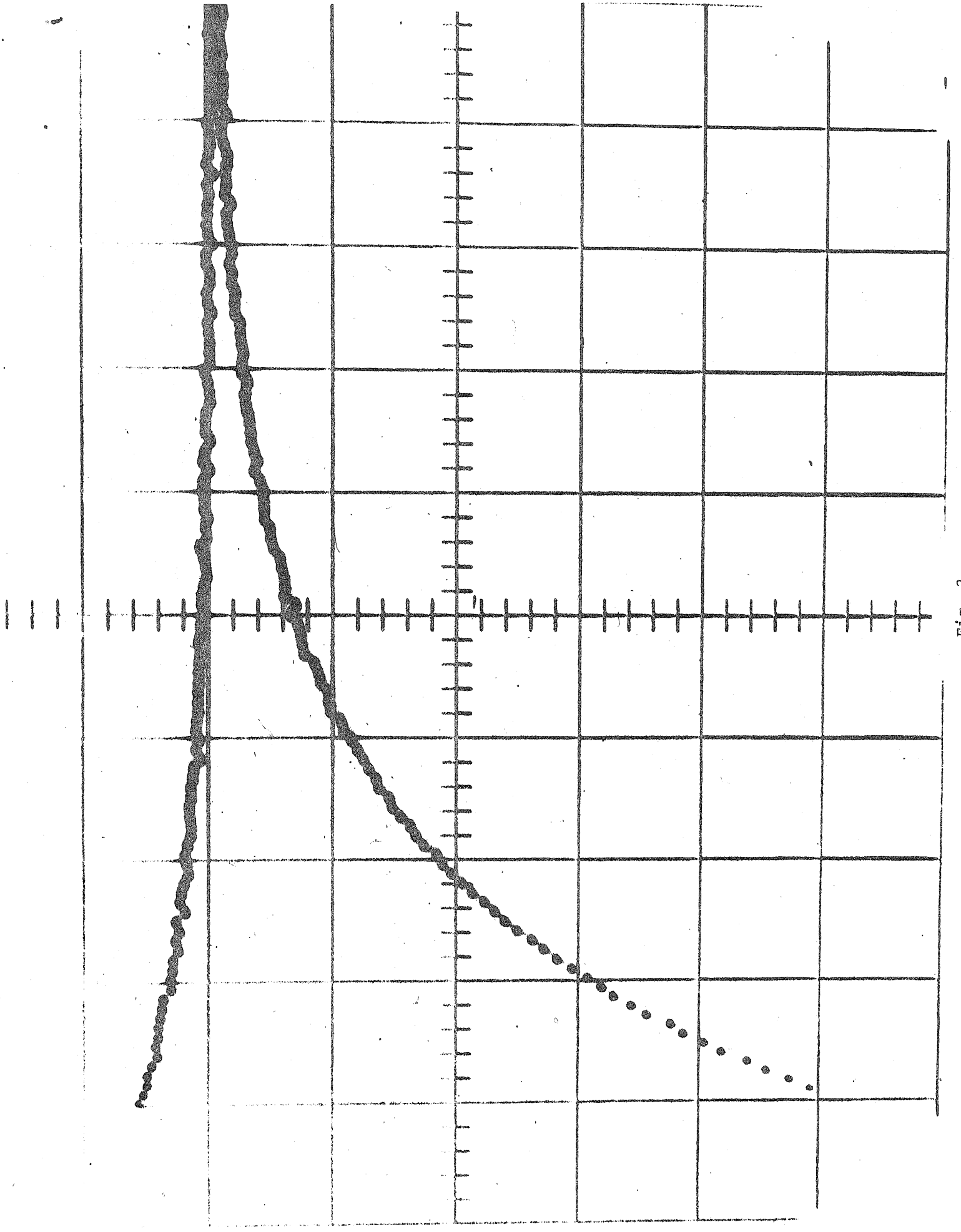

Fig. 2

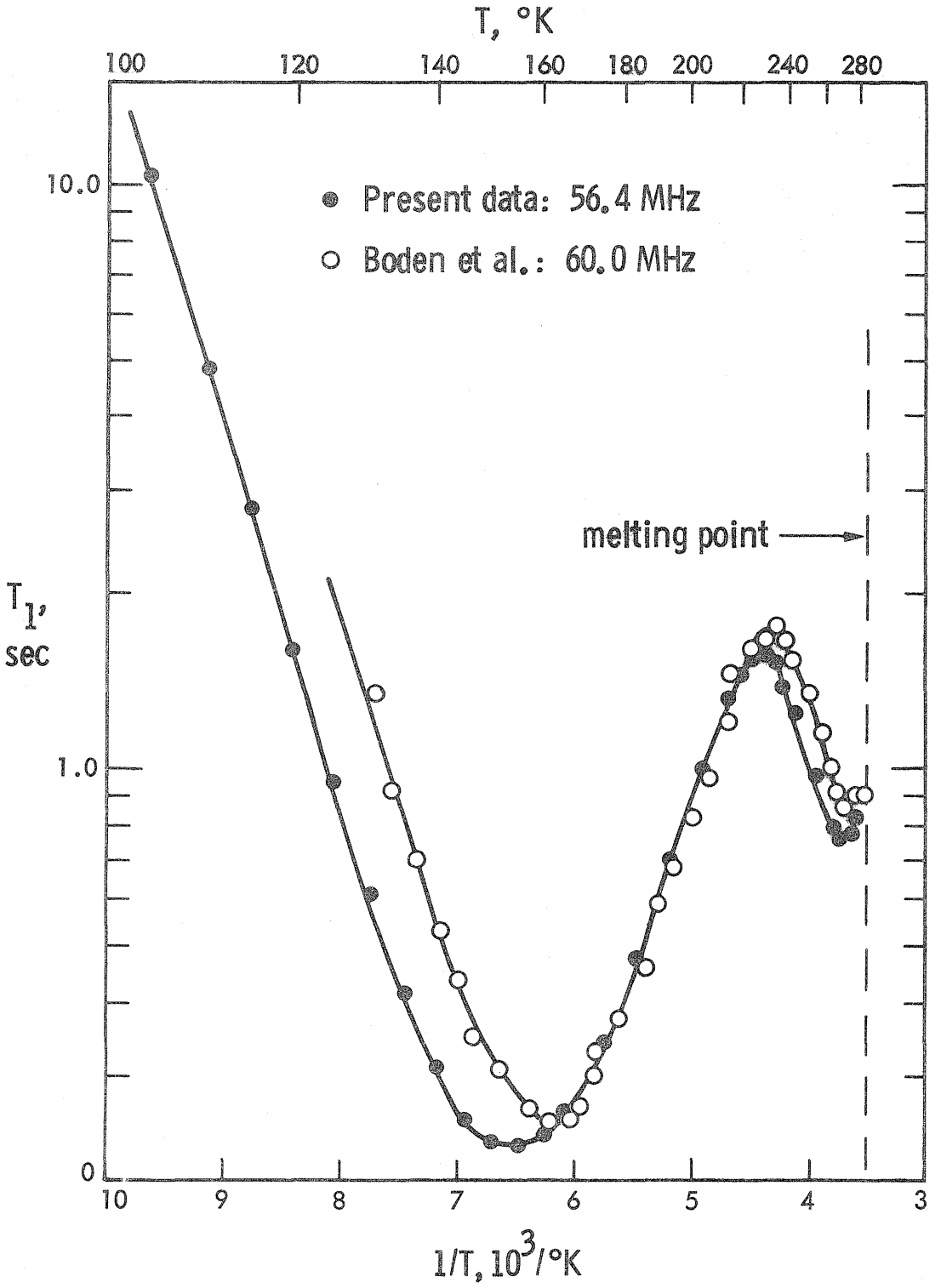
T, °K
100
120
140
160
180
200
240
280
10.0
1.0
0
Present data: 56.4 MHz
Boden et al.: 60.0 MHz
melting point
T1, sec
10
9
8
7
6
5
4
3
1/T, 10³/°K

Fig. 3

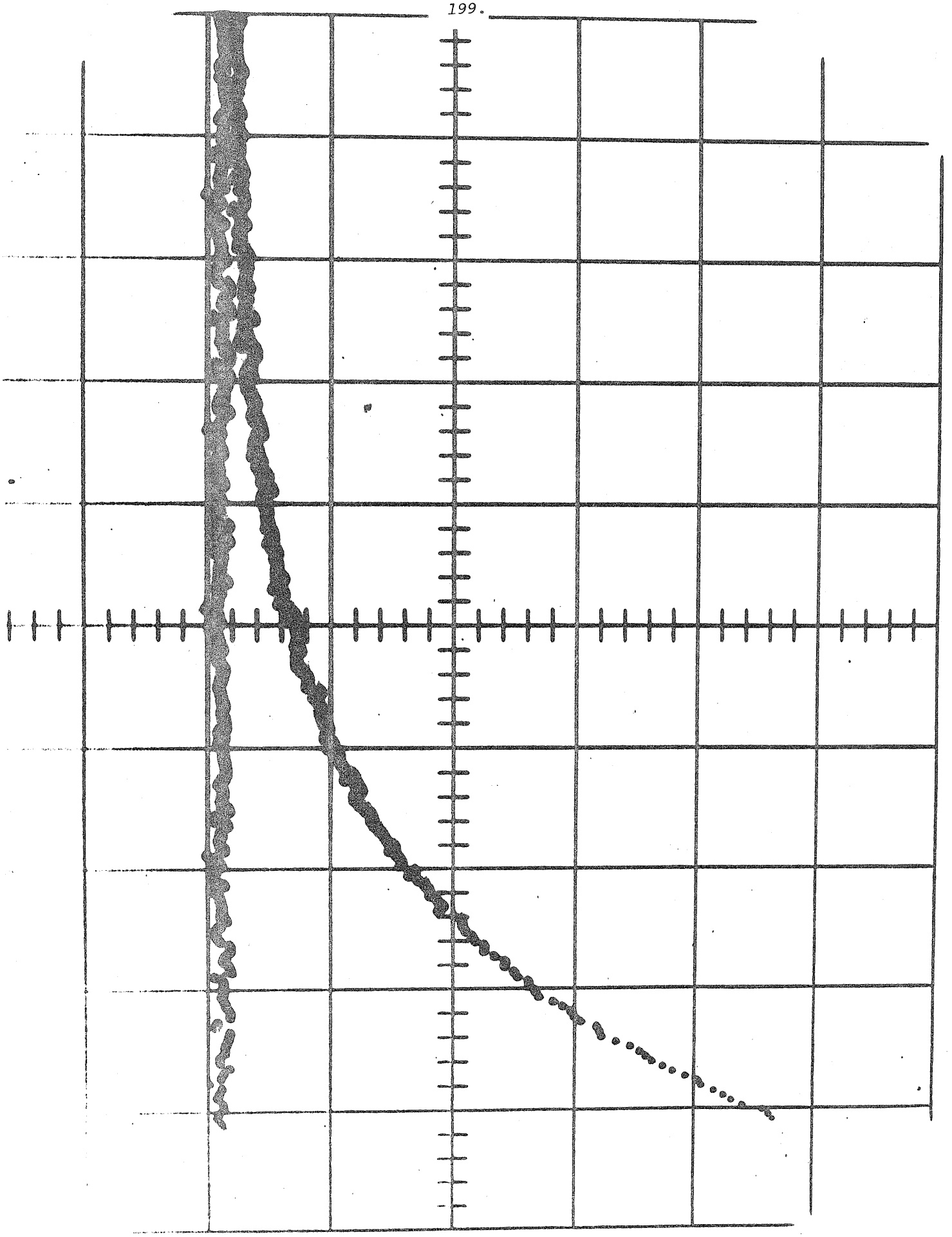

Fig. 4

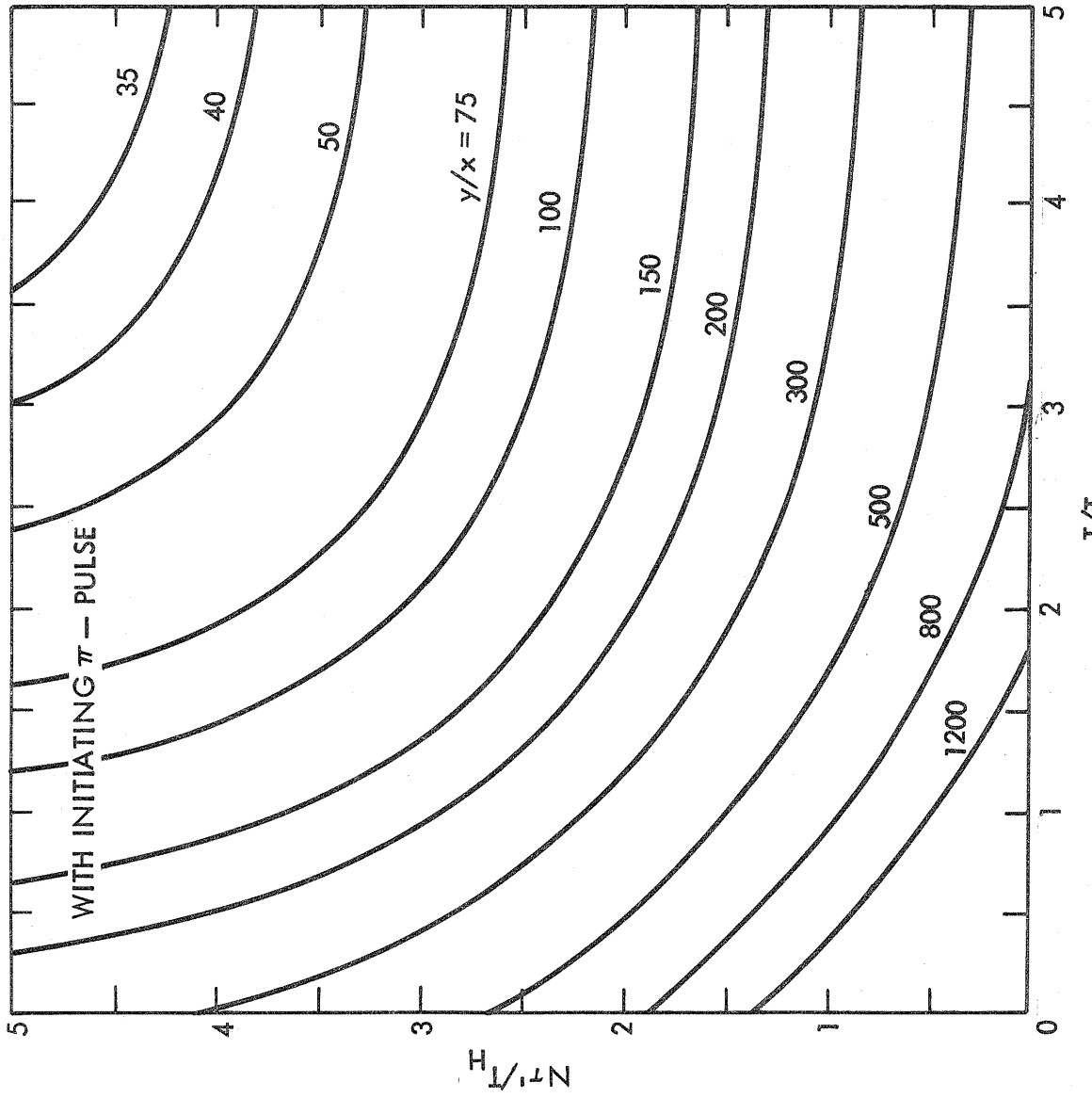
WITH INITIATING π — PULSE
35
40
50
y/x = 75
100
150
200
300
500
800
1200
0
1
2
3
4
5
Nτ'/T_H
T/T_1

Fig. 5

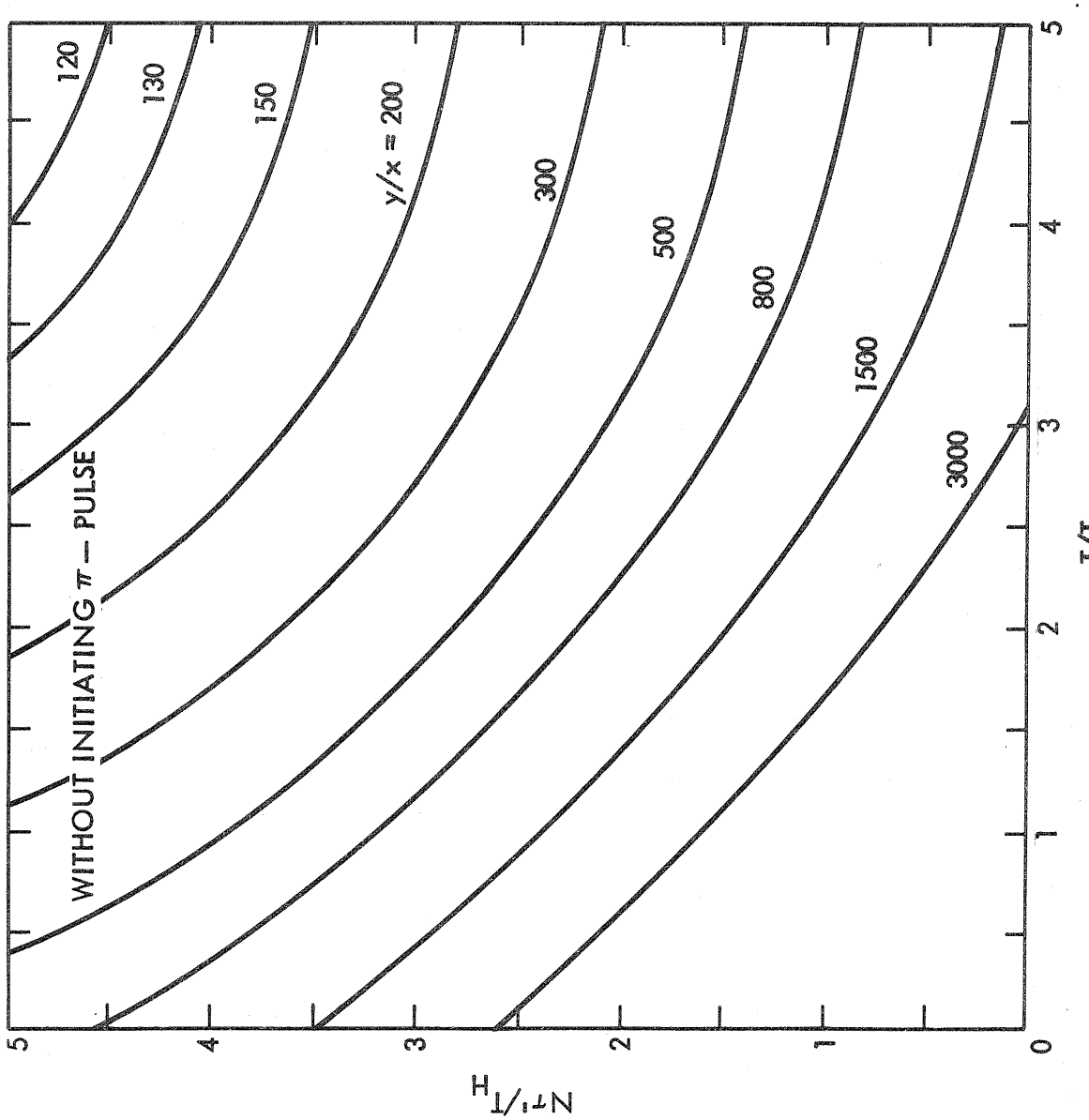
WITHOUT INITIATING π – PULSE
120
130
150
y/x = 200
300
500
800
1500
3000
0
1
2
3
4
5
N τ'/T_H
T/T_1

Fig. 6

APPENDIX

A SIMPLE, HIGHLY FLEXIBLE PULSE SEQUENCE GENERATOR

This appendix describes a simple yet highly flexible pulse sequence generator which was entirely designed a build in the laboratory using readily available components. Not only is this pulse generator a useful instrument, it also demonstrates that the seemingly complex experiments described in chapters 2 and 3 can be easily implemented using current technology.

A block diagram of the pulse sequence generator is shown in Figure 1. Although this device is essentially a special purpose computer, it does not utilize a micro-processor. Instead, it was found that a faster and more efficient instrument could be constructed using a high speed 256 x 16 bit memory and simple logic circuitry composed of TTL compatible gates, counters and multiplexers. A wide variety of experiments can be performed using this device, including single and double resonance experiments involving both cw and pulsed rf irradiation.

The pulse sequence generator can be controlled either from the front panel or via its interface to a PDP 11/10 computer. It has three types of output: Five primary outputs X1, Y1, -X1, -Y1 and Z1; five secondary outputs X2, Y2, -X2, -Y2 and Z2; and eight triggering outputs A-H. One primary output, one secondary output and any number of trigger outputs can be altered simultaneously. For example, a 1 μsec. pulse might appear at X1 at the same time that Y2 is turned on and trigger pulses appear at outputs A, E and H.

The block diagram of the pulse sequence generator given in figure 1 illustrates its basic operation. Programmed instructions are loaded into the 256 word x 16 bit (RAM) Memory either from the front panel or from the PDP 11/10 computer. The instruction cycle time, and thus the minimum time

between adjacent pulses, is 1.2 μsec. After being loaded, the pulse generator operates independently of the PDP 11/10. The Memory is addressed by a Program Counter which can be preset with a value from the Data Bus. The Program Counter is advanced by pulses from the Master Clock when the P.C. Flip-Flop enables the buffer between them.

Tables 1 and 2 summarize the pulse program instruction set. All timing is controlled by Function 1 instructions. When one of these instructions is executed a signal from the Output Multiplexer shown in figure 1 causes the value of τ given in bits 0-7 of the Data Bus to be loaded into the τ-Counter, which immediately begins counting pulses from the Master Clock. Simultaneously, the P.C. Flip-Flop is reset by the Output Multiplexer and the Master Clock begins advancing the Program Counter. Instructions in memory are executed until the next Function 1 appears on the Data Bus, at which point the Command Decoder sets the P.C. Flip-Flop and halts the Program Counter. Meanwhile, the τ-Counter continues to measure the elapsed time since the previous Function 1 instruction was executed. When it has received the specified number of clock pulses, the τ-Counter sends a Pulse Enable signal to the Output Multiplexer. The Function 1 instruction currently being addressed is still not executed until the Output Multiplexer subsequently receives a Pulse Fire signal from the Master Clock. If the Function 1 command does not require an external trigger, this will occur with the next Master Clock pulse. If a trigger is required, the Command Decoder will have set the Trigger Flip-Flop, isolating the Master Clock from the Output Multiplexer. In this case, the Function 1 instruction is not executed until an external trigger pulse resets the Trigger Flip-Flop and allows

the Pulse Fire signal to be transmitted to the Output Multiplexer. In either case all output is synchronized with the Master Clock. Note that the value of τ specified in a Function 1 command determines the time separating the execution of that command from the execution of the next Function 1, assuming that the second Function 1 does not require an external trigger.

All the other instructions shown in Table 1 are executed as rapidly as possible, the required time per instruction being 1.2 μsec. When a Function 2 command appears on the Data Bus, the Command Decoder causes bits 0-11 to be loaded into a latch in the Output Multiplexer. The appropriate secondary and trigger outputs then occur simultaneously with the next Function 1 execution.

Conditional program loops are generated using the Loop Counter. The number of loops is preset using the SET N command. When this command appears on the Data Bus, the Command Decoder causes bits 0-11 to be loaded into the Loop Counter. Whenever a LOOP command subsequently appears the Command Decoder signals the Loop Counter and also causes the Program Counter to jump to the address specified by bits 0-7 in the LOOP command. After the specified number of loops the Loop Counter disables the "Load" input of the Program Counter, and the next LOOP instruction is effectively ignored.

A BRANCH command of course has the same effect as a LOOP command, except that it does not interact with the loop counter and therefore is unconditional.

Table 2 summarizes the function codes for bits 8-11 of Function 1 and Function 2 commands. Note that output pulse lengths can be controlled

in two ways. For a "pulse" command such as X PULSE, the output pulse width is controlled by a one-shot and a timing potentiometer on the front panel. Alternatively, the pulse width can be set under program control by using separate X ON and X OFF commands. Of course, the pulse length must then be longer than the 1.2 μsec instruction cycle time. The use of a 10 MHz clock (Figure 1) allows values of τ to be specified in multiples of 0.1 μsec.

A pulse programming example is given in Table 3, which presents a set of instructions to generate the REV-8 pulse cycle shown in Figure 1 of chapter 2, section 3. The first command sets the loop counter to cause 1024 loops. The next two instructions cause the device to halt and wait for an external trigger pulse. When the pulse generator is triggered, a pulse is produced at output A. This can be used to trigger an oscilloscope or other data recording instruments. After 10 μsec. an X pulse is generated as a pre-pulse, and simultaneously a triggering pulse appears at output B to indicate a sampling window. Instructions 5-13 (octal) proceed to generate all but the last pulse in the REV-8 cycle. This final pulse is generated by looping back to instruction 3, so that the X pre-pulse becomes part of the cycle. Thus the following pulse sequence is generated by the series of instructions given in Table 3:

$$A - \tau' - [(X + B) - 2\tau - X - \tau - Y - 2\tau - \bar{Y} - \tau - \bar{X} - 2\tau - \bar{X} - \tau - Y - 2\tau - \bar{Y} - \tau -]_{1024} \qquad (1)$$

where $\tau' = 10.0$ μsec., $\tau = 3.0$ μsec. and $\bar{X} \equiv -X$, etc. The final instruction in the pulse program causes the entire procedure to repeat, so that the next external trigger pulse will initate another 1024 cycles. In this example all pulse lengths are set by means of the front panel one-shot controls.

Table 1

INSTRUCTION SET

INSTRUCTION	BINARY CODE															
	15	14	13	12	11	10	9	8	7	6	5	4	3	2	1	Ø
FUNCTION 1 (NO TRIGGER)	Ø	Ø	Ø	Ø	FUNCTION CODE[a]				←			T				→
FUNCTION 1: TRIGGERED	Ø	Ø	Ø	1	FUNCTION CODE[a]				←			T				→
FUNCTION 2	1	Ø	1	1	FUNCTION CODE[a]				H	G	F	E	D	C	B	A
SET N	1	Ø	1	Ø	←				N							→
LOOP	1	Ø	Ø	Ø	NOT USED				←			ADDRESS				→
BRANCH	1	Ø	Ø	1	NOT USED				←			ADDRESS				→

a. See Table 2.

Table 2

FUNCTION CODES

FUNCTION	FUNCTION CODE
No op.	Ø Ø Ø Ø
X PULSE	Ø Ø Ø 1
Y PULSE	Ø Ø 1 Ø
-X PULSE	Ø Ø 1 1
-Y PULSE	Ø 1 Ø Ø
Z PULSE	Ø 1 Ø 1
Z ON	Ø 1 1 Ø
Z OFF	Ø 1 1 1
X ON	1 Ø Ø Ø
X OFF	1 Ø Ø 1
Y ON	1 Ø 1 Ø
Y OFF	1 Ø 1 1
-X ON	1 1 Ø Ø
-X OFF	1 1 Ø 1
-Y ON	1 1 1 Ø
-Y OFF	1 1 1 1

Table 3

Program Example: REV-8

ADDRESS (OCTAL)	Instruction
0	SET N = 1024.
1	FN. 2 (NO OP) A
2	FN. 1: TRIGGERED (NO OP) τ = 10.0
3	FN. 2 (NO OP) B
4	FN. 1 (X PULSE) τ = 6.0
5	FN. 1 (X PULSE) τ = 3.0
6	FN. 1 (Y PULSE) τ = 6.0
7	FN. 1 (-Y PULSE) τ = 3.0
10	FN. 1 (-X PULSE) τ = 6.0
11	FN. 1 (-X PULSE) τ = 3.0
12	FN. 1 (Y PULSE) τ = 6.0
13	FN. 1 (-Y PULSE) τ = 3.0
14	LOOP TO 3
15	BRANCH TO 0

Figure Caption

Fig. 1. Block diagram of the pulse generator.

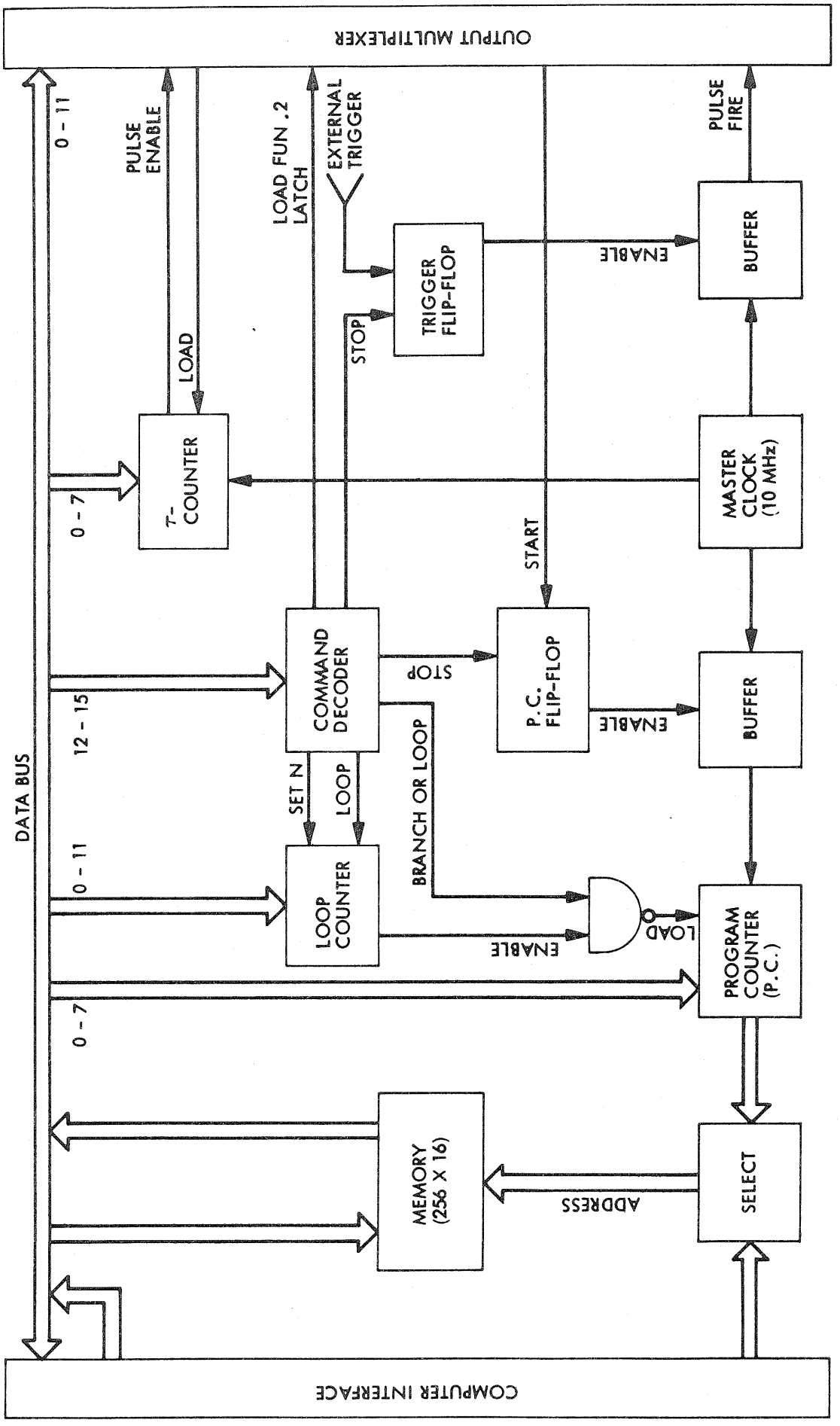
OUTPUT MULTIPLEXER
COMPUTER INTERFACE
DATA BUS
0 - 11
PULSE ENABLE
LOAD
LOAD FUN .2 LATCH
EXTERNAL TRIGGER
STOP
TRIGGER FLIP-FLOP
ENABLE
BUFFER
PULSE FIRE
τ- COUNTER
0 - 7
MASTER CLOCK (10 MHz)
START
COMMAND DECODER
STOP
P.C. FLIP-FLOP
ENABLE
BUFFER
12 - 15
SET N
LOOP
BRANCH OR LOOP
0 - 11
LOOP COUNTER
ENABLE
LOAD
PROGRAM COUNTER (P.C.)
0 - 7
MEMORY (256 X 16)
ADDRESS
SELECT

Fig. 1